Louisiana State University
LSU Digital Commons

LSU Doctoral Dissertations | Graduate School

8-5-2019

The Importance of Landscape Position Information and Elevation Uncertainty for Barrier Island Habitat Mapping and Modeling

Nicholas Matthew Enwright
Louisiana State University and Agricultural and Mechanical College, nick.enwright@gmail.com

Follow this and additional works at: https://digitalcommons.lsu.edu/gradschool_dissertations

Part of the Environmental Monitoring Commons, Geographic Information Sciences Commons, Geomorphology Commons, Physical and Environmental Geography Commons, Remote Sensing Commons, and the Spatial Science Commons

Recommended Citation
Enwright, Nicholas Matthew, "The Importance of Landscape Position Information and Elevation Uncertainty for Barrier Island Habitat Mapping and Modeling" (2019). *LSU Doctoral Dissertations*. 4838.
https://digitalcommons.lsu.edu/gradschool_dissertations/4838

This Dissertation is brought to you for free and open access by the Graduate School at LSU Digital Commons. It has been accepted for inclusion in LSU Doctoral Dissertations by an authorized graduate school editor of LSU Digital Commons. For more information, please contactgradetd@lsu.edu.

THE IMPORTANCE OF LANDSCAPE POSITION INFORMATION AND ELEVATION UNCERTAINTY FOR BARRIER ISLAND HABITAT MAPPING AND MODELING

A Dissertation

Submitted to the Graduate Faculty of the
Louisiana State University and
Agricultural and Mechanical College
in partial fulfillment of the
requirements for the degree of
Doctor of Philosophy

in

The Department of Geography and Anthropology

by
Nicholas Matthew Enwright
B.S., University of North Texas, 2007
M.S., University of North Texas, 2010
March 2019

For my wife, Megan, and daughter, Eleanor.

ACKNOWLEDGEMENTS

I thank my advisor, Dr. Lei Wang, for his patience, support, encouragement, inspiration, and guidance throughout my Ph.D. program. Besides my advisor, I extend my gratitude to my Ph.D. committee, which included Drs. Nina Lam, Charles Sasser, and Guangsheng Zhuang, for their time, helpful comments, and interest in my dissertation. For providing feedback and encouragement, I thank Dr. Stephen DeMaso from the U.S. Fish and Wildlife Service, Gulf Coast Joint Venture. I send my heartfelt gratitude to my past mentors from the University of North Texas, which include Drs. Bruce Hunter, Paul Hudak, and Joseph Oppong. All three of you have made a lasting impact on me and taught me the skills necessary to be successful in a Ph.D. program. I thank my supervisors at the U.S. Geological Survey, which include Stephen Hartley, Michelle Meyers, and Dr. Thomas Doyle, for allowing me to complete a Ph.D. program while working full time at the U.S. Geological Survey. I thank Dr. Greg Steyer from the U.S. Geological Survey for allowing me to work on the habitat mapping and modeling components of the “Alabama Barrier Island Restoration Assessment,” funded by the National Fish and Wildlife Foundation, which ultimately became this dissertation. For encouraging me to start this journey, I thank Drs. Michael Osland and Ken Krauss from the U.S. Geological Survey. I thank Sinéad Borchert from Borchert Consulting and Laura Feher, Richard Day, and Dr. Michael Osland from the U.S. Geological Survey for their assistance with field data collection for this research. I am grateful to Dr. Yi Qiang from the University of Hawaii for taking time to provide me guidance on using MATLAB for machine learning. Finally, I thank my wife, Megan, for her endless encouragement, support, and patience with me throughout this process. Thanks to you all!

TABLE OF CONTENTS

ACKNOWLEDGEMENTS iii

ABSTRACT v

CHAPTER 1. INTRODUCTION 1

CHAPTER 2. THE IMPACT OF LIDAR ELEVATION UNCERTAINTY ON MAPPING INTERTIDAL HABITATS ON BARRIER ISLANDS 5
- 2.1. Introduction 5
- 2.2. Methodology 10
- 2.3. Results 20
- 2.4. Discussion 27
- 2.5. Conclusion 31

CHAPTER 3. ADVANCING BARRIER ISLAND HABITAT MAPPING USING LANDSCAPE POSITION INFORMATION AND ELEVATION UNCERTAINTY 34
- 3.1. Introduction 34
- 3.2. Methodology 43
- 3.3. Results 53
- 3.4. Discussion 58
- 3.5. Conclusion 65

CHAPTER 4. MODELING BARRIER ISLAND HABITATS USING LANDSCAPE POSITION INFORMATION 67
- 4.1. Introduction 67
- 4.2. Methodology 72
- 4.3. Results 87
- 4.4. Discussion 93
- 4.5. Conclusion 98

CHAPTER 5. CONCLUSION 99

REFERENCES 110

APPENDIX A: HABITAT CLASS DEFINITIONS 124

APPENDIX B: HABITAT MAPPING THRESHOLDS 126

APPENDIX C: HABITAT MODELING 127

VITA 131

ABSTRACT

Barrier islands provide important ecosystem services, including storm protection and erosion control to the mainland, habitat for fish and wildlife, and tourism. As a result, natural resource managers are concerned with monitoring changes to these islands and modeling future states of these environments. Landscape position, such as elevation and distance from shore, influences habitat coverage on barrier islands by regulating exposure to abiotic factors, including waves, tides, and salt spray. Geographers commonly use aerial topographic lidar data for extracting landscape position information. However, researchers rarely consider lidar elevation uncertainty when using automated processes for extracting elevation-dependent habitats from lidar data. Through three case studies on Dauphin Island, Alabama, I highlighted how landscape position and treatment of lidar elevation uncertainty can enhance habitat mapping and modeling for barrier islands. First, I explored how Monte Carlo simulations increased the accuracy of automated extraction of intertidal areas. I found that the treatment of lidar elevation uncertainty led to an 80% increase in the areal coverage of intertidal wetlands when extracted from automated processes. Next, I extended this approach into a habitat mapping framework that integrates several barrier island mapping methods. These included the use of landscape position information for automated dune extraction and the use of Monte Carlo simulations for the treatment of elevation uncertainty for elevation-dependent habitats. I found that the accuracy of dune extraction results was enhanced when Monte Carlo simulations and visual interpretation were applied. Lastly, I applied machine learning algorithms, including K-nearest neighbor, support vector machine, and random forest, to predict habitats using

landscape position information extracted from topobathymetric data. I used the habitat map to assess the accuracy of the prediction model and I assessed the ability of the model to generalize by hindcasting habitats using historical data. The habitat model had a deterministic overall accuracy of nearly 70% and a fuzzy overall accuracy of over 80%. The hindcast model had a deterministic overall accuracy of nearly 80% and the fuzzy overall accuracy was over 90%. Collectively, these approaches should allow geographers to better use geospatial data for providing critical information to natural resource managers for barrier islands.

CHAPTER 1. INTRODUCTION

Barrier islands are subaerial expressions consisting of wave-, wind-, and/or tide-deposited sediments found along portions of coasts on every continent except Antarctica (Oertel, 1985; Stutz & Pilkey, 2011). Intertidal wetlands and supratidal/upland habitats on barrier islands provide numerous invaluable ecosystem services including storm protection and erosion control to the mainland, habitat for fish and wildlife, carbon sequestration in marshes, water catchment and purification, recreation, and tourism (Barbier et al., 2011; Feagin et al., 2010; Sallenger, 2000). However, barrier islands, face an uncertain future, particularly in the latter part of the 21st century. Numerous threats including hurricanes, accelerated sea-level rise, oil spills, and anthropogenic impacts may negatively influence the future of these islands (Pilkey & Cooper, 2014). Furthermore, climate-related threats to barrier islands may increase in the future (Hansen et al., 2016; Knutson et al., 2010). Therefore, to promote better management decisions, coastal resource managers require habitat mapping and models for insights with regard to how these islands are changing over time. This need can be filled by using geographic information science and remote sensing for monitoring the dynamic nature of barrier islands and modeling for predicting the future state of these ecosystems (Foster et al., 2017; Gutierrez, Plant, Thieler, & Tureck, 2015; Kindinger, Buster, Flocks, Bernier, & Kulp, 2013; Lucas & Carter, 2010; Passeri, Long, Plant, Bilskie, & Hagen, 2018).

Elevation data acquired via airborne topographic light detecting and ranging (lidar) sensors, are widely used in barrier island mapping and geomorphology studies (Brock, Krabill, & Sallenger, 2004; Foster et al., 2017; Gutierrez et al., 2015; McCarthy

& Halls, 2014). Due to their low-slope, barrier islands often contain a large amount of intertidal wetlands (Leatherman, 1979). While lidar technology has led to advancements in coastal wetland habitat mapping methodologies (Klemas, 2013), lidar vertical error often presents unique challenge for geospatial data applications in these low-relief environments. The level of uncertainty from data collected with conventional aerial topographic lidar systems is considerable within intertidal areas and can be as high as 60 cm in densely vegetated emergent wetlands (Buffington, Dugger, Thorne, & Takekawa, 2016; Medeiros, Hagen, Weishampel, & Angelo, 2015). Due to the lack of detailed error information, the uncertainty of lidar-based digital elevation models (DEMs) is often left unaddressed for habitat mapping efforts, yet the level of uncertainty becomes critical when studying low-relief environments, such as barrier islands, where centimeters can make a difference in the exposure to physically demanding abiotic conditions (e.g., inundation, salt spray, wave energy) (Anderson, Carter, & Funderbunk, 2016; Young, Brantley, Zinnert, & Vick, 2011). Advancements in sensor technology, such as single photon and Geiger-mode lidar sensors (Stoker, Abdullah, Nayegandhi, & Winehouse, 2016) and unmanned aerial system (UAS) lidar data collection (Jaakkola et al., 2010; Lin, Hyyppä, & Jaakkola, 2011), should lead to a greater frequency of high-quality elevation data for use by scientists and natural resource managers. As more and more data become available, one question that may arise for scientists is how to best leverage these data to produce automated inventories of elevation-dependent habitats in dynamic coastal environments to aid monitoring efforts. The first objective of this dissertation, covered in the second chapter, was to assess the impact of elevation

uncertainty on the delineation of intertidal habitats on barrier islands. This research was published in an article in *Remote Sensing.*

Maps of barrier island habitats provide natural resource managers with information needed to understand how habitats, such as beaches, intertidal flats, marshes, coastal dunes, and maritime forests, are changing over time (Kindinger et al., 2013; Lucas & Carter, 2010; Zinnert et al., 2016). As previously mentioned, with the increased availability of high-resolution lidar data, many researchers are utilizing elevation information along with aerial orthophotography for habitat mapping efforts specific to barrier islands (Chust, Galparsoro, Borja, Franco, & Uriate, 2008; Hantson, Kooistra, & Slim, 2012; Lucas & Carter, 2013; McCarthy & Halls, 2014). High-resolution elevation data can provide information about absolute elevation, but also relative topography, which has been shown to be helpful for delineating dune habitat (Wernette, Houser, & Bishop, 2016). The second objective of this dissertation, covered in the third chapter, was to develop a barrier island habitat mapping approach that incorporates elevation uncertainty information and relative topography from high-resolution lidar data.

Researchers have shown that barrier island habitats are related to barrier island morphology (Anderson et al., 2016; Foster et al., 2017; Young et al., 2011), yet models specific to barrier island habitats have rarely been developed. The relatively new field of machine learning includes efficient and powerful algorithms, such as K-nearest neighbor, support vector machine, and random forest (James, Witten, Hastie, & Tibshirani, 2013). Unlike classic data models, these flexible algorithms provide prediction tools that are free from assumptions related to the distribution of data (Breiman, 2001). The third objective of this dissertation, covered in the fourth chapter,

was to build on prior research with regard to linkages between barrier island morphology and habitat to assess how well machine learning algorithms can predict barrier island habitats using landscape position information (e.g., elevation and distance from the shoreline).

Due to the importance of barrier islands and the many ecosystem goods and services they provide, barrier island research often has a critical link to natural resource management. Finally, the fifth chapter concludes this dissertation with a summary of chapters two through four along with the implications of this research.

CHAPTER 2. THE IMPACT OF LIDAR ELEVATION UNCERTAINTY ON MAPPING INTERTIDAL HABITATS ON BARRIER ISLANDS

2.1. Introduction

Barrier islands are subaerial expressions consisting of wave-, wind-, and/or tide-deposited sediments found along portions of coasts on every continent except Antarctica (Oertel, 1985; Stutz & Pilkey, 2007). Due to their position along the land-sea interface, barrier islands often experience rapid episodic impacts related to storms as well as gradual changes related to anthropogenic activity, tides, and currents. Thus, natural resource managers are concerned with monitoring the extent and condition of these important coastal environments over time (Carruthers et al., 2013). Remote sensing provides an important tool for monitoring the dynamic nature of barrier island systems (Kindinger et al., 2013; Lucas & Carter, 2010).

Barrier islands provide numerous ecosystem services, including storm protection and erosion control to the mainland, habitat for fish and wildlife, salinity regulation in estuaries, carbon sequestration in marshes, water catchment and purification, recreation, and tourism (Barbier et al., 2011). Intertidal wetlands, which make up a substantial proportion of area on barrier islands, include areas that are regularly exposed to saline waters via high tides and areas that are periodically exposed to saline waters via extreme spring tides (Cowardin et al., 1979). Though difficult to value, these wetlands support ecosystem goods and services that are estimated to be worth U.S. $194,000 per hectare per year (Constanza et al., 2014). In addition to providing fish and

---

This chapter, previously published as “Enwright, N. M., Wang, L., Borchert, S. M., Day, R. H., Feher, L. C., & Osland, M. J. (2018). The Impact of Lidar Elevation Uncertainty on Mapping Intertidal Habitats on Barrier Islands. *Remote Sensing, 10*, 5.”

wildlife habitat, tidal wetlands can improve water quality, ameliorate flooding impacts, support coastal food webs, and protect coastlines (Barbier et al., 2011). Detailed wetland habitat mapping, such as the maps produced via the U.S. Fish and Wildlife National Wetlands Inventory Program, have commonly been developed using approaches that rely heavily on expert manual photointerpretation (Madden et al., 1999) and sometimes use elevation data as a guide (Maxa & Bolstad, 2009). Elevation information has also been combined with aerial photography for several habitat mapping efforts specific to barrier islands (Chust et al., 2008; McCarthy & Halls, 2014; Zinnert et al., 2016). For example, McCarthy and Halls (2014) mapped barrier island habitats in North Carolina and used elevation data to delineate habitats based on tidal regimes (e.g., intertidal and supratidal).

While lidar technology has led to advancements in coastal wetland habitat mapping methodologies (Klemas, 2013), lidar vertical errors can often present unique challenges for lidar applications in these low-slope environments. Lidar vertical error commonly varies by land cover type (Hodgson & Bresnahan, 2004), and vegetation cover has been found to be one of the greatest sources of error in lidar data (Su & Bork, 2006). The level of uncertainty from data collected with conventional aerial linear lidar systems is considerable within intertidal areas and can be as high as 60 cm in densely vegetated emergent wetlands (Buffington et al., 2016; Medeiros et al., 2015). Researchers have grappled with the challenges related to gauging the vertical error of lidar in intertidal areas and developing approaches to deal with these issues. These approaches have ranged from simple techniques, such as using a minimum bin approach (Schmid et al., 2011), to more complex regression-based corrections that

relate biomass estimation to the relative accuracy of digital elevation models (DEMs) estimated from Real-Time Kinematic Global Position System (RTK GPS) observations (Buffington et al., 2016; Medeiros et al., 2015). Due to the lack of detailed error information, the uncertainty of DEMs is often left unaddressed for habitat mapping efforts, yet the level of uncertainty becomes critical when studying low-relief environments where centimeters can make a difference in the exposure to physically demanding abiotic conditions (e.g., inundation, salt spray, wave energy) (Anderson et al., 2016; Young et al., 2011). In the near future, advancements in lidar technology, such as single photon and Geiger-mode lidar sensors (Stoker et al., 2016) and unmanned aerial system (UAS) lidar data collection (Jaakkola et al., 2010; Lin et al., 2011), should lead to higher frequency of high-quality elevation data for use by scientists and natural resource managers. As more and more data become available, one question that may arise for scientists is how to best leverage these data to produce automated inventories of elevation-dependent habitats in coastal environments for detailed monitoring of habitat changes over time.

One classic approach for dealing with vertical error in DEMs is through the use of Monte Carlo simulations (Hunter & Goodchild, 1995; Wechsler & Kroll, 2006). For example, one simple application of Monte Carlo simulations is to propagate error and determine the probability that the elevation is below a specific threshold for a set of iterations. This approach has become a popular way to incorporate vertical uncertainty in sea-level rise modeling applications (Cooper, Fletcher, Chen, & Barbee, 2013; Leon et al., 2014). Liu et al. (2007) used Monte Carlo simulations and error reported from lidar metadata to delineate the mean high water shoreline on the Bolivar Peninsula in

Texas, USA. Our work builds on this approach to extend the automated delineation to the full intertidal zone. In doing so, it is important to be sure that the error estimate incorporates vegetated land cover types and represents the 95th percentile error, since error commonly deviates from a normal distribution in vegetated land cover types (American Society for Photogrammetry and Remote Sensing, 2015). Furthermore, the utilization of a bias constraint in the Monte Carlo analyses (Weschler & Kroll, 2006) becomes critical as the intertidal boundary often extends into densely vegetated areas, which tend to lead to overestimation of elevation.

The primary objective of this study was to apply a simple approach to enhance results of automated intertidal area mapping using lidar data. I used tide gauge information, site-specific RTK GPS data, and information from a detailed relative accuracy report (i.e., lidar metadata) that followed the American Society of Photogrammetry and Remote Sensing's (ASPRS) standards (American Society for Photogrammetry and Remote Sensing, 2015) to simulate the propagation of elevation uncertainty into a lidar-based DEM using Monte Carlo simulations. I compared three different elevation error treatments, which included leaving error untreated and treatments that used Monte Carlo simulations to incorporate elevation vertical uncertainty using general information from lidar metadata and site-specific RTK GPS data, respectively. For each of the error treatments, I assessed the effect of error handling on automated delineation of low-lying lands (i.e., low-lying lands below the extreme high water spring (EHWS) tidal datum) and the delineation of the intertidal wetlands (Figure 2.1). In some cases, the collection of site-specific RTK GPS data may not be feasible and detailed metadata information with a relative elevation accuracy

assessment specific to vegetated low-lying land cover types may not be available. In these instances, researchers may opt to use information identified in literature from similar environments, specifically with regard to vegetation community. To aid researchers facing this predicament, I conducted a sensitivity test to explore how estimates of low-lying areas could be influenced by changes to error and bias. In this study, I investigated the following research questions: (1) How does extraction of low-lying lands compare for the three elevation error treatments in terms of areal coverage and accuracy?; (2) How does the extraction of intertidal wetlands compare for the three elevation error treatments in terms of areal coverage?; (3) How sensitive are error and bias parameters for the identification of low-lying lands?

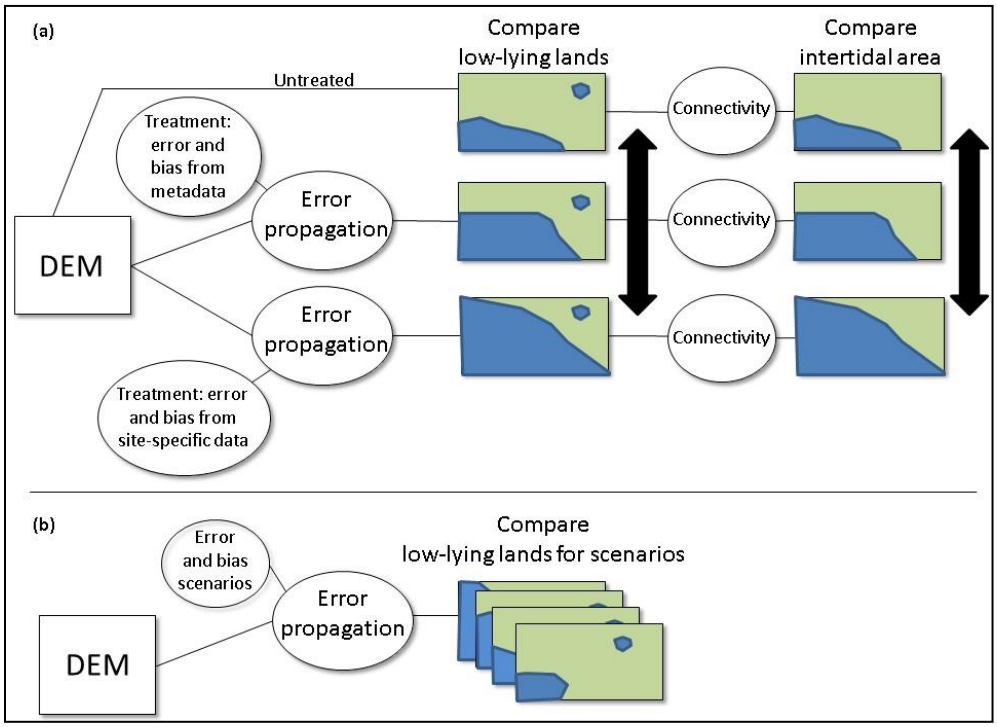

Figure 2.1. General overview of the study analyses. (a) Comparison of area with low-lying lands (i.e., elevation greater than or equal to the extreme high water spring tide level) and intertidal area using estimates from the three elevation error treatments. (b) Sensitivity analysis to assess how alternative error and bias values influence the identification of low-lying lands.

2.2. Methodology

2.2.1. Study Area

Dauphin Island (Alabama, USA) is a barrier island with a length of about 25 km, from about −88.34° to −88.07° longitude. At the widest point, the island extends from about 30.28° to 30.23° latitude (Figure 2.2). In December of 2015, the island had a subaerial area of about 13.6 km^2 (Enwright et al., 2017). The barrier island comprises a portion of a 105-km long Mississippi–Alabama wave-dominated barrier island chain that is backed by the shallow (<4-m depth) Mississippi Sound (Otvos & Carter, 2008). A tide gauge, first established in 1966 and operated by the National Oceanic and Atmospheric Administration (NOAA) (station ID: 8735180), is located on the eastern side of the island (Figure 2.2). The island is a microtidal environment, and experiences diurnal tides with a mean range of tide of about 0.36 m (i.e., height difference between mean low water and mean high water tidal datums), based on observations from the NOAA tide gauge on the island during the most recent North American Tidal Datum Epoch (NTDE; 1983 to 2001). The maximum observed water level at this gauge was about 2.01 m above mean sea level, which occurred during Hurricane Katrina in 2005. Numerous impacts from hurricanes have been documented on Dauphin Island with the most recent impacts occurring during Hurricane Katrina (Morton, 2008).

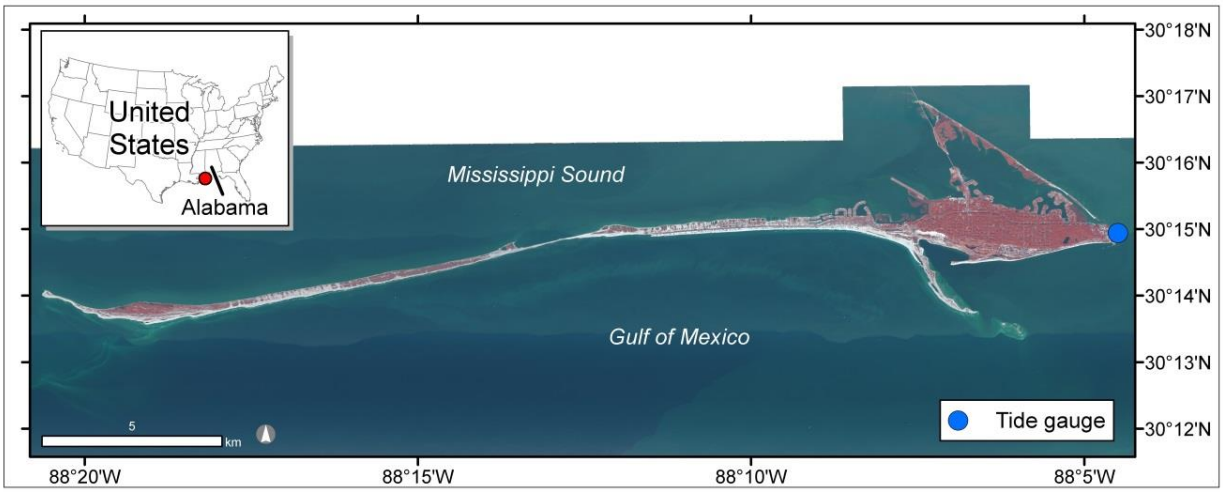

Figure 2.2. Study area and the location of the tide gauge. Basemap source data is 0.3-m color-infrared orthoimagery acquired in 2015 by Digital Aerial Solutions, LLC (DAS; Riverview, FL, USA) and the U.S. Geological Survey (USGS).

2.2.2. Elevation Data

I used aerial topographic linear lidar acquired during January 2015 by Digital Aerial Solutions, LLC (DAS; Riverview, FL, USA) and the U.S. Geological Survey (USGS). The lidar data were collected with the Leica ALS70 and ALS80 sensors. This data collection occurred over an extensive area (5,400 km^2) that included barrier islands in Alabama, Mississippi, and part of Louisiana. The acquisition area included 184 survey lines and 21 control lines positioned to have a nominal side overlap of 30%. These data were collected at an altitude of about 1,800 m and a ground speed of 155 knots. The laser rate was 132 kHz and the scan rate was 66.2 Hz. Airborne and ground GPS observations were collected at a frequency of 2 Hz and inertial measurement unit observations were collected at 200 Hz. These data were collected with a nominal pulse density of about 6 points per m^2 and adhered to the USGS quality level 2 standards (Heidemann, 2014). A 1-m DEM, which was used for this effort, was developed to support the USGS 3D Elevation Program (3DEP) (Sugarbaker et al., 2014) by DAS and the USGS. See Heidemann (2014) for information on USGS standards for lidar

acquisition and Arundel et al. (2015) for information on 1-m DEM development. The vertical datum of the data was the North American Vertical Datum of 1988 (NAVD88) GEOID 12a.

2.2.3. Tide and Water Level Data

I used tidal datum data from the NOAA Dauphin Island tide gauge (Figure 2.2). For this gauge, the mean sea level (MSL) was estimated to be 0.018 m higher than NAVD88 for the observations during the most recent NTDE. I transformed the vertical datum of the DEMs to MSL by adding this relative height difference to the DEM. Esri ArcMap 10.4.1 (Redlands, CA, USA) was used for all spatial analyses.

Intertidal wetlands fall above the extreme low water spring and below the EHWS tidal datums (Cowardin et al., 1979). I defined EHWS as the highest astronomical tide predicted for the Dauphin Island tide gauge (0.448 m relative to MSL), which is the highest predicted water level under astronomical conditions alone during the most recent NTDE.

2.2.4. Field Data Collection

I collected field data over two and a half weeks in November and December of 2015. Elevation data were collected using a high-precision RTK GPS connected to a Global Navigation Satellite System (GNSS) (Trimble R10 and TSC3, Trimble, Sunnyvale, CA, USA), coupled with the Continuously Operating Reference Station (CORS) network for Mississippi and Alabama (University of Southern Mississippi's network and Alabama Department of Transportation's CORS, respectively). The estimated precision from RTK GPS observations was about ±0.04 m (mean = 0.039, median = 0.037, interquartile range = 0.021). The habitat type was observed for each

elevation observation. These observations were collected via cluster sampling to support a habitat mapping effort (Enwright et al., 2017). Site accessibility related to private land was one of the main factors in the spatial distribution of the points. For more information on field data collection, see Enwright et al. (2017).

For this study, I created two subsets from the RTK GPS points. The first subset was used to conduct a relative accuracy assessment between the site-specific RTK GPS points and the 1-m DEM. A total of 62 points were collected in three different habitats which included intertidal flat (n = 7; Figure 2.3a), intertidal emergent marsh (n = 29; Figure 2.3b), and meadow (n = 26; Figure 2.3c). Meadows are supratidal areas with emergent herbaceous vegetation similar to wetlands found on the backslopes of the back-barrier. The second subset of the RTK GPS points was used to validate the results for identifying low-lying lands. I used datum information from the NOAA Dauphin Island tide gauge to transform the RTK GPS elevations to MSL. I restricted the subset to include points from any habitat that were below the elevation of 0.936 m (i.e., double the elevation of EHWS + 0.04 m; n = 86). A binary variable was created for these observations for which points with an elevation that was less than or equal to 0.488 m (EHWS + 0.04 m) were coded to “1” (n = 48) and those with an elevation greater than 0.488 m were coded to “0” (n = 38).

(a) (b) (c)

Figure 2.3. Examples of habitat types where data were collected for the relative accuracy assessment of the 1-m digital elevation model (DEM). (a) Intertidal flat. (b) Intertidal marsh. (c) Meadow.

2.2.5. Error and Bias

Propagation of lidar data vertical uncertainty by using Monte Carlo simulations requires an estimate of lidar DEM error and, if relevant, bias. I developed two different relative vertical error and bias estimates by comparing elevation collected via RTK GPS with the 1-m lidar DEM. The site-specific RTK GPS sample (n = 62) was right-skewed (i.e., skewness = 0.545) with a 95th percentile value of 0.415 m and a positive bias for 76% of the observations (Table 2.1). Based on the RTK GPS precision analyses, I assumed that points that were within ±0.04 m were not different for determining the percentage of observations with a positive bias (the DEM observation is higher than RTK GPS observation). Note, the bias identified in this study was similar to the bias found in a similar study in coastal wetlands by Buffington et al. (2016). The second error and bias estimate was based on information reported in the metadata for the lidar DEM product. These data came from RTK GPS observations throughout the extensive lidar acquisition extent from areas classified as either open, nonvegetated terrain, tall weed, brush land, forest, or urban. To make this analysis comparable to the site-specific analysis, I only used points from the open, nonvegetated terrain (n = 22) and tall weed (n = 18) classes that fell below 1 m relative to NAVD88. The pooled sample (n = 40)

was right-skewed (i.e., skewness = 0.959) with a 95th percentile value of 0.326 m and a positive bias for 54% of the observations (Table 2.1). For both vertical error assessments, the bias for nonvegetated and vegetated areas were combined to develop a simple average bias value which was rounded to nearest integer. SigmaPlot 12.5 (Systat Software, Inc., San Jose, CA, USA) was used for all nonspatial statistical analyses in this study, unless otherwise noted.

Table 2.1. Relative error accuracy assessment between the 1-m DEM and the Real-Time Kinematic Global Position System (RTK GPS) observations.

Measure	**Site-specific RTK GPS data**	**Lidar metadata**
Positive bias (%)	Nonvegetated (*n* = 7): 57.1 Vegetated (*n* = 55): 94.5 Average (*n* = 62): 76.0	Nonvegetated (*n* = 22): 36.3 Vegetated (*n* = 18): 72.2 Average (*n* = 40): 54.0
Skewness	0.545	0.959
95th percentile error (m)	0.415	0.326

2.2.6. Monte Carlo DEM Error Propagation

Monte Carlo analyses provide an efficient way to simulate the propagation of vertical error into DEMs for coastal applications involving tidal datums and sea-level rise (Cooper & Chen, 2013). In this study, error propagation followed an approach similar to that of Cooper and Chen (2013), with the addition of enhancements such as a neighborhood spatial autocorrelation filter and bias constraint used by Wechsler and Kroll (2006).

Figure 2.4 shows a general overview of the Monte Carlo simulation process used in this study. The first step in the error propagation was the development of a random field. In our case, I used a raster with a normal distribution with a mean of 0 and a standard deviation of 0.5. I forced the bias to be either positive or negative for each random field, collectively based on the proportional positive bias identified in the relative elevation analyses (Table 2.1). Next, a local filter (a 3-by-3-pixel neighborhood) was

used to incorporate spatial autocorrelation into the simulated random fields (Wechsler & Kroll, 2006). The filtered raster was multiplied by the 95th percentile error (Table 2.1) and added to the original DEM. The use of the 95th percentile error is recommended by the ASPRS when dealing with vertical error for areas that include vegetated areas (American Society for Photogrammetry and Remote Sensing, 2015). The result of adding the product of the 95th percentile error and the random field to the DEM is the simulation of the propagation of error into the DEM. For each iteration, pixels less than or equal to EHWS were coded as a binary variable as being true ("1") or false ("0"). These steps were repeated for 500 iterations. The binary rasters were summed, and the probability of a pixel being less than or equal to EHWS was determined by dividing the sum by the iteration count (n = 500).

I developed a presence-absence raster from the probability surface by coding pixels with a probability of greater than 0.5 to be "1" (presence) or "0" (absence) otherwise. This raster identified areas considered to be low-lying lands with an elevation less than or equal to EHWS. This low-lying lands raster includes some isolated low-lying areas that are not influenced by tides (Figure 2.1). I applied a connectivity constraint to this raster to create a presence-absence raster for intertidal areas. Specifically, I used the 8-side rule which includes cardinal and diagonal directions (Poulter & Halpin 2008) to remove isolated low-lying areas and retain only interconnected cells that receive tidal influence (Figure 2.4; for example, see Enwright et al. (2016) (p. 310)).

I repeated the steps above to develop a probability raster, presence-absence raster for low-lying lands, and a presence-absence raster for intertidal areas for the DEM using both error treatments (Table 2.1). I also created presence-absence rasters

for low-lying lands and intertidal areas for the untreated DEM. Our analyses were limited to the landward boundary of the intertidal zone (i.e., above MSL) since the airborne topographic lidar data I used did not include bathymetric data.

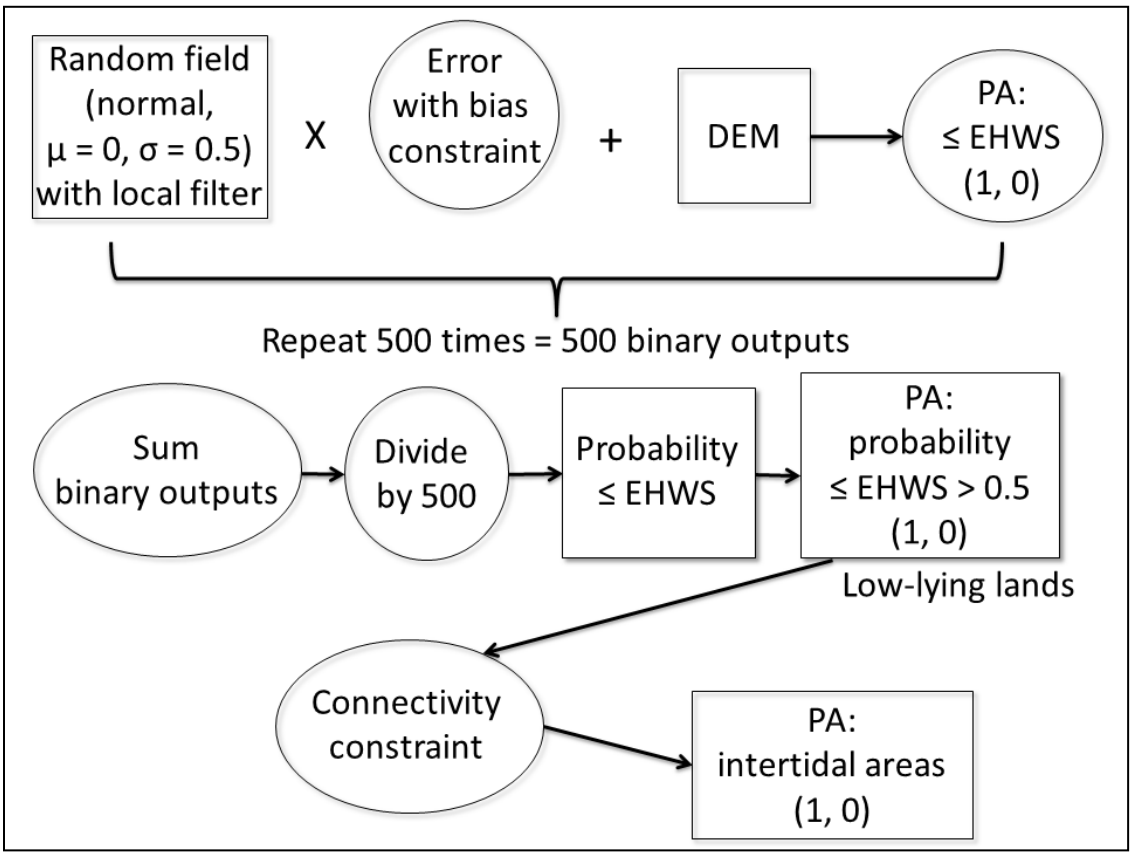

Figure 2.4. An overview of the Monte Carlo error propagation process for estimating the probability of pixels being considered low-lying lands (i.e., elevation ≤ extreme high water spring), the presence-absence raster for pixels likely to be low-lying lands, and the presence-absence raster for pixels likely to be intertidal areas. DEM: Digital elevation model; EHWS: Extreme high water spring; PA: Presence-absence raster.

2.2.7. Data Analyses

I compared the areal coverage of low-lying lands for the uncorrected DEM and for both error treatments. I also used the site-specific RTK GPS observations described in Section 2.2.4 as validation data to assess the performance of each DEM error treatment for identifying low-lying lands (Figure 2.5). For each treatment, I calculated the producer's accuracy (omission errors) and user's accuracy (commission errors) of

each presence-absence raster for low-lying lands. This accuracy assessment generally adhered to guidelines suggested by Congalton and Green (2009).

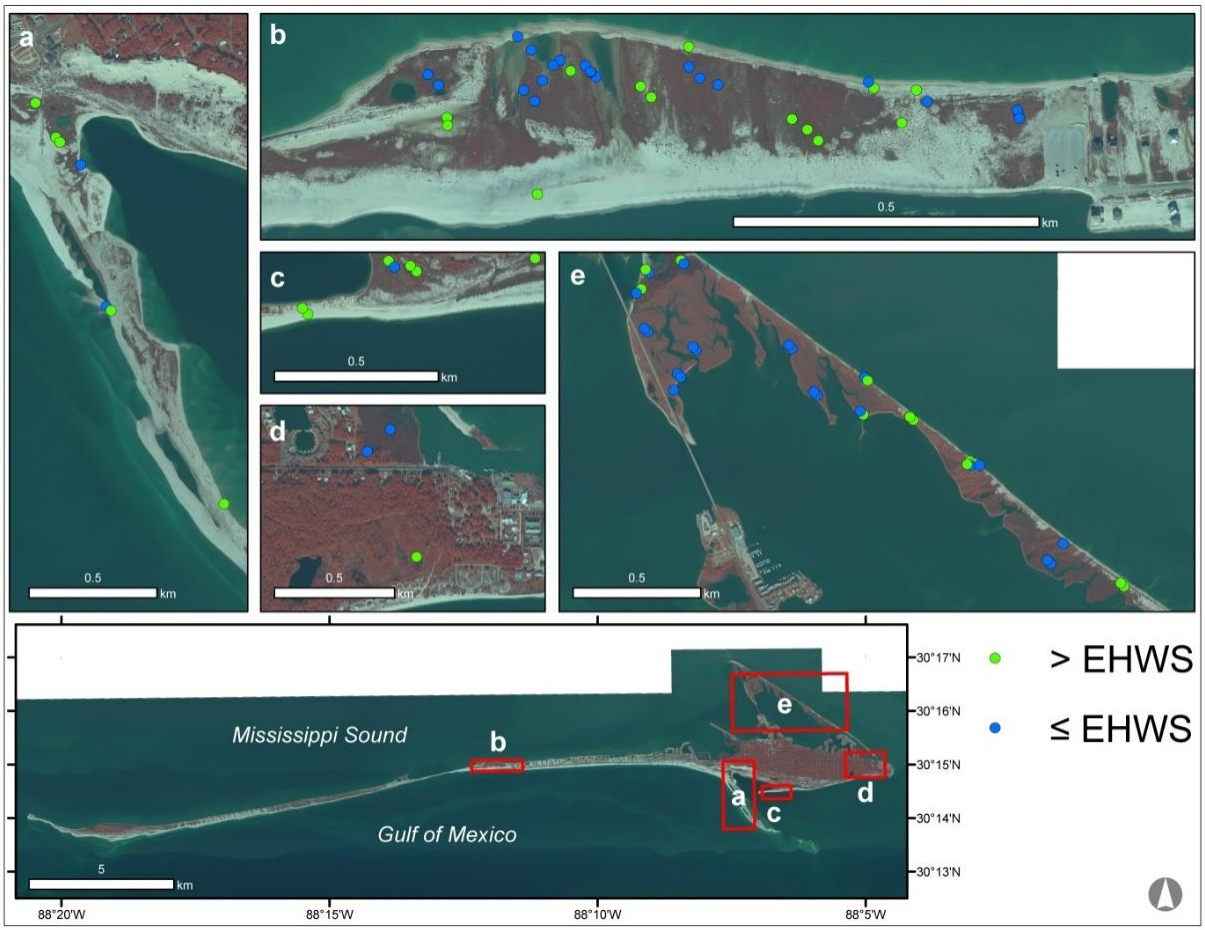

Figure 2.5. Validation points for assessing the presence-absence rasters for low-lying lands (a–e). Basemap source data is 0.3-m color-infrared orthoimagery acquired in 2015 by the DAS and the USGS.

I compared the areal coverage of intertidal areas delineated from each error treatment for the entire island. I conducted a more detailed comparison for a few specific areas of interest (AOI) with abundant intertidal areas. For each AOI, I calculated the percent of the AOI that is intertidal for each treatment.

In some cases, the collection of site-specific RTK GPS data may not be feasible and detailed metadata information with a relative elevation accuracy assessment specific to vegetated low-lying land cover types may not be available. In these

instances, researchers may opt to use information identified in literature from similar environments, specifically with regard to vegetation community. To aid researchers facing this predicament, I conducted a sensitivity analysis to explore how estimates of low-lying areas could be influenced by changes to error and bias. I ran the Monte Carlo error propagation for a suite of alternative error and bias values. I used the error treatment based on site-specific RTK GPS data as the baseline.

In total, I tested nine different alternative positive bias values (Table 2.2) and eight different error values (Table 2.3). To reduce the number of combinations, I held the bias constant (76%) while modifying error values and used a constant error of 0.415 m for bias modifications. I calculated the Kappa statistic (Cohen, 1960) to assess the agreement between each sensitivity scenario and the baseline scenario for identifying low-lying lands. Thus, the results of the sensitivity analysis show how minor adjustments to the error and bias affect the results of delineating low-lying lands. Ultimately, by gauging the similarity of results of minor error or bias adjustments, I aim to provide researchers with information for gauging whether it would be reasonable to use literature-derived error and bias values for similar environments.

Table 2.2. Positive bias values used in the sensitivity analysis.

Positive bias (%)
50
55
60
65
70
76[a]
80
85
90
95

[a]Baseline positive bias value.

Table 2.3. Error values used in the sensitivity analysis.

Error (m)
0.250
0.300
0.350
0.375
0.395
0.415[a]
0.435
0.450
0.500

[a]Baseline error value.

2.3. Results

2.3.1. Identification of Low-Lying Lands

The areal coverage of low-lying lands identified from the DEM varied by error treatment (Table 2.4). The range for the coverage of these lands extracted from the DEMs was 1.3 km^2. The untreated DEM resulted in the least amount of low-lying lands with an areal coverage of about 1.8 km^2, whereas the DEM with error treatment using site-specific RTK GPS data resulted in the most low-lying lands with an areal coverage of about 3.1 km^2.

In terms of validation, the range of both producer's accuracy and user's accuracy was nearly 30% (Table 2.4). Similar to areal coverage, there was a positive relationship between producer's accuracy and the sophistication of error treatment. The untreated DEM had a producer's accuracy of about 60% and the DEM with error propagation using site-specific RTK GPS data had a producer's accuracy of nearly 88%.

In contrast, a negative relationship was found between user's accuracy and sophistication of error treatment. The untreated DEM had a user's accuracy of about

96% and the DEM with error propagation using site-specific RTK GPS data had an accuracy of about 69%.

Table 2.4. Areal coverage, producer's accuracy, and user's accuracy for low-lying lands for each error treatment.

Error treatment	Area of low-lying lands (km^2)	Producer's accuracy (%)	User's accuracy (%)
Untreated	1.8	60.4	96.4
Information from lidar metadata	2.5	79.2	84.4
Site-specific RTK GPS data	3.1	87.5	68.9

2.3.2. Intertidal Wetlands

The overall trend in areal coverage of intertidal wetlands delineated for each treatment (Table 2.5) was consistent with the results of low-lying lands (Table 2.4). The range of intertidal area delineated from the DEMs was 1.3 km^2. The percent change in the coverage of intertidal areas from the untreated DEM increased by about 44% when intertidal areas were delineated using DEM with error treatment using information from metadata (i.e., increase from 1.6 km^2 to 2.3 km^2). This figure increased to 81% when intertidal areas were delineated using DEM with error treatment using site-specific RTK GPS data (i.e., increase from 1.6 km^2 to 2.9 km^2).

Table 2.5. Areal coverage of intertidal areas delineated for each error treatment.

Error treatment	Intertidal area (km^2)
Untreated	1.6
Information from lidar metadata	2.3
Site-specific RTK GPS data	2.9

Figures 2.6–2.8 show the extent of the intertidal area delineated for each error treatment for three different AOIs. Figure 2.6 includes back-barrier wetlands on the western tip of Dauphin Island. The percent of the AOI that contained intertidal areas increased by 190% when these areas were delineated using the DEM with error treatment using information from the lidar metadata. This figure increased to about

373% when intertidal areas were delineated using the DEM with error treatment using site-specific data. Figure 2.7 highlights an area with back-barrier wetlands near the island breach that occurred during Hurricane Katrina (named “Katrina Cut”). The percentage of the AOI that contained intertidal areas increased by 150% when these areas were delineated using the DEM with error treatment using information from the lidar metadata. This figure increased to about 294% when intertidal areas were delineated using the DEM with error treatment using site-specific RTK GPS data. Figure 2.8 includes intertidal marsh near Graveline Bay. Here, the differences amongst the three error treatments were much less pronounced; the difference between percent of the AOI that contained intertidal wetlands was ±10% for all three treatments.

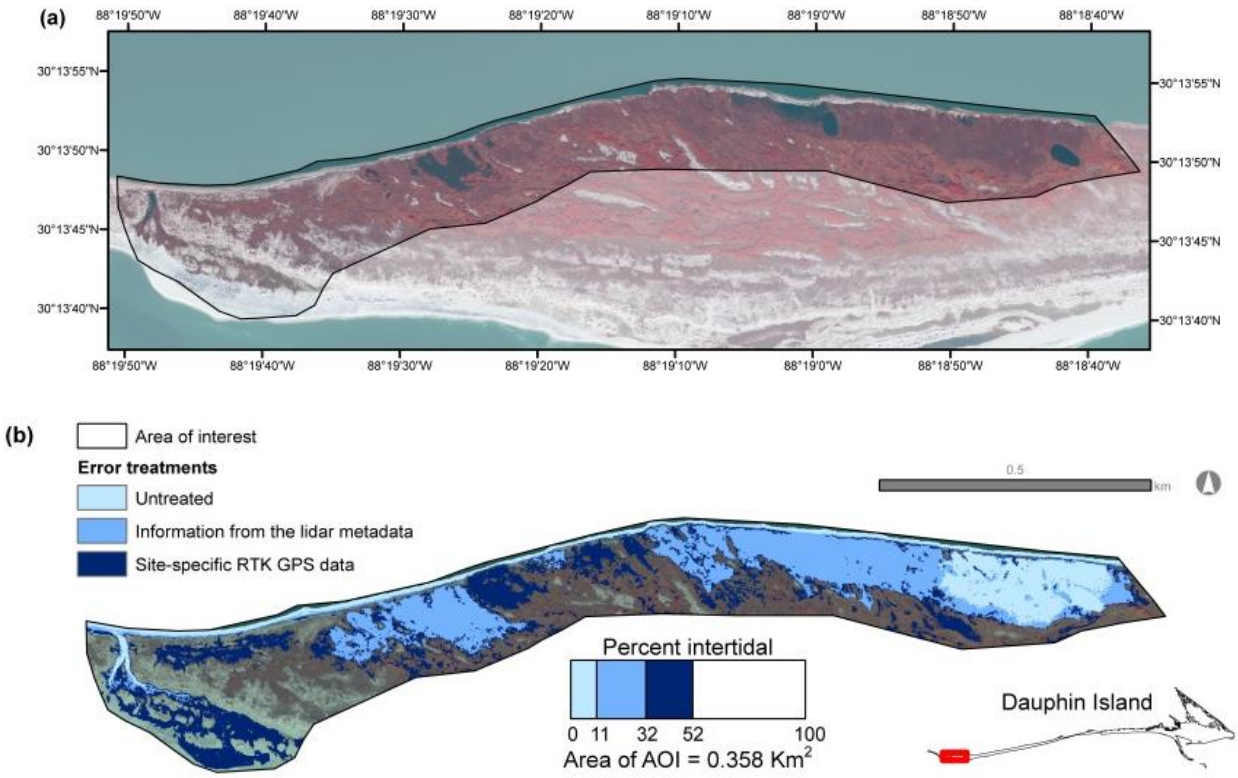

Figure 2.6. Comparison of intertidal area delineated for each error treatment for back-barrier wetlands located near the western tip of Dauphin Island. (a) Color-infrared orthoimagery for the AOI. Imagery is 0.3-m color-infrared acquired in 2015 by DAS and the USGS. (b) Intertidal area delineated with each DEM within the AOI. To visualize the full extent of a given treatment it is necessary to consider areas with less sophisticated treatment(s) (e.g., include the extent of all treatments for visualizing the extent of the treatment with site-specific RTK GPS data). The percentage of total area within the AOI below delineated as intertidal (rounded to nearest percent) is shown graphically below the map. The location of the AOI is depicted on a generalized overview map of Dauphin Island (Enwright et al., 2017). AOI: Area of interest; RTK GPS: Real-Time Kinematic Global Position System.

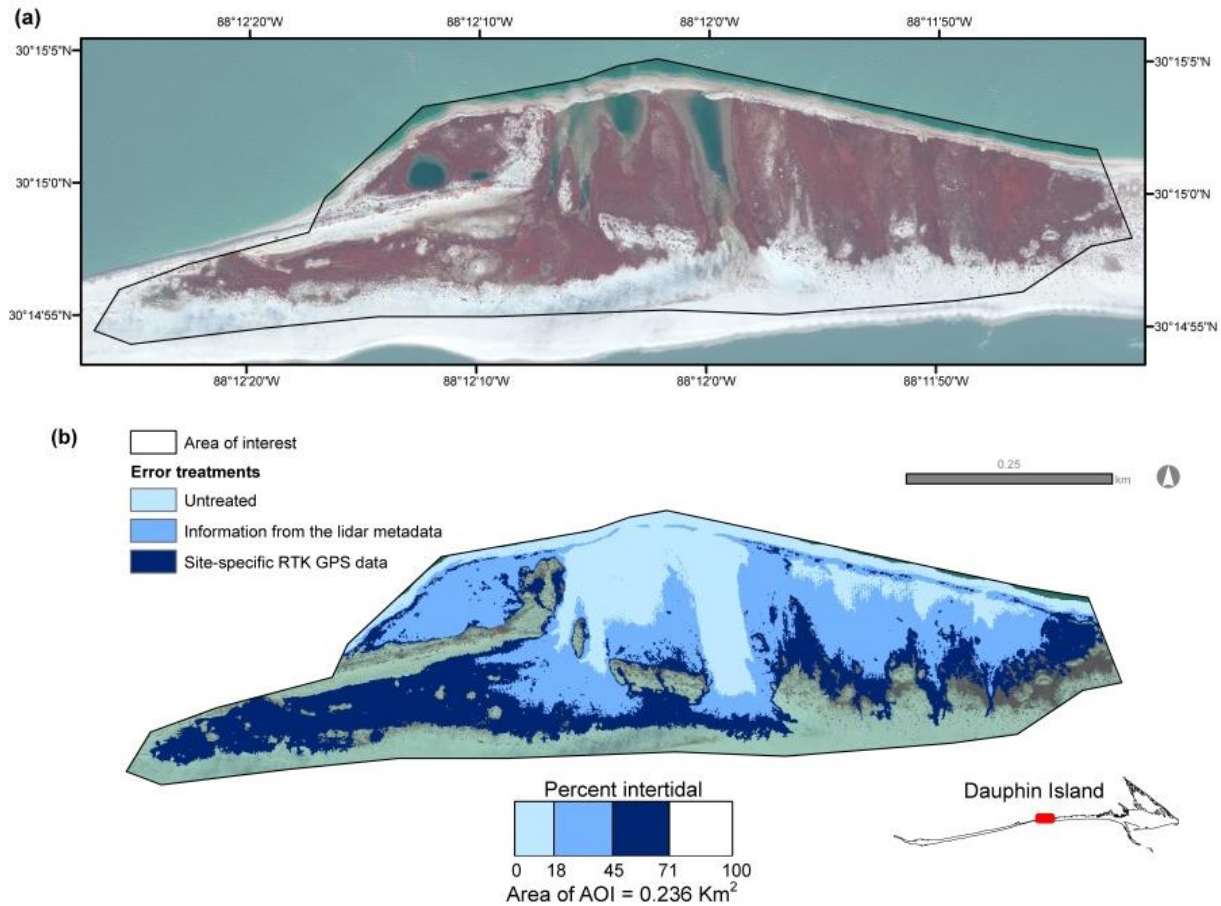

Figure 2.7. Comparison of intertidal area delineated for each error treatment for back-barrier wetlands located east of Katrina Cut. (a) Color-infrared orthoimagery for the AOI. Imagery is 0.3-m color-infrared acquired in 2015 by DAS and the USGS. (b) Intertidal area delineated with each DEM within the AOI. To visualize the full extent of a given treatment it is necessary to consider areas with less sophisticated treatment(s) (e.g., include the extent of all treatments for visualizing the extent of the treatment with site-specific RTK GPS data). The percentage of total area within the AOI delineated as intertidal (rounded to nearest percent) is shown graphically below the map. The location of the AOI is depicted on a generalized overview map of Dauphin Island (Enwright et al., 2017). AOI: Area of interest; RTK GPS: Real-Time Kinematic Global Position System.

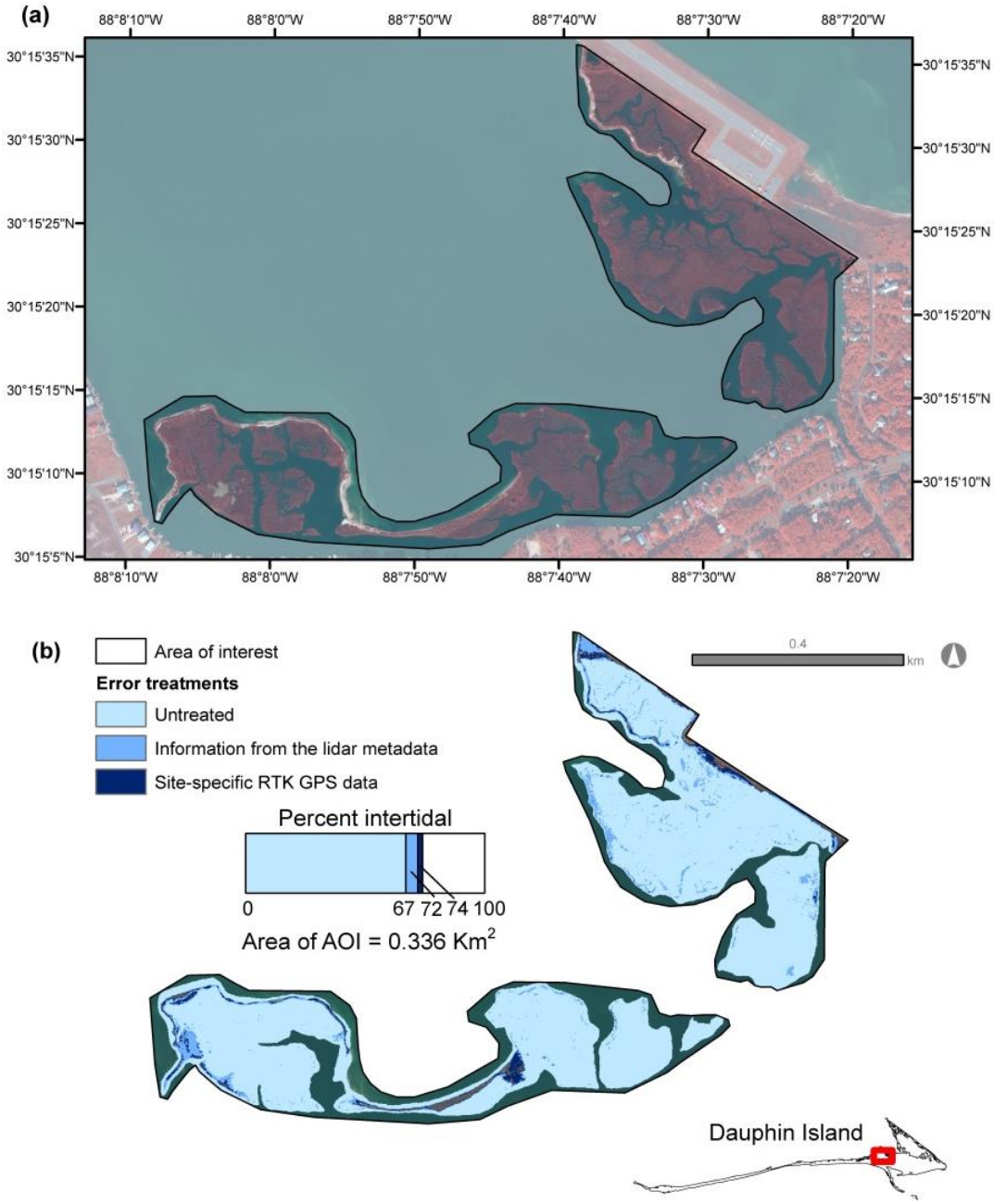

Figure 2.8. Comparison of intertidal area delineated for each error treatment for back-barrier wetlands located near Graveline Bay. (a) Color-infrared orthoimagery for the AOI. Imagery is 0.3-m color-infrared acquired in 2015 by DAS and the USGS. (b) Intertidal area delineated with each DEM within the AOI. To visualize the full extent of a given treatment it is necessary to consider areas with less sophisticated treatment(s) (e.g., include the extent of all treatments for visualizing the extent of the treatment with site-specific RTK GPS data). The percentage of total area within the AOI delineated as intertidal (rounded to nearest percent) is shown graphically below the map. The location of the AOI is depicted on a generalized overview map of Dauphin Island (Enwright et al., 2017). AOI: Area of interest; RTK GPS: Real-Time Kinematic Global Position System.

2.3.3. Sensitivity Analysis

Figure 2.9 shows the results from the sensitivity analysis. Overall, adjustments to the error (Figure 2.9a) had a greater effect on the agreement of results with the baseline than adjustments to positive bias (Figure 2.9b). Scenarios had a Kappa of 0.85 with error values that ranged from 0.375 m to 0.450 m (baseline error = 0.415 m), whereas scenarios had a Kappa of 0.85 for positive bias that ranged from 60% to 95% (baseline positive bias = 76%). Results produced using a 50% positive bias (DEM overestimates elevation only 50% of the time) were very different from the baseline (Kappa = 0.25).

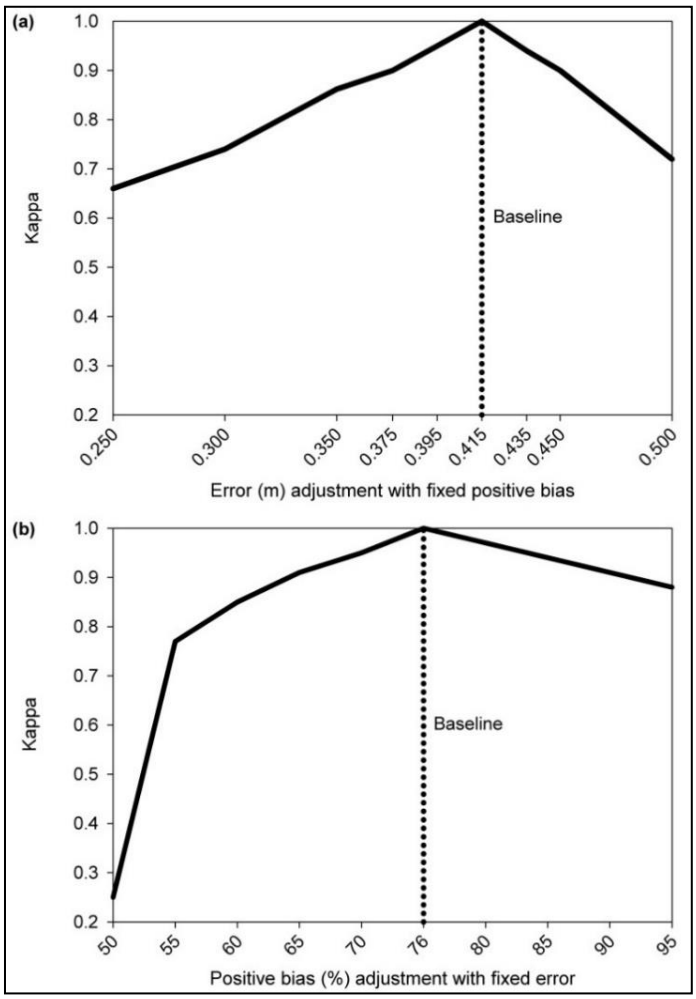

Figure 2.9. Plots of the sensitivity analysis results. (a) Agreement between the baseline scenario and scenarios with alternative error values with a fixed positive bias (76%). (b) Agreement between the baseline scenario and scenarios with alternative positive bias values with a fixed error (0.415 m).

2.4. Discussion

In this study, I applied a simple probabilistic approach to more accurately use lidar data in coastal settings for delineation of the landward intertidal boundary. Our results confirmed findings of others, which suggest that lidar DEMs can have a substantial level of vertical uncertainty in intertidal areas (Buffington et al., 2016; Medeiros et al., 2015; Schmid et al., 2011), and this uncertainty should be accounted for if data are directly used in classification algorithms for habitat mapping or for use in sea-level rise modeling efforts (Alizad et al., 2016; Schile et al., 2014). Our findings highlighted that optimal results with regard to the maximum identification of actual intertidal areas (i.e., highest producer's accuracy) are likely produced when site-specific RTK GPS data are used. Due to the overall importance and the dynamic nature of intertidal ecosystems, a natural resource manager may prefer an approach that better ensures all intertidal areas are captured even if the methodology used may include some level of reasonable overestimation rather than underestimation. In the absence of site-specific data, using information from the lidar metadata to parameterize error and bias should provide better results than maps produced with error left untreated. With a lower vertical error estimate, the Monte Carlo analyses with information from the lidar metadata provided relatively balanced results with regard to producer's accuracy and user's accuracy. This was likely due to the moderate error and lower bias compared to the site-specific error and bias. Ultimately, the decision on how a researcher balances omission error (producer's accuracy) or commission error (user's accuracy) should be based on their research questions and mapping objectives.

By using connectivity constraints, I extended the Monte Carlo analyses to map areas likely to be intertidal wetlands. The impact of error treatments was explored for the entire island and for three different AOIs (Figures 2.6–2.8). While the untreated DEM was more suitable for the intertidal marsh application near Graveline Bay (Figure 2.8), the differences were more magnified for other back-barrier marshes (Figures 2.6 and 2.7). The similarity of the treatments for the marsh near Graveline Bay is likely the result of a lower overall elevation of the marsh platform in that area, but differences in vegetation community can also be a factor that affects localized lidar error, for example (Buffington et al., 2016). Clearly, a map of intertidal areas developed from untreated DEM would result in a gross underestimation of intertidal wetlands similar to results from other researchers (Buffington et al., 2016; Kidwell et al., 2017). However, both maps with treatment of error could provide reasonable intertidal wetland estimates based on lidar data alone or as an initial step that could be refined via minor manual photointerpretation. In other words, these maps can serve as a stand-alone inventory of area falling within the intertidal zone similar to the work of Liu et al. (2007) or be used to as a foundation to develop a detailed habitat map (Enwright et al., 2017).

The decision regarding use of site-specific RTK GPS data or information from the lidar metadata should be driven by project budget and research questions. In some cases, the lidar metadata may not provide sufficient information to assess the 95th percentile error for vegetated areas and estimate the bias. Under these circumstances, error treatment may only be feasible using error and bias values identified from literature that include analyses of lidar datasets with similar acquisition characteristics (e.g., point spacing) and vegetation community. I conducted a sensitivity analysis to

provide insights on how results produced with minor adjustments to either error or bias compare to the results produced with site-specific RTK GPS data. Our results suggest selection of an appropriate error value may be more critical than bias; however, it seems important to have a bias value that is higher than 50% for study areas with vegetated areas. If it is necessary to rely on literature for error and bias values, then a thorough visual inspection of the results may be warranted to ensure parameters are producing reasonable results for the particular study area.

Due to the local scale of our study, I was able to transform vertical datum of the DEM from an orthometric datum to a locally relevant tidal datum using a tide gauge on the island. However, studies that cover a larger spatial extent may need to use a vertical datum transformation software, such as NOAA VDatum (Parker, 2003) to transform orthometric datums to locally relevant tidal datums. This step can lead to additional vertical uncertainty, and if quantified for the transformation model, this uncertainty can be combined with the source data uncertainty and incorporated into the Monte Carlo simulations (Cooper et al., 2013).

A byproduct of delineating the upper intertidal boundary is information on the extent and areal coverage of supratidal habitat. On barrier islands, supratidal areas include habitats such as beach, dune, and barrier flat (i.e., meadow, nonvegetated barrier flat, and forest). Monitoring these supratidal areas is equally important to resource managers (Lucas & Carter, 2010) because these areas provide important habitat for resident and migratory shorebirds (Galbraith, DesRochers, Brown, & Reed, 2014), neotropical migrants (Lester, Ramierez, Kneidel, & Heckscher, 2016), and sea turtles (Katselidis, Stamou, Dimopoulos, & Pantis, 2014). Besides providing habitat for

wildlife, dunes deliver erosion control for shorelines (Plant, Thieler, & Passeri, 2016). Dune crest elevation plays a critical role in the level of this protective capacity, and thus, in determining coastal vulnerability (Plant et al., 2016; Sallenger, 2000; Stockdon, Doran, Thompson, Sopkin, & Sallenger, 2012). A Monte Carlo process similar to the one used in this study can be applied to determine areas with elevation that is greater than a typical extreme water level associated with storms using site-specific RTK GPS data collected in dune environments (Enwright et al., 2017).

The objective of this study was to develop a straightforward approach for treating vertical uncertainty in lidar-based DEMs. This study leveraged RTK GPS data collected with a cluster sampling design that was obtained to serve as validation data for a habitat classification mapping effort (Enwright et al., 2017). For this reason, I chose to use a simple method of introducing spatial autocorrelation into the Monte Carlo processing by using a low-pass filter rather than a more complex approach, such as the weighted spatial dependence approach (Wechsler & Kroll, 2006). A more systematic sampling of lidar error in intertidal areas similar to the approaches applied by Medeiros et al. (2015) or Buffington et al. (2016) would allow for a more complex treatment of spatial autocorrelation. As stated earlier, analyses in this effort were restricted to intertidal areas above MSL due to the use of topographic lidar. The methodology used in this study could be modified to more accurately delineate the full intertidal zone (i.e., boundary between subtidal and intertidal habitats and boundary between supratidal and intertidal habitats) if used with topobathymetric lidar. Lidar intensity data has been shown to enhance habitat classifications in coastal environments (Brennan & Webster, 2006; Chust et al., 2008). Future efforts could explore the application of spatially

variable error and bias based on a simple vegetation presence-absence classification based on lidar intensity. Additionally, the use of intensity information would allow researchers to extend this work to examine the habitat-specific impacts of not treating lidar error when delineating the intertidal zone. One potential issue related to this enhancement could be that high-quality intensity information may not be available for all lidar acquisitions. Finally, technological advancements like next-generation lidar sensors and on-demand lidar via UAS should greatly enhance how dynamic habitats like barrier islands are monitored. As data availability increases, this approach could be calibrated with next-generation lidar sensors such as single photon and Geiger-mode lidar platforms which enable data collection with much higher nominal point spacing (e.g., greater than 20 points per m^2) as compared to conventional linear lidar (i.e., lidar used in this study was about 6 points per m^2) (Stoker et al., 2016) or data collected via on-demand lidar via an UAS (Jaakkola et al., 2010; Lin et al., 2011). Another potential improvement of using these methods with UAS data would be the ability to collect elevation data and optical imagery concurrently.

2.5. Conclusion

In intertidal areas, the elevation estimated from conventional aerial linear lidar can be much higher than the actual elevation due to dense vegetation cover. The uncertainty of DEMs is often not addressed for habitat mapping efforts, yet the level of uncertainty becomes critical when studying these low-relief and intertidal environments where centimeters can greatly influence the exposure to physically demanding abiotic conditions. In this study, I applied tide gauge information, RTK GPS data, and information from a detailed relative accuracy report that followed the ASPRS standards

to simulate the propagation of elevation uncertainty into a DEM using Monte Carlo simulations. The primary objective of this study was to apply a simple approach to enhance results of automated intertidal area mapping using lidar data. I analyzed three different elevation error treatments which included leaving error untreated and treatments that used Monte Carlo simulations to incorporate elevation vertical uncertainty using lidar metadata and site-specific RTK GPS data, respectively.
Our work shows that the untreated DEM underestimated coverage of low-lying areas and intertidal areas. I found that the DEMs with treatment of error had higher producer's accuracy and user's accuracy for identifying low-lying areas below the EHWS. For the entire island, the percent intertidal lands increased by up to 80% when using Monte Carlo analyses to treat vertical uncertainty. Results from the sensitivity analysis suggest that it could be reasonable to use error and positive bias values from literature for similar environments, conditions, and lidar acquisition characteristics in the event that collection of site-specific data is not feasible and information in the lidar metadata is insufficient. In this event, I found that bias values may be less sensitive than error, although it is critical to select a bias value greater than 50% if the study area has abundant vegetation cover.

Results from this study should interest researchers that use lidar data in coastal morphology and habitat mapping studies, but especially those studying elevation-dependent ecological patterns and processes in coastal areas. The methodology outlined in this study could be used to develop stand-alone products with the simple aim of providing land managers with an accurate areal coverage of intertidal and supratidal habitats or to serve as a foundation for identification of tidal regimes for detailed habitat

mapping efforts. The approach outlined in this study should be applicable to future technological advancements, such as next-generation lidar sensors and on-demand lidar via unmanned aerial systems.

CHAPTER 3. ADVANCING BARRIER ISLAND HABITAT MAPPING USING LANDSCAPE POSITION INFORMATION AND ELEVATION UNCERTAINTY

3.1. Introduction

Barrier islands are dynamic coastal environments that consist of wave-, wind-, and/or tide-deposited sediments located along the estuarine-marine interface. These islands are found along portions of coasts on every continent except Antarctica (Oertel, 1985; Stutz & Pilkey, 2011). Comprised of a diverse mosaic of habitats, these islands can include beaches, dunes, marshes, intertidal flats, and coastal forests. Barrier islands provide many valuable ecosystem services, including storm protection and erosion control to the mainland, habitat for fish and wildlife, carbon sequestration in marshes, water catchment and purification, recreation, and tourism (Barbier et al., 2011; Feagin et al., 2010; Sallenger, 2000). However, barrier islands face an uncertain future, particularly in the latter part of the 21st century as numerous threats, including hurricanes, accelerated sea-level rise, oil spills, and anthropogenic impacts, may influence the future of these islands (Pilkey & Cooper, 2014). Furthermore, climate-related threats to barrier islands are expected to increase in the future (Knutson et al., 2010; Hansen et al., 2016). Thus, to better inform both present and future management decisions, coastal resource managers require insights into how these dynamic islands are changing over time. Geographers and remote sensing scientists can fill this critical need through the development of habitat maps and models created using geographic information science and remote sensing (Campbell, Wang, Christiano, & Stevens, 2017; Jeter & Carter, 2015; Kindinger et al., 2013; Lucas & Carter, 2010; Zinnert et al., 2016).

3.1.1. Mapping Methodologies

Barrier island monitoring efforts require the development of custom habitat map products. This is due to a need for greater thematic resolution than is often included in readily available, regional land cover products such as the U.S. Geological Survey's (USGS) National Land Cover Database (NLCD; Homer et al., 2015) and the National Oceanic and Atmospheric Administration's (NOAA) Coastal Change Assessment Program (C-CAP; Dobson et al., 1995), which include general land cover types such as bare lands, marshes, and woody vegetation but lack classification of habitats like beaches, dunes, and intertidal flats. These regional products also often lack specific information related to regional microhabitats such as relic beach ridges (e.g., Chenier Plain region of Texas and Louisiana, USA). Similarly, the U.S. Fish and Wildlife Service's National Wetland Inventory maps (Cowardin et al., 1979) provide detailed information in coastal areas, but only for wetland habitats. Also, the spatial resolution of regional map products like NLCD and C-CAP are often too coarse (i.e., 30 m) for barrier islands, which may only span a handful of pixels for relatively narrow portions of an island. In some cases, researchers may find the accuracy of NLCD and C-CAP products for barrier islands to be suboptimal for a given research objective since these classifications are developed for expansive areas that extend well beyond barrier islands rather than focusing explicitly on developing targeted algorithms for habitat classification on barrier islands. As a result, barrier island-specific habitat mapping efforts are prevalent and include a wide array of habitat class types, source data, and mapping approaches (Table 3.1).

Table 3.1. Examples of barrier island or coastal beach-dune habitat mapping efforts. For each mapping effort, I outlined the types of classes, mapping unit, source data, general mapping approach, and location of the study. Studies that included both species-level classes and general morphology-based habitat classes were listed under both class categories. HI: Hyperspectral imagery; HO: High-resolution orthophotography; HS: High-resolution satellite imagery; KB: Knowledge-based ruleset; LI: Topographic lidar elevation data; ML: Machine learning algorithm; MS: Moderate-resolution satellite imagery; OB: object-based; PB: Pixel-based; PI: Photointerpretation; SC: Supervised classification; UAS: Unmanned aerial system; and UC: Unsupervised classification.

Types of classes	Unit	Source data	Mapping approach	Study	Location
Species-level	PB	HI	SC and UC	Bachmann et al. (2002)	U.S. East Coast
		HI and LI	SC and UC	Young et al. (2011)	U.S. East Coast
		HO, HS, and LI	ML	Timm and McGarigal (2012)	U.S. East Coast
		HO and LI	SC	Chust et al. (2008)	Spain
				Hantson et al. (2012)	Netherlands
		HO and LI	SC	Hantson et al. (2012)	Netherlands
		HS, HO, and LI	ML	Campbell et al. (2017)	U.S. East Coast
		HS and LI	KB	Brownett and Mills (2017)	England
National/regional classification schemes	PB	HO	PI	Acosta et al. (2003)	Italy
		HS	UC	Wang et al. (2007)	U.S. East Coast
General morphology-based barrier island habitats (e.g., beach, dune, and backslopes)	PB	HO	UC	Fearnley et al. (2009)	U.S. East Coast
		HS and LI	UC and SC	McCarthy and Halls (2014)	U.S. East Coast
		HO	SC	Jeter and Carter (2015)	U.S. East Coast
		HO and LI	SC	Anderson et al. (2016)	U.S. East Coast
		HI and LI	SC	Lucas and Carter (2010)	U.S. East Coast
				Lucas and Carter (2013)	U.S. East Coast
		MS	SC	Zinnert et al. (2016)	U.S. East Coast
		MS and LI	SC	Zinnert et al. (2011)	U.S. East Coast
	OB	HS, HO, and LI	ML	Campbell et al. (2017)	U.S. East Coast
		UAS and LI	ML	Sturdivant et al. (2017)	U.S. East Coast
		HS and LI	KB	Brownett and Mills (2017)	England

A critical starting point for habitat mapping efforts is the development or adoption of an existing classification scheme (i.e., a set of mapping targets with clear definitions). Table 3.1 includes a list of commonly used classification scheme types for barrier island and coastal beach-dune habitat mapping efforts. Some studies used detailed classification schemes that include species-level habitat mapping (Bachmann et al., 2002; Brownett & Mills, 2017; Campbell et al., 2017; Chust et al., 2008; Hantson et al., 2012; Timm & McGarigal, 2012; Young et al., 2011). In some cases, barrier island habitat mapping efforts utilized existing standardized classification schemes, such as the U.S. National Vegetation Classification System (Wang, Traber, Milstead, & Stevens, 2007) or the European CORINE (coordination of information on the environment)

system (Acosta et al., 2003). However, most barrier island habitat mapping efforts used or included general, user-defined barrier island habitat classes with an emphasis on geomorphic features including beaches, dunes, and barrier flats (Anderson et al., 2016; Brownett & Mills, 2017; Campbell et al., 2017; Fearnley et al., 2009; Halls, Frishman, & Hawes, 2018; Jeter & Carter, 2015; Leatherman, 1979; Lucas & Carter, 2010, 2013; McCarthy & Halls, 2014; Timm & McGarigal, 2012; Zinnert, Shifflett, Vick, & Young, 2011; Zinnert et al., 2016).

The mapping unit is another critical decision in developing a mapping methodology. Here, options include traditional pixel-based methods, where each pixel is classified individually, and geographic object-based image analysis (GEOBIA; Blaschke et al., 2014), which involves classification of image objects (i.e., a group of neighboring pixels that are considered to be similar). A few benefits of GEOBIA are the ability to easily integrate spatial information into a mapping process through data fusion (O'Neil-Dunne, MacFaden, & Royar, 2014; Zhang, 2015; Zhang, Xie, & Selch, 2013) and the ability to reduce salt-and-pepper issues associated with pixel-based mapping (Yu et al., 2006). These advantages are most often realized when using high-resolution source data (e.g., high-resolution orthophotography, high-resolution satellite imagery). While the popularity of GEOBIA is rapidly increasing in coastal remote sensing applications (Dronova, 2015; Heumann, 2011), the technique was not found to be as prevalent in barrier island and coastal beach-dune habitat mapping literature (Table 3.1). A few examples of use of GEOBIA in coastal-beach dune settings include the work of Brownett and Mills (2017) and Hantson et al. (2012).

Source data are another critical component for habitat mapping efforts. Species-level mapping efforts commonly used hyperspectral imagery, yet most barrier island habitat mapping efforts used high-resolution orthophotography or satellite imagery (Table 3.1). High-resolution imagery is well-suited to developing detailed maps (Brownett & Mills, 2017; Campbell et al., 2017), whereas moderate-resolution satellite imagery such as Landsat or Sentinel-2 imagery offers the advantage of developing multi-temporal analyses to explore change in these dynamic systems (Zinnert et al., 2011, 2016). Both products can provide valuable insights to barrier island monitoring. A high-resolution, bare-earth digital elevation model (DEM) produced from data collected from aerial topographic lidar systems provides valuable information for coastal applications on barrier islands (Brock & Purkis, 2009), and these data were often combined with imagery for habitat mapping efforts (Table 3.1). Increasingly, researchers are using bare-earth DEMs developed from lidar data and tide data for automated delineation of intertidal and supratidal habitats (Brownett & Mills, 2017; Halls et al., 2018; McCarthy & Halls, 2014). Raw lidar data also have general applicability to mapping efforts as researchers can use these data for estimating the height and morphology of building footprints (Meng, Wang, & Currit, 2009) and, despite uncertainty issues due to lidar penetration in densely vegetated areas (Meng, Currit, & Zhao, 2010), for estimates of the height of vegetation (Brownett & Mills, 2017; Hantson et al., 2012; Hudak, Evans, & Smith, 2009; O'Neil-Dunne et al., 2014).

Lastly, the mapping approach is another crucial factor to consider. Several algorithms have been used with traditional pixel-based mapping frameworks for barrier island habitat mapping efforts (Table 3.1). The most common algorithm was the

maximum likelihood classifier (Anderson et al., 2016; Chust et al., 2008; Strahler, 1980; Hantson et al., 2012; Jeter & Carter, 2015; Lucas & Carter, 2010, 2013; McCarthy & Halls, 2014; Sturdivant et al., 2017; Zinnert et al., 2011, 2016), although some studies used unsupervised techniques (Bachmann et al., 2002; Ball & Hall, 1965; Fearnley et al., 2009; McCarthy & Halls, 2014; Wang et al., 2007). While supervised machine learning approaches can be used with GEOBIA (Campbell et al., 2017; Dronova, 2015; Timm & McGarigal, 2012), researchers often use a rule-based approach that classifies habitat types in a step-wise fashion using interpretation and expert knowledge (Brownett & Mills, 2017; Dronova, 2015; Gao, Chen, Zhang, & Zha, 2004; Myint Gober, Brazel, Grossman-Clarke, & Weng, 2011; O'Neil-Dunne et al., 2014). For instance, Brownett and Mills (2017) used high-resolution satellite imagery, a bare-earth DEM, a canopy height model, tide information, and ecological knowledge to develop a rule-based approach to classify coastal dune habitats in England.

3.1.2. Intertidal Wetlands and Lidar Vertical Uncertainty

Intertidal wetlands include areas that are periodically exposed to saline waters via extreme spring tides (Cowardin et al., 1979). Barrier islands often include a substantial amount of low-lying lands. Thus, these wetlands often make up a large proportion of area on barrier islands. As previously mentioned, DEMs are increasingly being used for automated delineations of intertidal and supratidal habitats in coastal applications despite issues related to vertical uncertainty. Yet, the level of uncertainty from data collected with conventional aerial topographic lidar systems has been found to be as high as 60 cm in densely vegetated emergent wetlands throughout the U.S. (Buffington et al., 2016; Enwright et al., 2018b; Medeiros et al., 2015). For barrier island

habitat mapping efforts, the vertical uncertainty is often left unaddressed due to the lack of detailed error information. However, the level of uncertainty becomes critical when studying low-relief environments, including barrier islands, where centimeters can make a difference in the exposure to physically demanding abiotic conditions (e.g., inundation, salt spray, wave energy) or in the potential for inundation by storm surges or rising sea levels (Anderson et al., 2016; Young et al., 2011; Zinnert, Stallins, Brantley, & Young, 2017).

Monte Carlo simulations are one classic approach for dealing with vertical uncertainty in DEMs (Hunter & Goodchild, 1995; Wechsler & Kroll, 2006). For example, a simple application of Monte Carlo simulations is to propagate error and determine the probability that the elevation of a given DEM cell is below or above a specific elevation threshold for a set of iterations. This approach has been used for coastal shoreline mapping applications. For instance, Liu et al. (2007) used Monte Carlo simulations and error reported from lidar metadata to delineate the mean high water shoreline from noisy lidar data on the Bolivar Peninsula in Texas, USA. Enwright et al. (2018b) extended this approach using field data to map the full intertidal zone using the highest astronomical tide for a barrier island off the coast of Alabama, USA. The results from these efforts confirmed the findings of others (Alizad et al., 2016; Buffington et al., 2016; Medeiros et al., 2015; Schmid et al., 2011) and underscore the importance of considering elevation uncertainty when using a DEM for automated delineation of intertidal habitats.

3.1.3. Dune Delineation

Dunes are geomorphic features formed by aeolian transport of sediments. These features provide important habitat for wildlife (Gieder et al., 2014; Katselidis et al., 2014) and can influence coastal vulnerability by buffering coastal erosion and flooding during storm surges (Sallenger, 2000; Stockdon et al., 2012; Plant et al., 2016). Remote sensing of dune features is complicated due to the ambiguity and subjectivity often associated with the delineation of these features (Hugenholtz et al., 2012; Wernette et al., 2016, 2018). Dunes with a high relative topography (i.e., steep slopes) can often be easily distinguished in high-resolution lidar-based DEMs. Wernette et al. (2016) proposed the use of relative relief as an approach for automated dune delineation. Their multi-scaled approach shows promise for detailed, automated dune extraction, but the focus on foredune (i.e., first seaward dune) extraction could potentially limit the applicability to broad island-scale habitat mapping efforts. Another approach is the use of the topographic position index (TPI), which was first proposed by Weiss (2001). This index can be used to identify slope positions such as ridges and upper slopes. This approach has been used by Halls et al. (2018) for automated dune extraction from a DEM. However, when using a TPI-based approach, elevation becomes important because ridges and upper slopes can also be located at lower elevations, including on features such as beach berms. One possible workaround could be using an elevation threshold based on extreme storm water levels to remove low-lying ridges and upper slopes that were identified as dune based on the TPI extraction alone. The rationale here is that frequent impacts from storm water levels would prevent dunes from forming at lower elevations (Sallenger, 2000). Similar to intertidal areas, the vertical uncertainty

in DEMs for dune habitats could be impacted by vegetation, but slope could also be a factor (Su & Bork, 2006). Thus, Monte Carlo analyses could be used to develop probabilistic outputs for the probability of a pixel being above an extreme storm water level. While the techniques discussed so far have been focused on two-dimensional mapping of dunes, researchers are also interested in understanding one-dimensional (i.e., transect-based) geomorphic characteristics of beach-dune systems (Stockdon et al., 2012) and moving beyond dune delineation to categorizing dune topographic state space (Monge & Stallins, 2016).

3.1.4. Aim

In addition to providing a review of barrier island habitat mapping efforts, I aimed to use a case study to outline a GEOBIA barrier island habitat mapping framework (Figure 3.1) that includes advances in dune delineation and integrates the treatment of elevation uncertainty for the extraction of elevation-dependent habitats. The framework builds on the GEOBIA approach outlined by Brownett and Mills (2017) and includes the following advancements: (1) use of relative elevation for automated dune delineation approaches (Halls et al., 2018; Wernette et al., 2016); (2) use of a Monte Carlo approach for addressing vertical uncertainty to develop a dune elevation threshold based on extreme storm water levels; and (3) treatment of vertical uncertainty for delineating intertidal and supratidal habitats.

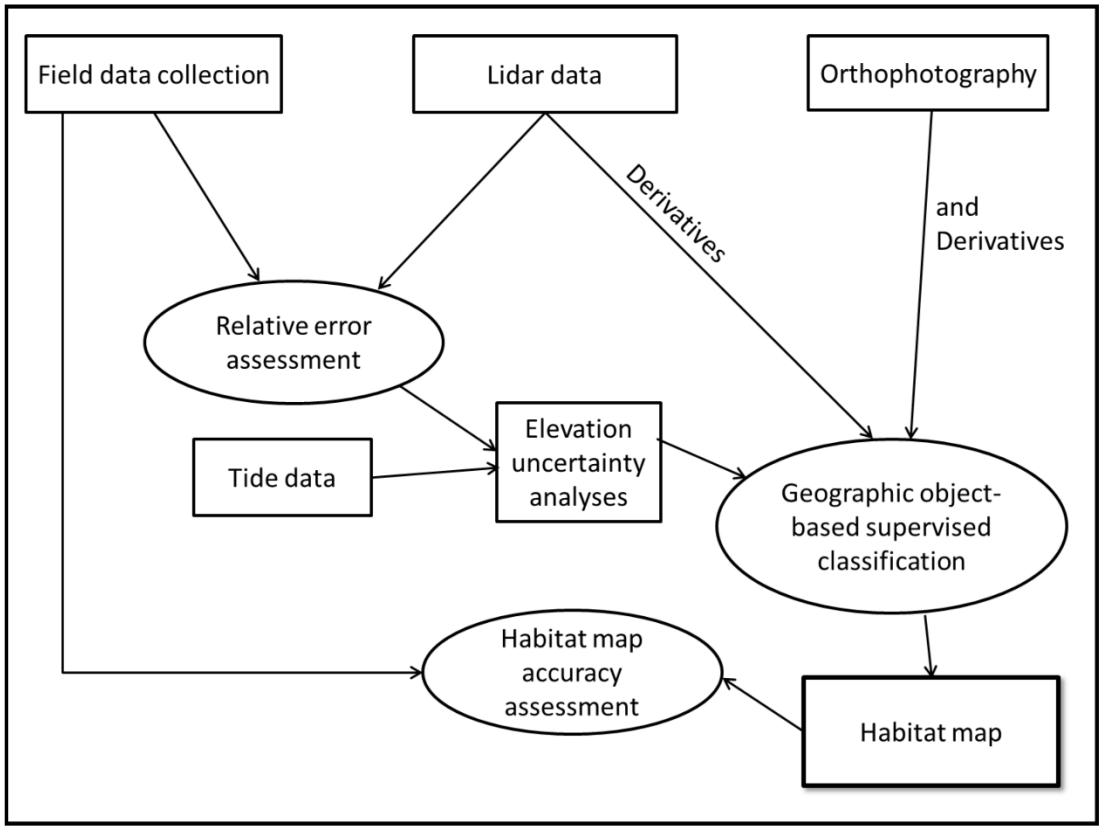

Figure 3.1. An overview of the development of the barrier island habitat map for Dauphin Island, Alabama, 2015.

3.2. Methodology

3.2.1. Study Area and Data

Dauphin Island, Alabama, USA is a part of a 105 km-wide barrier island chain that is backed by the shallow (<4-m deep) Mississippi Sound and is located along the north central Gulf of Mexico Coast of the USA (Otvos & Carter, 2008) (Figure 3.2). As of December 2015, the island had a length of about 25 km, from about 88.34° W to 88.07° W and, at its widest point, the island extended from about 30.28° N to 30.23° N and had a subaerial area of about 13.60 km^2 (Guy, 2015). The island is a microtidal environment with diurnal tides that have a tidal range of about 0.36 m from mean low water tide to mean high water tide based on observations from the NOAA tide gauge (station ID:

8735180) on the island during the most recent North American Tidal Datum Epoch (NTDE; 1983−2001).

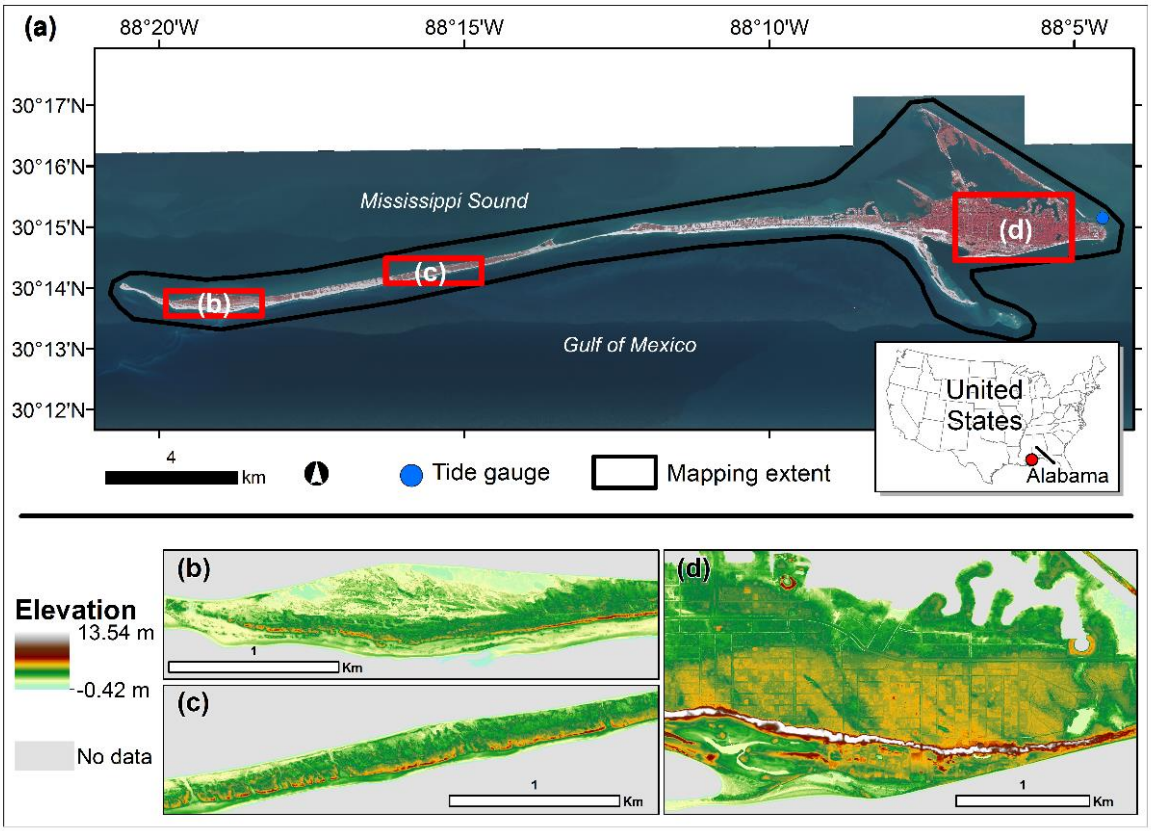

Figure 3.2. Study area, location of National Oceanic and Atmospheric Administration's tide gauge, and lidar data for the barrier island habitat mapping effort on Dauphin Island, AL, 2015. (a) Basemap source data is 0.3-m color-infrared orthophotography acquired in 2015 by Digital Aerial Solutions, LLC (DAS; Riverview, FL, USA) and the U.S. Geological Survey (USGS). (b−d) 1-m lidar bare-earth digital elevation model acquired in January 2015 by DAS and the USGS.

As outlined for previous studies, barrier island habitat monitoring efforts require detailed source data for map production. I used field data, tide data, high-resolution orthophotography, and lidar data for mapping habitats on Dauphin Island (Figure 3.1). Habitat type and elevation data were collected during two and a half weeks in November and December of 2015 by using cluster sampling (i.e., relatively dense sampling in a limited number of targeted areas) along 67 different transects located

across seven different sites on the eastern portion of Dauphin Island. Site selection was driven predominantly by accessibility. The transects targeted 10 general habitat types including: (1) beach, (2) dune-bare; (3) dune-herbaceous; (4) dune-wooded; (5) forested; (6) intertidal flat; (7) intertidal marsh; (8) meadow; (9) scrub/shrub; and (10) unvegetated barrier flat (Appendix A). Transect locations were randomly selected within homogenous areas of habitats per site based on a generalized map I developed from heads-up digitizing of 1-m color-infrared orthophotography acquired in 2013 by the U.S. National Agriculture Imagery Program. For each transect, I collected data for three points along the transect and for a set of eight points radiating from the center point at a distance of about 25 m at intervals of 45-degree angles. I collected the center transect point using a high-precision real-time kinematic (RTK) global positioning system (GPS) connected to a Global Navigation Satellite System (GNSS; Trimble R10 and TSC3, Trimble, Sunnyvale, CA, USA), coupled with the continuously operating reference station (CORS) network for Mississippi and Alabama (University of Southern Mississippi's CORS network or the Alabama Department of Transportation's CORS). I used a laser rangefinder (Laser Technology, Inc., 360 R, Centennial, CO, USA) to efficiently collect additional data for transect ends and points radiating off the transect center. Habitats were identified within a 1-m quadrat for transect locations and radial points. In total, data were collected at 749 points. SigmaPlot 12.5 (Systat Software, Inc., San Jose, CA, USA) was used for all nonspatial statistical analyses in this study, unless otherwise noted. The distribution of precision estimates for all the RTK GPS observations was right-skewed (i.e., skewness = 1.09) with a median root mean square error (RMSE) of ±0.04 m. All geospatial data for this study were native to, or otherwise

projected to, the Universal Transverse Mercator Zone 16 North projected coordinate system with the North American Datum of 1983. For more information on this field data collection, see Enwright et al. (2017).

Tide data were obtained from the NOAA tide gauge on the eastern end of Dauphin Island (Figure 3.2). I used these data to understand the relationship between the North American Vertical Datum of 1988 (NAVD88), mean sea level (MSL), and spring tide levels. Intertidal wetlands are situated above the extreme low water spring and below the extreme high water spring (EHWS) tides (Cowardin et al., 1979). I defined EHWS as the highest astronomical tide predicted for the Dauphin Island tide gauge (0.45 m relative to MSL), which is the highest predicted water level under astronomical conditions alone during the most recent NTDE. As a wave-dominated barrier island (McBride et al., 2013), storms play a large role in the regulation of barrier island morphology and habitats on Dauphin Island (Morton, 2008). Thus, I used the NOAA's Extreme Water Analyses for Dauphin Island based on observations between 1966 and 2010 (Zervas, 2013) to identify an elevation associated with extreme water levels. Specifically, I used the extreme water level with a 10-percent annual exceedance probability updated for 2016 (1.13 m relative to MSL) to account for the sea-level rise trend observed at the Dauphin Island tide gauge (NOAA, 2013).

Similar to numerous other barrier island habitat mapping efforts, I utilized both high-resolution orthophotography and lidar data. I used 0.3-m color-infrared aerial orthophotography acquired on December 4, 2015 by Digital Aerial Solutions, LLC (DAS; Riverview, FL, USA) and the USGS. The orthophotography was collected with a Leica ADS100 digital camera (Wetzlar, Germany) when water levels were near the MSL. I

used a 1-m bare-earth DEM from January 2015 produced by DAS. The source data was aerial topographic lidar data acquired with the Leica ALS70 and ALS80 sensors. These data were collected with a nominal pulse density of about 6 points per m^2. I used first returns from the lidar point cloud to create 1-m and 5-m digital surface models (DSMs) by using the maximum bin algorithm (i.e., assigning the DSM cell to be equal to the maximum first return in the cell). I used the information from the NOAA tide gauge to transform the vertical datum of the 1-m DEM from the NAVD88 to MSL.

3.2.2. Addressing Uncertainty

Monte Carlo simulations were used to propagate error and determine the probability that the elevation of a given DEM cell is above or below a specific elevation threshold for a set of iterations. These analyses were used to determine the probability of a pixel being intertidal and the probability of a pixel being above the elevation during extreme water levels associated with storms. Error propagation followed an approach similar to that of Cooper and Chen (2013), with the addition of enhancements such as using the 95th percentile error instead of the RMSE due to vegetated cover (American Society for Photogrammetry and Remote Sensing, 2015) along with the use of a neighborhood spatial autocorrelation filter and bias constraint outlined by Wechsler and Kroll (2006). I used a relative error assessment to determine the error and bias for the DEM for dune habitat. This assessment was conducted using field data collected on dunes below 3.00 m relative to MSL. This elevation cutoff was selected because higher dunes are both well above the extreme storm water threshold and also may have higher uncertainty due to issues with horizontal displacement along steeper slopes (Su & Bork, 2006). The observations (n = 29) had a median elevation of 1.44 m (relative to MSL)

and an interquartile range of 1.54 m. These data were left-skewed (skewness = –2.58) with a positive bias (i.e., DEM was higher than RTK GPS elevation) for 55% of the observations and a 95th percentile error of 0.16 m. The Monte Carlo analyses included a total of 1,000 iterations. Probabilistic outputs were developed using binary raster for each pixel with regard to whether elevation was greater than or equal to the 10-percent extreme storm water level. For determining the probability of a pixel being intertidal, my approach was similar to Enwright et al. (2018b).

3.2.3. Barrier Island Mapping Framework

I developed a custom 17-class habitat classification scheme through the review of barrier island habitat mapping efforts (Figure 3.3; Appendix A). Similar to Brownett and Mills (2017), I used a semi-automated GEOBIA approach to classify the habitats. A few preprocessing steps included conducting a principal component analysis (PCA) of the four-band orthophotography and calculating a normalized difference vegetation index (NDVI). I used multiresolution segmentation (Trimble, 2016) in Trimble eCognition Developer 9.2 (Munich, Germany) to segment the imagery into objects based on spatial and spectral similarities with regard to derivatives of orthophotography including the first two PCA components, NDVI, and elevation. I determined the optimal segmentation parameters (i.e., bands, weights, and scale of objects) using a trial-and-error approach similar to Myint et al. (2011).

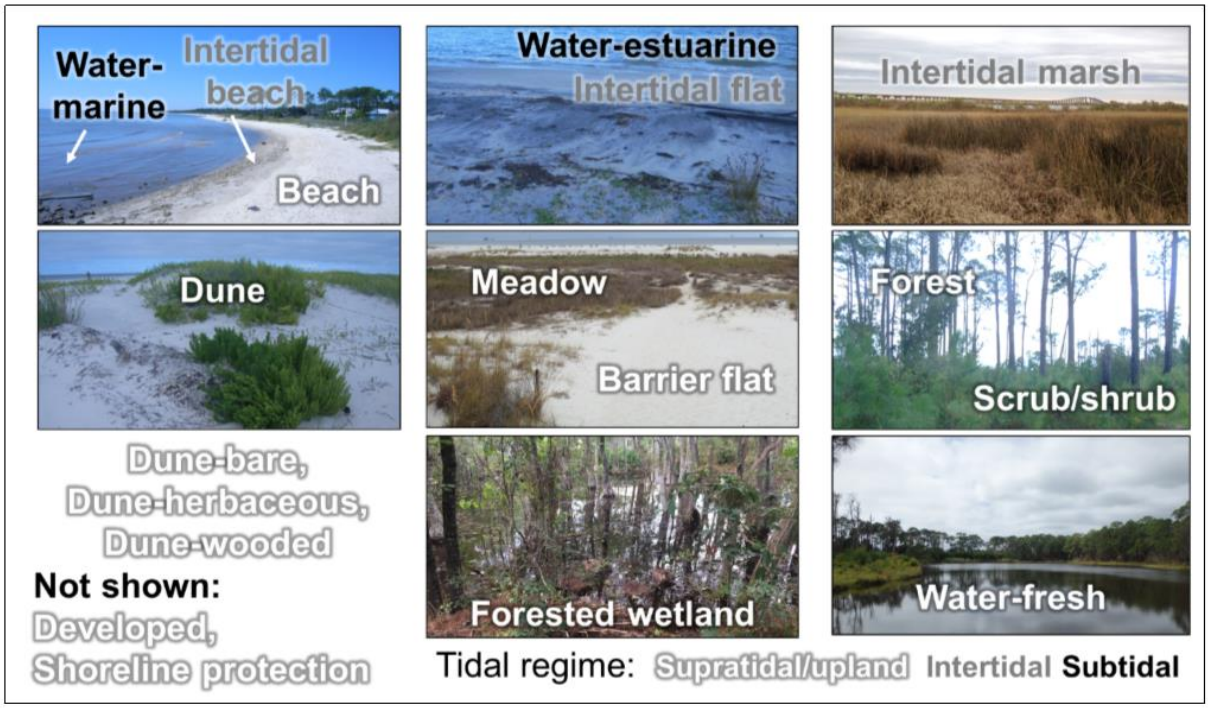

Figure 3.3. Photos of the habitat classes (*n* = 17) for the barrier island habitat mapping effort on Dauphin Island, AL, 2015. The classification scheme delineates habitats by tidal regime (see legend in lower right). The developed and shoreline protection are not depicted. For habitat definitions, see Appendix A.

I used a hierarchical approach to classify the image segments based on object-level statistics (e.g., mean, SD, and minimum pixel value). First, I classified the image segments as either land or water using thresholds for the NDVI and the near infrared band and manual editing. Next, I used a similar approach to classify land segments into vegetated and unvegetated categories. I used general rule-based thresholds to further subdivide vegetated and unvegetated areas into detailed habitats according to habitat definitions (Appendix A). For a given step, threshold-based rules were developed to classify habitats while minimizing commission and omission errors as gauged by visual inspection of results (Figure 3.4). For example, a generalized rule to identify objects in the meadow class would include rules to target “non-tidal vegetated areas that lack relative topography and woody vegetation.” After applying general decision rules for

each habitat in a step-wise fashion, photointerpretation was used to refine habitats through manual editing including editing segment boundaries as needed (Figure 3.4). For more information on general thresholds used in the mapping process for most of the classes, see Appendix B. It is important to note that these thresholds are often specific to source data and can vary based on many factors such site vegetation community, time of year, image quality, and image bit-depth. Thresholds can also vary from image to image and sometimes within images due to color balancing issues.

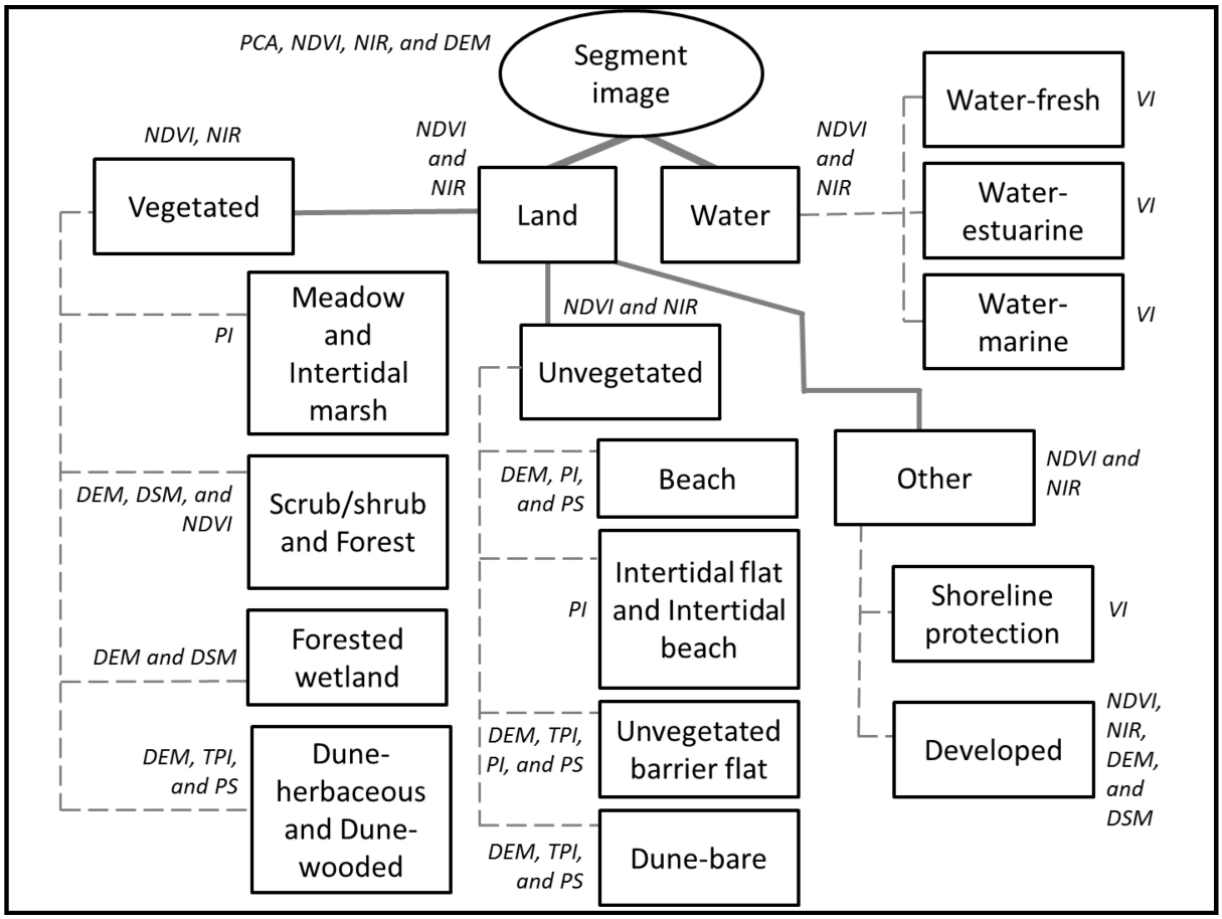

Figure 3.4. An overview of the mapping process used for the barrier island habitat map for Dauphin Island, AL, 2015. The italic text indicates data or techniques used for classifying each habitat. DEM: Digital elevation model; DSM: Digital surface model; NDVI: Normalized difference vegetation index; NIR: Near infrared band; PCA: Principal component analysis; PI: Probability of being intertidal; PS: Probability of being above water levels during extreme storms; TPI: Topographic position index; and VI: Photointerpretation. VI was used for all mapping steps and classes.

Several elevation derivatives were developed to assist with mapping various classes, including woody vegetation (i.e., scrub/shrub and forested habitats), developed areas, intertidal habitats, and the dune classes. First, the relative difference between the DSMs and the DEM provided information on the difference in the heights of objects such as tree canopy or buildings and was used to map the scrub/shrub, forested, and developed classes. Second, the probabilistic outputs with regard to intertidal areas from Enwright et al. (2018b) were used as a guide for mapping intertidal habitats (i.e., intertidal beach, intertidal marsh, and intertidal flat). Image objects were classified as intertidal if the object intersected an area considered likely to be intertidal based on pixel elevations. These areas were refined, as needed, using visual inspection of orthophotography and lidar data. This approach was used for identifying the intertidal/supratidal boundary, whereas the intertidal/subtidal boundary was identified via photointerpretation of the imagery due to the lack of bathymetric information. Lastly, I used the TPI, which was developed by comparing the elevation for a pixel with the mean for the neighborhood (De Reu et al., 2013; Weiss, 2001), to identify slope position. First, I excluded pixels from the DEM with an elevation less than zero and ran a low-pass filter on the DEM to smooth random noise. Then, I estimated the TPI for a 30-m circular neighborhood. While a detailed dune geomorphology study may be interested in use of multiple scales (Wernette et al., 2016), I opted for a single scale as a multi-scaled approach may not be feasible for large-scale habitat mapping efforts (e.g., maps for one or a few islands). I used visual inspection and confirmed 30 m was a reasonable neighborhood size. Halls et al. (2018) used a similar scale (i.e., 40 m) for dune delineation. Dunes were defined as pixels with TPI values that were indicative of

ridges or upper slopes (i.e., values greater than one-half SD from the mean) (De Reu et al., 2013; Weiss, 2001). Dunes were further refined by: (1) excluding ridges and upper slopes with a probability of less than 0.5 for being greater than or equal to extreme water levels associated with storms; (2) excluding any areas less than 40 m^2; and (3) revising ridges and upper slopes based on visual inspection of orthophotography and lidar data. This last step included manually removing areas that were not dunes via visual inspection and geomorphic setting (e.g., small ridges behind the dune backslope on eastern end of Dauphin Island in developed areas), filling in holes in dunes based on TPI scale limitations (i.e., would be considered dune if a larger scale was used), and adding in well-defined dunes that were missed by using a single scale. The reduction in the areal coverage of ridges and upper slopes was quantified for these steps.

Several post-processing steps were conducted to refine the barrier island habitat map with an emphasis on noise reduction. First, I converted the image objects to a 1-m raster. The rationale for converting the image objects to a raster was to efficiently remove sliver polygons created via manual editing through a majority filter for a 3-by-3 pixel neighborhood in the raster data structure. To further reduce noise not removed by the major filter and standardize the identification of small features, I applied a 40 m^2 minimum mapping unit (MMU). I selected this MMU as a reasonable balance between noise reduction and loss of detail evaluated through visual inspection. This mapping unit is well below the smallest MMU (2,500 m^2) suggested by the USGS and the U.S. National Park Service for mapping vegetation in U.S. National Parks (Lea & Curtis, 2010).

Lastly, I conducted an accuracy assessment using the previously discussed field data. The accuracy assessment generally adhered to guidelines by Congalton and Green (2009) regarding sample design and procedures. Instead of assessing map accuracy with points, I buffered field data to have area equal to the size of the minimum mapping unit. For the accuracy assessment, the map data label was assigned to be the majority class that fell within the buffered area and the reference data label (Appendix A) came from the field data collection and, in some instances, photointerpretation. In order to have at least 30 accuracy points per class, supplemental data were added for the following habitat classes: (1) beach (n = 1); (2) developed (n = 30); (3) dune-bare (n = 9); (4) forested wetland (n = 30); (5) intertidal beach (n = 25); (6) shoreline protection (n = 30); (7) water-estuarine (n = 30); (8) water-fresh (n = 30); (9) water-marine (n = 30). These supplemental points were attributed by using visual inspection of orthophotography and lidar data. The accuracy assessment included overall accuracy, Kappa statistic (Cohen, 1960), and producer's and user's accuracy estimates for each class.

3.3. Results

Like Halls et al. (2018), I found that the TPI proved to be an effective approach for delineating dunes. I found the application of an elevation threshold and manual refinement enhanced TPI-based dune extraction. The refinement of the ridges and upper slopes by using the probabilistic output with regard to storm water levels led to an 18.1% decrease in areal coverage (50 hectares (ha); Figure 3.5). While the removal of small areas below the minimum mapping unit reduced noise, the step only resulted in a decrease in areal coverage of ridges and upper slopes of about 2 ha. Manual editing of

the ridges and upper slopes layer resulted in the largest reduction in areal coverage (84 ha; Figure 3.5). Collectively, the refinements led to a 49.1% decrease in the areal coverage of dunes (Figure 3.5).

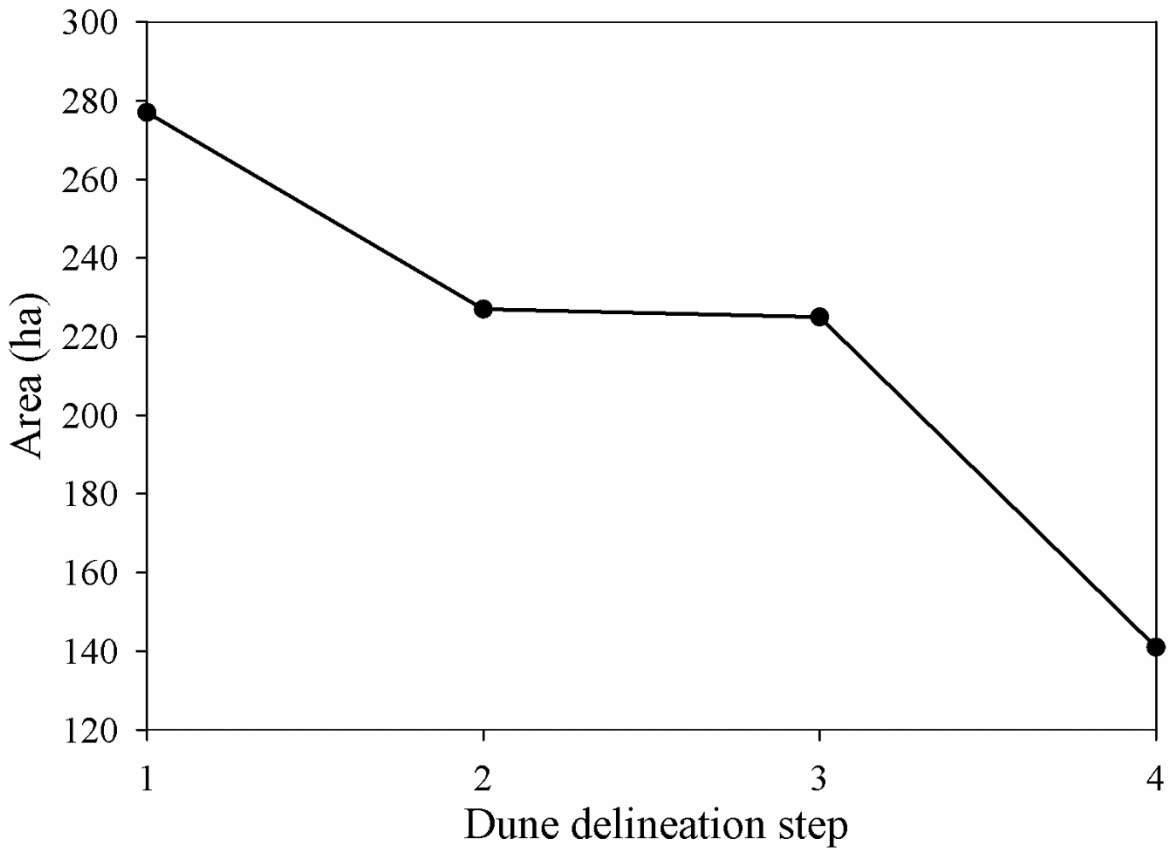

Figure 3.5. Areal coverage in hectares (ha) for ridges and upper slopes for each step in the TPI-based dune delineation process for the habitat mapping effort for Dauphin Island, AL, 2015. The numbers along the x-axis represent the steps in the dune delineation process. 1: Initial ridges and upper slope extraction; 2: Exclusion of ridges and upper slopes below extreme storm water levels; 3: Exclusion of ridges and upper slopes smaller than the minimum mapping unit; and 4: Manual refinement of ridges and upper slopes using visual inspection.

The habitat map produced for Dauphin Island is shown in Figures 3.6 and 3.7. Table 3.2 shows areal coverage of each habitat by tidal zone. For nonwater habitats, much of the island was within the supratidal/upland elevation range (85.5%; Table 3.2). Of the nonwater, nondeveloped, subaerial habitats, the most abundant habitats were:

(1) meadow (360 ha, 29.2%); (2) forest (292 ha; 23.7%); (3) all dune classes, collectively (141 ha, 11.4%); (4) intertidal marsh (122 ha, 9.9%); (5) unvegetated barrier flat (105 ha, 8.5%); and (6) all beach classes, collectively (103 ha, 8.4%).

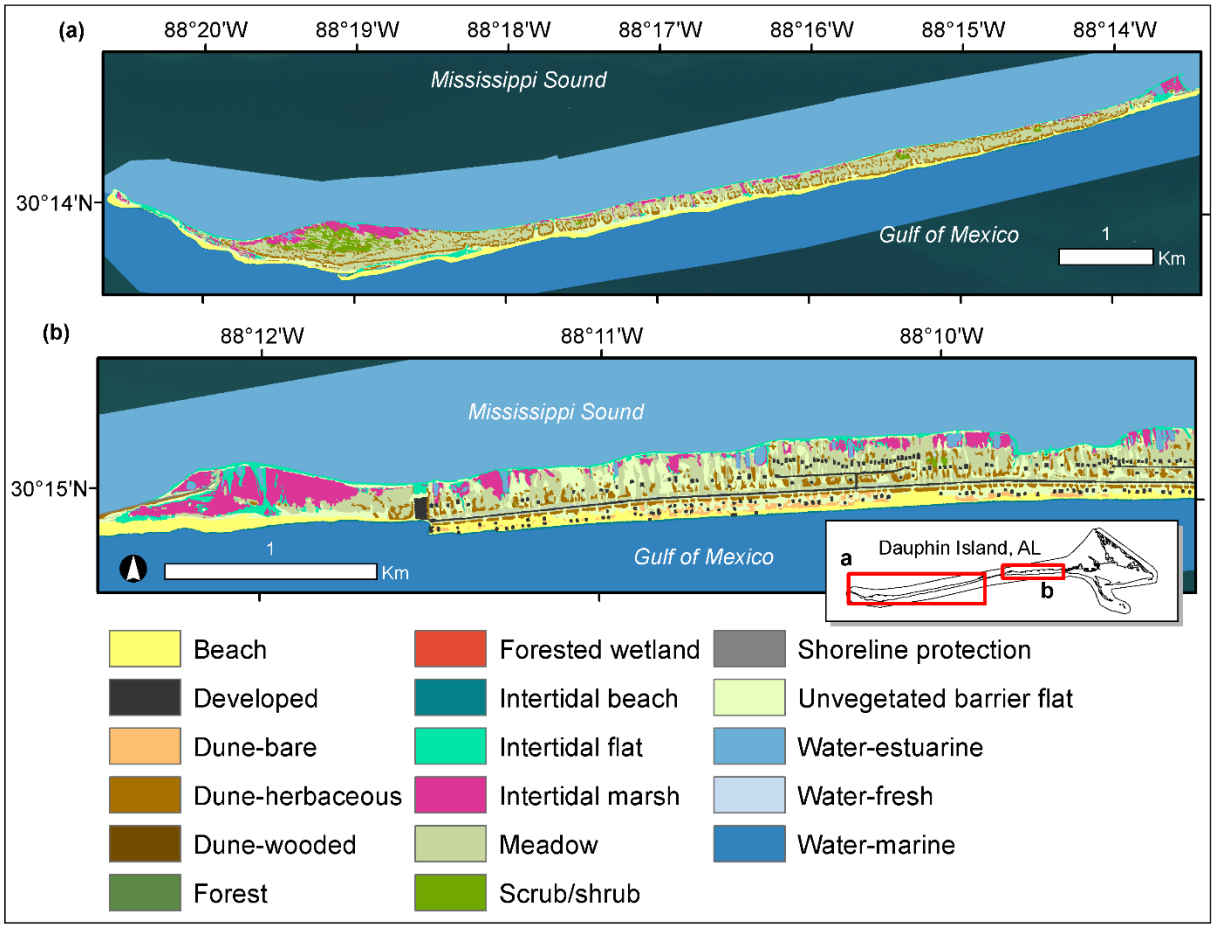

Figure 3.6. Habitat map for the western two-thirds of Dauphin Island, AL, 2015.

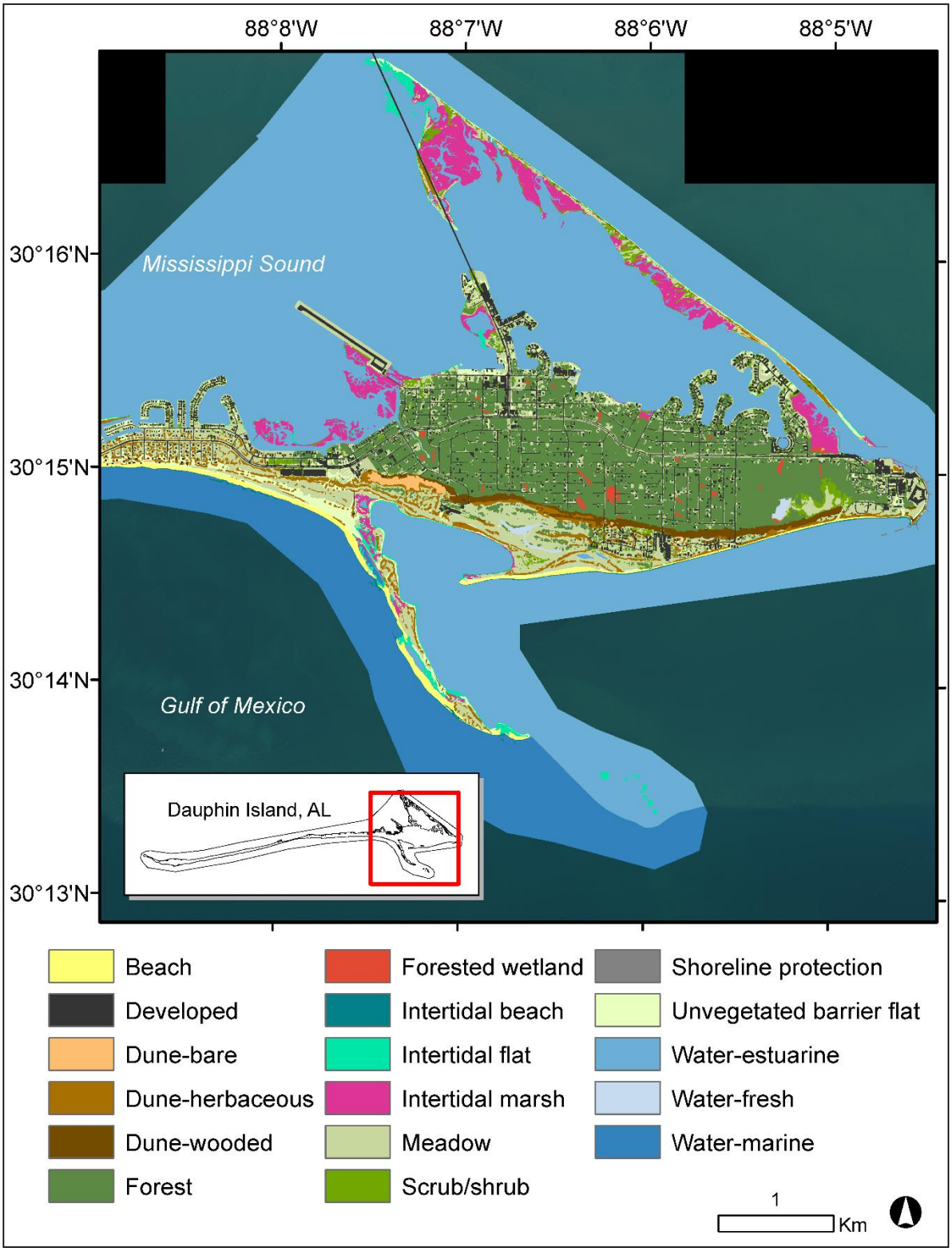

Figure 3.7. Habitat map for the eastern one-third of Dauphin Island, AL, 2015.

Table 3.2. Areal coverage for each habitat class summarized by tidal regime for the barrier island habitat map for Dauphin Island, AL, 2015.

Tidal regime	Habitat class	Areal coverage (ha)
Subtidal	Water-marine	1,335
	Water-estuarine	2,849
Subtidal total		4,184
Intertidal	Intertidal beach	19
	Intertidal flat	55
	Intertidal marsh	122
Intertidal total		196
Supratidal/upland	Beach	84
	Dune-bare	10
	Dune-herbaceous	109
	Dune-wooded	22
	Meadow	360
	Unvegetated barrier flat	105
	Scrub/shrub	47
	Forest	292
	Forested wetland	6
	Water-fresh	5
	Developed	121
	Shoreline protection	3
Supratidal/upland total		1,164
Total		5,544

The map had an overall accuracy of 79.2% and a Kappa statistic of 0.77 (Table 3.3). Excluding water classes, shoreline protection and developed, the classes with the highest user's accuracies were: (1) forest (97.3%); (2) dune-bare (90.3%); (3) intertidal beach (86.7%); (4) forested wetland (85.7%); and (5) beach (84.4%). The dune-wooded and meadow class had the lowest user's accuracy at 65.1% and 65.7%, respectively. For the meadow class, most of the confusion was from misclassification as dune-herbaceous areas mapped as meadow. The classes with the highest producer's accuracies were: (1) intertidal beach (95.0%); (2) intertidal marsh (93.8%); (3) dune-bare (93.3%); (4) beach (93.3%); and (5) forested wetland (86.7%). The dune-herbaceous class had the lowest producer's accuracy of 46.2% with majority of the confusion coming from dune-herbaceous areas mapped as meadow. Dunes were

mapped at a higher accuracy when lumped into a single dune class. Collectively, the dune classes had a mean user's accuracy of 78.4% and a producer's accuracy of 72.4%.

3.4. Discussion

Barrier island habitat maps provide researchers and natural resource managers with critical information needed to understand changes to these dynamic ecosystems. In this study, I reviewed barrier island habitat mapping literature to highlight habitat class types, mapping units, source data, and mapping approaches commonly used by researchers. As is the case for remote sensing applications for other environments, researchers utilize many approaches for barrier island habitat mapping. Having so many classification schemes and methodologies can create semantic challenges when a researcher is assessing whether habitat maps from different dates or geographic extents can be conflated for regional or time series analyses (Feranec et al., 2014). Gibson and Looney (1992) highlight this issue for barrier island mapping efforts by crosswalking habitats from four different barrier island mapping efforts. Similarly, Wernette et al. (2016, 2018) show how several commonly used dune delineation techniques can yield different results using the same data. To help reduce these issues, I developed a GEOBIA approach for mapping general morphology-based barrier island habitats that uses landscape position information and addresses elevation uncertainty for extracting elevation-dependent habitats.

Table 3.3. Confusion matrix for the 2015 barrier island habitat map for Dauphin Island, AL. B: Beach; CT: Column total; DB: Dune-bare; DH: Dune-herbaceous; DV: Developed; DW: Dune-wooded; F: Forest; FW: Forested wetland; IB: Intertidal beach; IF: Intertidal flat; IM: Intertidal marsh; M: Meadow; OA: Overall accuracy; PA: Producer's accuracy; RT: Row total; SP: Shoreline protection; SS: Scrub/shrub; UA: User's accuracy; UBF: Unvegetated barrier flat; WE: Water-estuarine; WF: Water-fresh; and WM: Water-marine.

		Reference data																		
	Class	DB	DH	DW	M	UBF	SS	F	FW	IB	B	IF	IM	SP	DV	WE	WF	WM	RT	UA (%)
Map data	DB	**28**	2	1	0	0	0	0	0	0	0	0	0	0	0	0	0	0	31	90.3
	DH	1	**36**	4	4	1	0	0	0	0	0	0	0	0	0	0	0	0	46	78.3
	DW	1	4	**28**	2	0	1	7	0	0	0	0	0	0	0	0	0	0	43	66.7
	M	0	32	2	**113**	1	16	3	0	0	0	1	4	0	0	0	0	0	172	65.7
	UBF	0	3	0	4	**24**	1	0	0	0	0	4	0	0	0	0	0	0	36	73.9
	SS	0	0	0	8	0	**47**	2	0	0	0	0	2	0	0	0	0	0	59	79.7
	F	0	0	1	1	0	0	**73**	0	0	0	0	0	0	0	0	0	0	75	97.3
	FW	0	0	0	0	0	0	5	**30**	0	0	0	0	0	0	0	0	0	35	85.7
	IB	0	0	0	0	0	0	0	0	**26**	1	3	0	0	0	0	0	0	30	86.7
	B	0	1	0	0	0	0	0	0	3	**38**	3	0	0	0	0	0	0	45	84.4
	IF	0	0	0	3	4	0	0	0	0	1	**47**	2	0	0	4	0	0	61	77.0
	IM	0	0	0	36	0	4	2	0	0	0	1	**136**	0	0	1	0	0	180	76.0
	SP	0	0	0	2	0	0	0	0	0	0	0	0	**30**	0	3	0	0	35	85.7
	DV	0	0	0	1	0	0	0	0	0	0	0	0	0	**30**	0	0	0	31	96.8
	WE	0	0	0	0	0	0	0	0	0	0	7	0	0	0	**22**	0	0	29	75.9
	WF	0	0	0	0	0	0	0	0	0	0	0	0	0	0	0	**30**	0	30	100.0
	WM	0	0	0	0	0	0	0	0	1	0	0	1	0	0	0	0	**30**	32	93.8
	CT	30	78	36	174	30	69	92	30	30	40	66	145	30	30	30	30	30	**970**	
	PA (%)	93.3	46.2	77.8	64.9	80.0	68.1	79.4	86.7	95.0	93.3	71.2	93.8	100.0	100.0	73.3	100.0	100.0		

OA (%): 79.2; Kappa: 0.77

As higher-resolution remote sensing data becomes increasingly available in the future, GEOBIA should become a more and more popular approach for detailed habitat mapping (Ma et al., 2017). The step-wise GEOBIA approach outlined in this study relies heavily on the use of lidar data for understanding the geomorphologic settings on a barrier island (Leatherman, 1979; Zinnert et al., 2017). One challenge with existing lidar data can be limited temporal and spatial coverage. In some areas, lidar is only collected every several years. Some lidar monitoring programs, such as those that collect lidar data to monitor shoreline change, only collect lidar data for a narrow band along shorelines in order to monitor nearshore change and often do not collect data for back-barrier habitats. I expect that advancements in sensor technology, such as single photon and Geiger-mode lidar sensors (Stoker et al., 2016) and unmanned aerial system (UAS) lidar data collection (Jaakkola et al., 2010; Lin et al., 2011), should lead to a greater frequency and coverage of high-quality elevation data for use by scientists and natural resource managers. Researchers are already using digital surface models created via structure-from-motion for geomorphic feature extraction and habitat classification for coastal beach-dune systems (Sturdivant et al., 2017). The techniques outlined in this study provide insights for researchers on how to best leverage elevation data to enhance mapping of elevation-dependent habitats like dunes and intertidal areas and increase the efficiency and repeatability of barrier island habitat monitoring efforts.

Dune delineation from remote sensing data can be challenging and is often ambiguous. Both Halls et al. (2018) and Wernette et al. (2016) have shown the utility of using relative topography from DEMs for automated dune extraction. While my research

confirmed the utility of relative topography information for dune extraction, I also found the need to incorporate elevation thresholds and allow for refinement via visual interpretation. As a relative measure, the TPI considers relative topography independent of elevation relative to locally relevant datums. Therefore, an elevation threshold can be important for removing high beach berms, which could be considered a ridge or upper slope when based solely on a TPI value, from the results of an automated dune extraction routine. Storms can shape dune morphology (Sallenger, 2000), thus extreme water levels associated with storms can serve as a reasonable dune elevation threshold. Researchers recommend that vertical uncertainty be considered for coastal studies using lidar data for the automated delineation of elevation-dependent habitats (Buffington et al., 2016; Enwright et al., 2018b; Kidwell et al., 2017; Liu et al., 2007). The vertical uncertainty of lidar in dunes can be impacted by both vegetation cover and slope (Su & Bork, 2006). Here, I applied a similar approach as Enwright et al. (2018b) to use Monte Carlo simulations to determine the probability of a pixel being above an extreme water level associated with storms from field data and tide data for automated dune extraction. While the application of the elevation threshold had a smaller relative impact for the entire island compared to visual inspection (Figure 3.5), it is expected that the relative reduction in areal coverage would likely be greater if the assessment were limited to the beach-dune area instead of the entire island. The use of relative topography provides an enhancement to existing techniques for dune delineation, yet the approach also warrants manual refinement through visual inspection when used for broad habitat mapping. For instance, some areas on a dune backslope (i.e., meadow and unvegetated barrier flat) or behind dunes can have relative relief and be higher than

an extreme storm tide, such as areas that exhibit disturbance-resisting morphology (Zinnert et al., 2017), yet perhaps not all areas should be considered dune habitat particularly in areas with anthropogenic impacts (i.e., spoil banks). Finally, temporal gaps between lidar and imagery acquisition along rapidly changing dynamic coasts can cause issues for habitat mapping, which typically uses the imagery as the primary source data and elevation data for supplemental information related to landscape position.

The level of uncertainty from data collected with conventional aerial topographic lidar systems has been found to be as high as 60 cm in densely vegetated emergent wetlands throughout the U.S. (Buffington et al., 2016; Enwright et al., 2018b; Medeiros et al., 2015). Thus, the consideration of vertical uncertainty is critical for producing accurate areal coverage estimates for intertidal and supratidal habitats from DEMs and tide data (Buffington et al., 2016; Campbell & Wang, 2018; Enwright et al., 2018b; Kidwell et al., 2017). Enwright et al. (2018b) includes a detailed overview of the impacts of not incorporating uncertainty into intertidal area identification efforts on Dauphin Island. I applied the methodology outlined in Enwright et al. (2018b) to develop probabilistic outputs that considered vertical uncertainty for use as a guide for delineating intertidal and supratidal habitats. The approaches for handling vertical uncertainty for both dunes and intertidal areas can be extended into other study areas although the vertical uncertainty may depend on factors such as lidar technology, lidar point spacing, vegetation community, vegetation density, and slope. In this study, field data were used to determine the error and bias of the lidar dataset; however, if field data cannot be acquired, then I recommend using the lidar metadata for the Monte

Carlo analysis similar to Liu et al. (2007) and Enwright et al. (2018b) instead of leaving vertical uncertainty untreated.

The results from the accuracy assessment highlight some minor challenges associated with mapping barrier island habitats with regard to data processing and semantics. Most of the confusion was associated with dunes, specifically, for the dune-herbaceous class. To a large extent, these areas were determined to be poorly defined hummocky dunes in the field, yet they were classified as meadow or unvegetated barrier flat per the classification scheme. This error is largely caused by the difficulty in identifying small hummocky dunes that often lack the defined relative topography needed to easily delineate with remote sensing data. However, if hummocky dunes are of interest to a researcher, then it may be possible to map these areas using some combination of texture metrics, a finer-scaled TPI, and visual inspection. For example, Halls et al. (2018) extracted hummock features from a DEM using geomorphology information like mean elevation, fine-scaled TPI, and shape indices. While this process shows promise, the hummock class was found to be difficult to classify with an omission error of just over 50%. The FRAGSTAT metrics used by Monge and Stallins (2016) to characterize state space may also prove to be useful for hummock dune extraction. These results also highlighted confusion for the intertidal marsh and meadow and intertidal flat classes. This was likely due to the difficulty of determining intertidal areas on a single site visit when water levels were observed at a narrow window within the tidal range. Also, as previously mentioned, the temporal gaps between lidar data orthophotography acquisition can introduce challenges when mapping intertidal beach and intertidal flat along dynamic shorelines. Due to the dynamic nature of these

habitats, researchers should consider using both a deterministic and fuzzy accuracy assessment (Congalton & Green, 2009; Woodcock & Gopal, 2000). Still, the framework outlined in this study provides a roadmap for efficiently processing remote sensing data while also making progress toward tackling semantic challenges for barrier island habitat maps using landscape position information and the treatment of vertical uncertainty. The framework presented here can be modified by increasing the detail of the habitat classes, adding new habitat classes (e.g., mangrove, freshwater wetland, interdunal swale, and/or hummock), and/or dropping certain habitat classes, or if a researcher opts to use a traditional pixel-based approach. If any of these modifications are needed to suit the objectives of a researcher, the basic concepts outlined in this framework regarding landscape position and elevation uncertainty would still be applicable and provide value to the mapping effort. For example, this mapping approach can be extended beyond barrier islands to beaches, dunes, and marshes found on mainland areas as well as areas that include mangrove forests (Enwright et al., 2018a). While this framework relies heavily on high-resolution orthophotography, it is important that researchers studying barrier islands continue to utilize moderate-resolution imagery for multi-temporal analyses to study dynamic changes (Zinnert et al., 2011, 2016) that may not be captured in periodic mapping from high-resolution orthophotography or UAS data collections. The utilization of both approaches, where applicable, will provide natural resource managers with key insights on how these systems are changing over time.

3.5. Conclusion

Due to their dynamic nature, monitoring of barrier islands is critical for advancing understanding of how these ecosystems change over time from gradual processes such as tides and currents to more episodic events like storms. Because of their size and unique geomorphic habitats, barrier island habitat monitoring efforts often require custom habitat map development rather than using readily available, regional land cover datasets. One challenge when mapping geomorphic habitats on barrier islands with remotely sensed data is reducing semantic issues caused by ambiguity in class definitions and variability in delineation techniques. In response, I outlined a GEOBIA approach for mapping general morphology-based barrier island habitats that includes landscape position information and treatment of elevation uncertainty. A few highlights of the approach include advancements in dune delineation and integration of vertical uncertainty into the barrier island habitat mapping process. While DEMs provide valuable information regarding geomorphic setting, the level of uncertainty can be substantial in these data from barrier islands. To address this uncertainty, I used field data, tide data, and Monte Carlo analyses to develop probabilistic outputs based on the elevation relative to extreme storm water levels and extreme spring tides. The dune refinement using extreme storm water levels led to an 18% decrease in areal coverage and combined with manual edits from visual inspection for a 49% reduction in dune area. The Monte Carlo techniques outlined in this study provide a repeatable and more accurate method for automated extraction of elevation-dependent habitats. Collectively, the framework outlined in this study provides a roadmap for efficiently processing remote sensing data while also enhancing the semantics of barrier island habitat maps

through the use of landscape position information and treatment of elevation uncertainty to enhance map comparison through time and map conflation for regional analyses.

CHAPTER 4. MODELING BARRIER ISLAND HABITATS USING LANDSCAPE POSITION INFORMATION

4.1. Introduction

Barrier islands are subaerial expressions consisting of wave-, wind-, and/or tide-deposited sediments (Oertel, 1985). These islands are found along portions of every continent except Antarctica (Stutz & Pilkey, 2011) and provide numerous important ecosystem services, including storm surge reduction, wave attenuation, erosion control to the mainland, habitat for fish and wildlife, carbon sequestration in marshes, water catchment and purification, recreation, and tourism (Barbier et al., 2011; Feagin et al., 2010; Sallenger, 2000). Barrier islands tend to be dynamic due to their location along the estuarine-marine interface. Collectively, these factors make barrier island monitoring a critical need of natural resource managers for coastal management, such as planning for coastal protection and restoration. As a result, natural resource managers often use habitat maps developed by geographers and remote sensing scientists to gain insights into how these islands are changing over time (Campbell et al., 2017; Jeter & Carter 2015; Kindinger et al., 2013; Lucas & Carter 2010; Zinnert et al., 2016). Besides gradual changes caused by constant forces, such as currents and tides, barrier islands face numerous threats including hurricanes, accelerated sea-level rise, oil spills, and anthropogenic impacts (Pilkey & Cooper, 2014). These threats are likely to influence the future of barrier islands in the latter part of the 21st century, especially as climate-related threats to coastal areas are expected to increase in the future (Hansen et al., 2016; Knutson et al., 2010). Thus, to better inform both current and future management decisions, natural resource managers often lean on scientific models that predict what

barrier island systems may look like in the future with regard to morphology (Guiterrez et al., 2015, Passeri et al., 2018) and habitat for fish and wildlife (Foster et al., 2017).

Geomorphology is a critical component of barrier island habitat configuration as certain foundation species (*sensu* Dayton, 1972), such as saltmeadow cordgrass (*Spartina patens* (Aiton) Muhl.), seaoats (*Uniola paniculata* L.), and slash pine (*Pinus elliottii*) tend to thrive in specific topographic settings or disturbance regimes (Zinnert et al., 2017). Geomorphology regulates many abiotic factors that influence the performance of foundation plant species, including wave energy, salinity, inundation frequency, sea spray, Aeolian transport, and nutrient availability (Young et al., 2011). Researchers have established linkages between barrier island habitats and specific landscape position variables, such as distance from shoreline (Young et al., 2011) and elevation (Anderson et al., 2016; Foster et al., 2017; Halls et al., 2018; Young et al., 2011).

Geocomputational models can incorporate landscape position information, including elevation and relative topography, to predict barrier island geomorphic features and habitats. For example, Halls et al. (2018) developed a model that uses landscape position to produce maps of geomorphic features (e.g., intertidal, supratidal, dune, hummock, swale, and overwash) using information extracted from a digital elevation model (DEM) for an area in North Carolina, USA. To predict geomorphic features, their model uses elevation relative to tidal datums, relative topography, shape, and general location information (e.g., proximity). Similarly, Gutierrez et al. (2015) developed a Bayesian network to model barrier island morphologic characteristics, including dune crest height, beach presence-absence, and beach width using

contemporary data, such as a lidar-based DEM and orthophotography for Assateague Island, off the coasts of Maryland and Virginia, USA. Their approach also uses data representing longer-term, larger-scale processes, including long-term shoreline change rates, barrier island width, barrier island elevation, proximity to inlets, and anthropogenic modification. Researchers often use data-driven, machine learning algorithms, such as K-nearest neighbor (KNN; Barandela & Juarez, 2002; Manton et al., 2005), support vector machine (SVM; Guo Kelly, & Graham, 2005; Heumann, 2011; Xu, Dai, Xu, & Lee, 2012,), and random forest (RF; Prasad, Iverson, & Liaw, 2006; Rogan, Franklin, & Roberts, 2002) to develop geocomputational models to make predictions from geospatial data. These algorithms could also be effective tools for determining the relationship between landscape position and barrier island habitats. For example, Foster et al. (2017) developed a naïve Bayes model to predict the overall habitat coverage based on elevation for Cape Canaveral Florida, USA, under alternative sea-level rise scenarios. Despite these productive examples and the demonstrated importance of landscape position, most researchers have not fully leveraged landscape position-habitat linkages to develop predictive models.

Incorporation of elevation uncertainty for extracting elevation-dependent habitats and post-processing model results using expert knowledge of barrier island habitats may enhance machine learning-based habitat prediction for barrier islands. Habitats on barrier islands can be tied to tidal regimes (Enwright et al., in press), which could allow for targeted models to be developed for each tidal regime. Researchers can extract these tidal regimes directly from DEMs by using information regarding locally relevant tidal datums, such as extreme high water spring (EHWS), extreme low water spring

(ELWS), and storm water levels (Enwright et al., 2018b, in press; Halls et al., 2018; McCarthy & Halls, 2014). When using automated extraction of elevation-dependent habitats, researchers are advised to address vertical uncertainty in DEMs (Buffington et al., 2016; Enwright et al., 2018b; Medeiros et al., 2015). This is especially critical for low-relief environments, such as barrier islands, where centimeters can make a difference in the exposure to physically demanding abiotic conditions (e.g., inundation, salt spray, wave energy; Anderson et al., 2016; Young et al., 2011). Enwright et al. (2018b) highlighted the impact of the treatment of vertical uncertainty within intertidal areas. Relative topography can be helpful for extracting dune habitat (Enwright et al., in press; Halls et al., 2018; Wernette et al., 2016), yet elevation relative to storm water levels can also be a factor as dunes can be eroded by high wave runup during storms (Sallenger, 2000). Thus, elevation uncertainty analyses could also be used to evaluate the likelihood of areas depicted by a DEM being above a common extreme storm water level (Enwright et al., in press). Data-driven, machine learning algorithms are powerful tools for teasing out patterns and relationships in data; however, one potential issue is that they require the assumption that the data used to train the model is representative of the phenomena being modeled. Because change can sometimes occur rapidly on a barrier island, post-processing could be used to ensure that spatially explicit habitat predictions match my expectations based on expert theoretical knowledge of the specific barrier island being modeled (e.g., for a high energy barrier island I would not expect marsh to be located on the ocean-facing shoreline; Roland & Douglass, 2005).

Here, I built upon recent barrier island habitat model efforts by Foster et al. (2017) and Halls et al. (2018) to develop a habitat model for Dauphin Island, Alabama,

USA. The model incorporates elevation uncertainty for elevation-dependent habitat extraction and yields spatially explicit predictions of general barrier island habitats based on landscape position information, such as elevation, distance from shoreline, and relative topography (Figure 4.1). For this study, I explored three research questions: (1) how well can machine learning algorithms, such as KNN, SVM, and RF, predict contemporary barrier island habitats from landscape position information; (2) does the use of post-processing routines, such as expert rules based on the theoretical understanding of a barrier island (e.g., marsh should not be located along the high energy shoreline of the island), enhance model accuracy; and (3) how well does this model generalize to predict historical habitats (i.e., hindcast)?

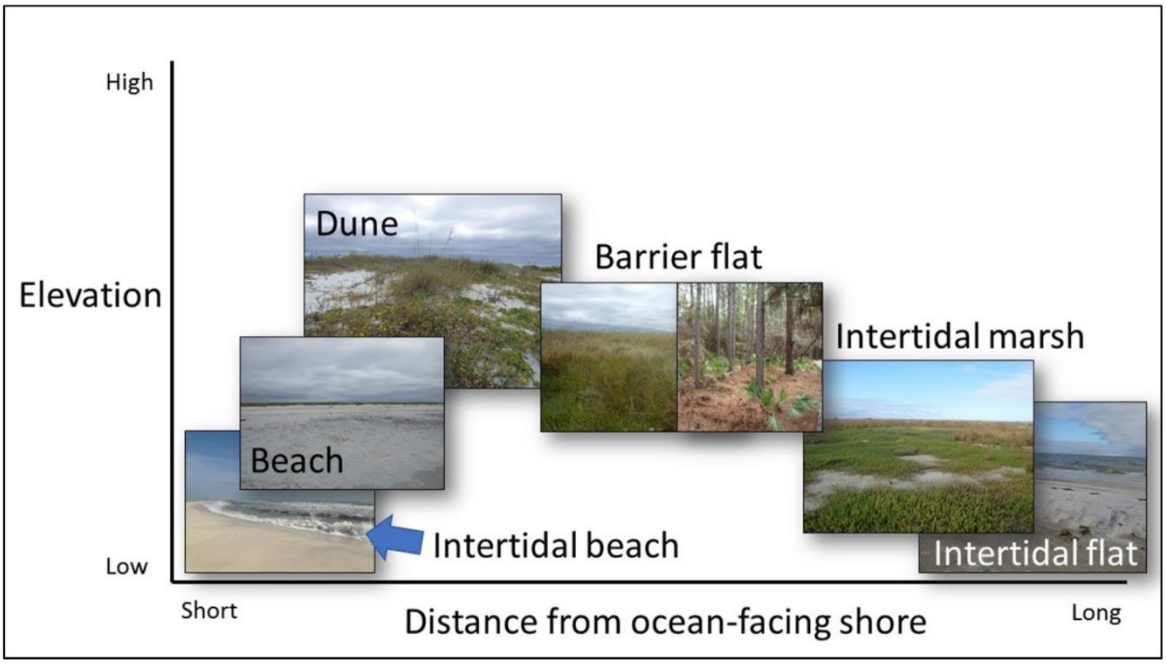

Figure 4.1. Hypothesized relationship between elevation and distance from ocean-facing shoreline for general barrier island habitats based on literature (Leatherman, 1979; Young et al., 2011).

4.2. Methodology

4.2.1. Study Area

Dauphin Island is part of a 105-km wide Mississippi-Alabama wave-dominated barrier island chain (McBride et al., 2013; Otvos & Carter, 2008; Figure 4.2). The island is backed by the shallow (<4-m deep) Mississippi Sound (Otvos & Carter, 2008) and is flanked to the east by Mobile Bay. In 2015, the length of Dauphin Island was about 25 km and the subaerial portion of the island was estimated to be about 15.8 km^2 (Enwright et al., 2017, in press). Situated in the northern Gulf of Mexico, Dauphin Island experiences diurnal tides with a mean tidal range of about 0.36 m (i.e., mean low water to mean high water), based on observations during the most recent North American Tidal Datum Epoch (NTDE; 1983 to 2001) from a National Oceanic and Atmospheric Administration tide gauge (station ID: 8735180) on the island. I developed the modeling domain for this study (dashed outline in Figure 4.2) by buffering the maximum extent of Dauphin Island shorelines from 1940 to 2015 (Henderson, Nelson, Long, & Smith, 2017) by 2.5 km. I used Esri ArcMap 10.5.1 (Redlands, CA, USA) for all spatial analyses.

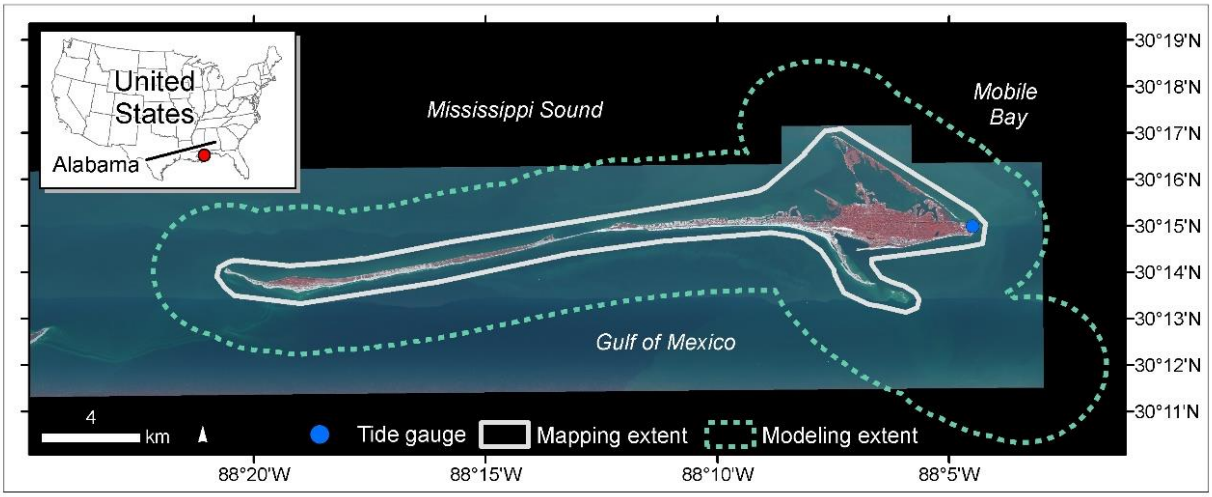

Figure 4.2. Modeling domain and the extent of baseline mapping data for habitat modeling effort on Dauphin Island, Alabama, USA. The basemap source data is 0.3-m color-infrared orthophotography acquired in December 2015 by Digital Aerial Solutions, LLC (Riverview, Florida, USA) and the U.S. Geological Survey. The area that is outside the 2015 imagery acquisition zone is shown in black.

4.2.2. Barrier Island Habitats

I set the model targets to be generalized habitat classes from a geomorphology-based habitat classification scheme that was recently used for a 2015 Dauphin Island habitat map (Table 4.1; Figure 4.3; Enwright et al., in press). The habitat generalizations that I applied involved combining habitat classes that may occupy the same geomorphic setting yet are regulated by factors that I did not include in the model, such as disturbance. Specifically, these included combining meadow and unvegetated barrier flat habitats into a single habitat class (i.e., barrier flat) and, likewise, combining forest and scrub/shrub into a single habitat class (i.e., woody vegetation). Each habitat in the model classification scheme is linked to a tidal zone (i.e., subtidal, intertidal, supratidal/upland; Figure 4.3). My research questions are mainly focused on predicting habitats; therefore, I did not make any predictions of changes to developed areas. These developed areas were extracted from the 2015 Dauphin Island habitat map and excluded from the machine learning prediction model input and output.

Table 4.1. Descriptions of the habitat classes included in the Dauphin Island habitat model.

Habitat	Description	Source
Barrier flat	Barrier flat includes flat or gently sloping supratidal/upland areas that are located on the backslope of dunes, unvegetated washover fans, and areas along estuarine shorelines. Barrier flat habitat can be unvegetated or vegetated (i.e., meadow).	Leatherman (1979); Lucas and Carter (2010)
Beach	Beach includes bare or sparsely vegetated supratidal areas that are located upslope of the intertidal beach and marine-water habitats. These habitats are located along shorelines with high wave energy.	Cowardin et al. (1979)
Developed[a]	Developed includes areas dominated by constructed materials (i.e., transportation infrastructure, residential, and commercial areas).	Homer et al. (2015)
Dune	Dunes are supratidal features developed via Aeolian processes with a well-defined relative elevation. Dune habitat can be vegetated or unvegetated.	Acosta et al. (2005)
Intertidal beach	Intertidal beach includes bare or sparsely vegetated intertidal wetlands located along the ocean-facing side of the island that are adjacent to high energy shorelines.	Cowardin et al. (1979)
Intertidal flat	Intertidal flat includes bare or sparsely vegetated intertidal wetlands that are adjacent to estuarine-water and along low energy shorelines.	Cowardin et al. (1979)
Intertidal marsh	Intertidal marsh includes all intertidal wetlands with 30% or greater areal cover by erect, rooted, herbaceous hydrophytes.	Cowardin et al. (1979)
Water-estuarine	Water-estuarine includes all areas of subtidal water and ponds on the back-barrier side of the island. These areas rarely have salinity greater than 30 ppt and generally has less than 30% cover of vegetation.	Cowardin et al. (1979)
Water-fresh	Water-fresh includes all areas of supratidal/upland water that generally have less than 30% cover of vegetation.	Cowardin et al. (1979)
Water-marine	Water-marine includes all areas of subtidal water found offshore of the ocean-facing side of the island. These areas are found along high energy coastlines and/or are areas that occasionally experience salinity levels greater than or equal to 30 ppt and generally has less than 30% cover of vegetation.	Cowardin et al. (1979)
Woody vegetation	Woody vegetation includes supratidal/upland scrub/shrub and forested areas where woody vegetation height is greater than about 0.5 m. Woody vegetation coverage should generally be greater than 30 percent.	Homer et al. (2015); Cowardin et al. (1979)
Woody wetland	Woody wetland includes all supratidal/upland wetlands dominated by woody vegetation with a vegetation height greater than about 0.5 m. Woody vegetation coverage should generally be greater than 30 percent.	Cowardin et al. (1979)

[a]Developed was not modeled in this effort. I assumed there were no changes in developed areas from the 2015 habitat map.

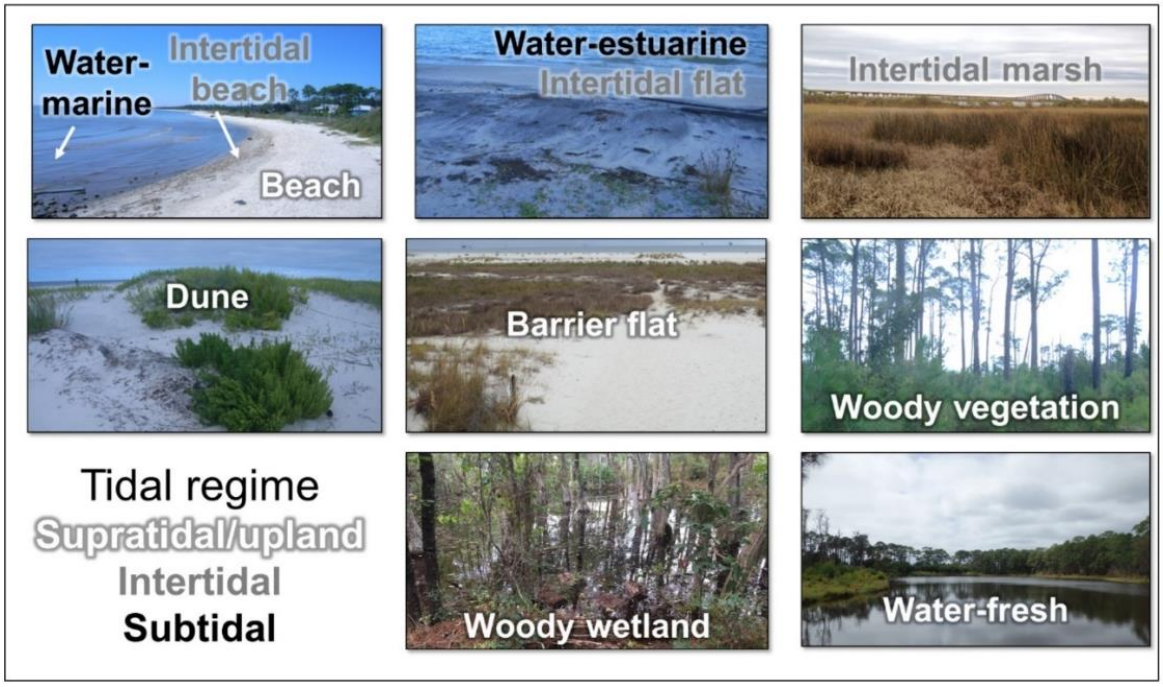

Figure 4.3. Examples of the habitat classes for the barrier island habitat modeling effort on Dauphin Island, Alabama, USA. The classes are linked to tidal regime (see legend in lower left corner of the figure). The developed class was not shown since it was not explicitly modeled in this effort. Modified from Enwright et al. (in press) with permission.

4.2.3. Remote Sensing Data and *In Situ* Data

I used topobathymetric DEMs (TBDEMs) as the primary data source for landscape position information. The contemporary TBDEM was developed from a 1-m bare-earth DEM from lidar data collected in January 2015 by Digital Aerial Solutions, LLC (DAS, Riverview, Florida, USA). The TBDEM was produced by DAS and the U.S. Geological Survey (USGS). The contemporary bathymetric data for much of the nearshore area was from a 20-m DEM developed from single-beam sonar surveys by the USGS in 2015 (DeWitt et al., 2015). Bathymetric data for the remainder of the study area was from the 3-m USGS Coastal National Elevation Database TBDEM (CoNED; Thatcher et al., 2016) for the northern Gulf of Mexico, which includes historical data from various periods between 1920 through 1988. I developed a seamless 10-m TBDEM by converting the rasters to points and using inverse distance weighted

interpolation to combine the datasets. The rationale for selecting 10 m for the model resolution was to use a spatial resolution that could provide insights on whether this habitat model framework could be used with spatial resolutions that could be compatible with irregular grids from hydrodynamic numerical models for forecasting geomorphology (Passeri et al., 2018).

The CoNED TBDEM was used for the hindcast TBDEM. Topographic data for the subaerial portion for most of the island in this dataset was from data collected via the USGS Experimental Advanced Airborne Research Lidar (Bonisteel et al., 2009) in 2007, although a small area along the northern portion of eastern Dauphin Island and Little Dauphin Island (i.e., the narrow island on the northeastern end of the study area that runs from northwest to the southeast; Figure 4.2) was from lidar data from 2002 collected by Mobile County, Alabama. I resampled the CoNED to 10 m using bilinear interpolation.

I used orthophotography as ancillary data for model validation via photointerpretation. The contemporary orthophotography was ~0.3-m color-infrared aerial orthophotography acquired on 4 December 2015, by DAS and the USGS. The imagery was collected with a Leica ADS100 digital camera (Wetzlar, Germany) when water levels were near or just below mean sea level (MSL). The hindcast orthophotography was 0.5-m true color orthophotography collected with a Leica ADS40 digital camera (Wetzlar, Germany) by the USGS on 1 February 2008 for all but the western tip of Dauphin island. For this area, I used 1-m orthophotography captured with a Z/I digital mapping camera by Photo Science, Inc (Norcross, Virginia, USA) in October 2008 due to a lack of coverage in the February orthophotography.

I used tide data to understand the relationship between the North American Vertical Datum of 1988 (NAVD88), MSL, extreme spring tide levels, and extreme water levels. These data were obtained from the NOAA tide gauge on the eastern end of Dauphin Island (Figure 4.2). All TBDEMs were transformed from NAVD88 to MSL using relative height differences from the NOAA tide gauge during the current NTDE. Habitat type and elevation data were collected during two and a half weeks in November and December of 2015 at 67 different transects located across seven different sites on the eastern half of Dauphin Island. These data were collected using a high-precision real-time kinematic global positioning system (RTK GPS) connected to a Global Navigation Satellite System (GNSS, Trimble R10 and TSC3, Trimble, Sunnyvale, CA, USA). These data were used to develop two separate relative error assessments for the 2015 DEM. The first assessment explored relative error for intertidal and low-lying herbaceous areas, whereas the second assessment quantified relative error in dunes. I assumed that the error and bias in the historical TBDEM were similar to the contemporary TBDEM. For more information on the field data collection and relative error assessments, see Enwright et al. (2017, in press).

4.2.4. Probability Surfaces

I used Monte Carlo simulations to develop probability surfaces that indicated the likelihood that a pixel in the TBDEM is either in an intertidal geomorphic setting or above an extreme water level. To do this, I simulated the propagation of error uncertainty using information from the relative error assessments (i.e., error and bias). For subaerial areas, the Monte Carlo simulation to create the probability surface related to intertidal areas used the assessment from intertidal and low-lying herbaceous areas, whereas the

Monte Carlo simulation for the likelihood of being above a storm water level used the dune assessment. For submerged areas for both simulations, I used recommendations from Byrnes, Baker, and Li (2002) for the RMSE of bathymetry data for nearshore waters and assumed bias was negligible. The lower and upper elevation thresholds for the intertidal probability surface were the lowest astronomical tide and the highest astronomical tide observed during the NTDE at the Dauphin Island, respectively (Cowardin et al., 1979). The elevation threshold for the extreme water probability surface was set to be the extreme water level with a 10% annual exceedance probability from the NOAA's Extreme Water Analyses for Dauphin Island (Zervas, 2013) that was updated for 2016 (1.13 m relative to MSL) to account for the sea-level rise trend observed at the Dauphin Island tide gauge (NOAA, 2013). For more information on the probability rasters and Monte Carlo simulations, see Enwright et al. (2018, in press).

4.2.5. Tidal zone determination

Because the habitat classes are linked to tidal zones (Figure 4.3), it is important to be able to automate the extraction of tidal zones from the TBDEM. I used the intertidal probability surfaces to separate the model domain by tidal zone. Subtidal areas were pixels that had a probability of being intertidal that was less than 0.5 and had an elevation less than MSL. Intertidal areas were areas with a probability of being intertidal greater than or equal to 0.5. The connectivity of the raster cells was defined by the queen's move rule, which searches for interconnected cells to expand tidal influence in both cardinal and diagonal directions and removes isolated low-lying areas (Poulter

& Halpin, 2008). After subtidal and intertidal areas were identified, the remaining areas, which included the isolated low-lying areas, were classified as supratidal/upland.

4.2.6. Predictor variable processing

I used the TBDEM to develop numerous landscape position predictor variables based on literature-derived linkages of landscape position to barrier island ecology and habitat distribution (Anderson et al., 2016; Foster et al., 2017; Halls et al., 2018; Young et al., 2011). The predictor variables were related to elevation or X,Y coordinates (i.e., proximity and direction; Figure 4.4). I determined the value of these predictor variables for each 10-m pixel in the TBDEM. I used the topographic position index, which was first proposed by Weiss (2001), as a measure of relative topography. This is calculated by subtracting the elevation for a single pixel to that of a neighborhood. Halls et al. (2018) used the topographic position index to extract dune habitat. The elevation to the south variables were calculated by taking the median of the maximum elevation for three 22-degree wedge-shaped kernels radiating to the south with radii of 1-km and 8-km. The distance from the Mobile-Tensaw River Delta was a cost distance, which restricted the distance calculation to subtidal areas identified from the TBDEMs. To do this, I created a cost surface that only included subtidal areas (i.e., intertidal, supratidal, and upland areas were set to “NoData”). For the Euclidean direction from the center variable (Figure 4.4), I determined Euclidean direction from centroids of 5-m cross-shore transects. I recoded this variable to “1” for directions between 90 degrees and 270 degrees, otherwise the value was set to “0”.

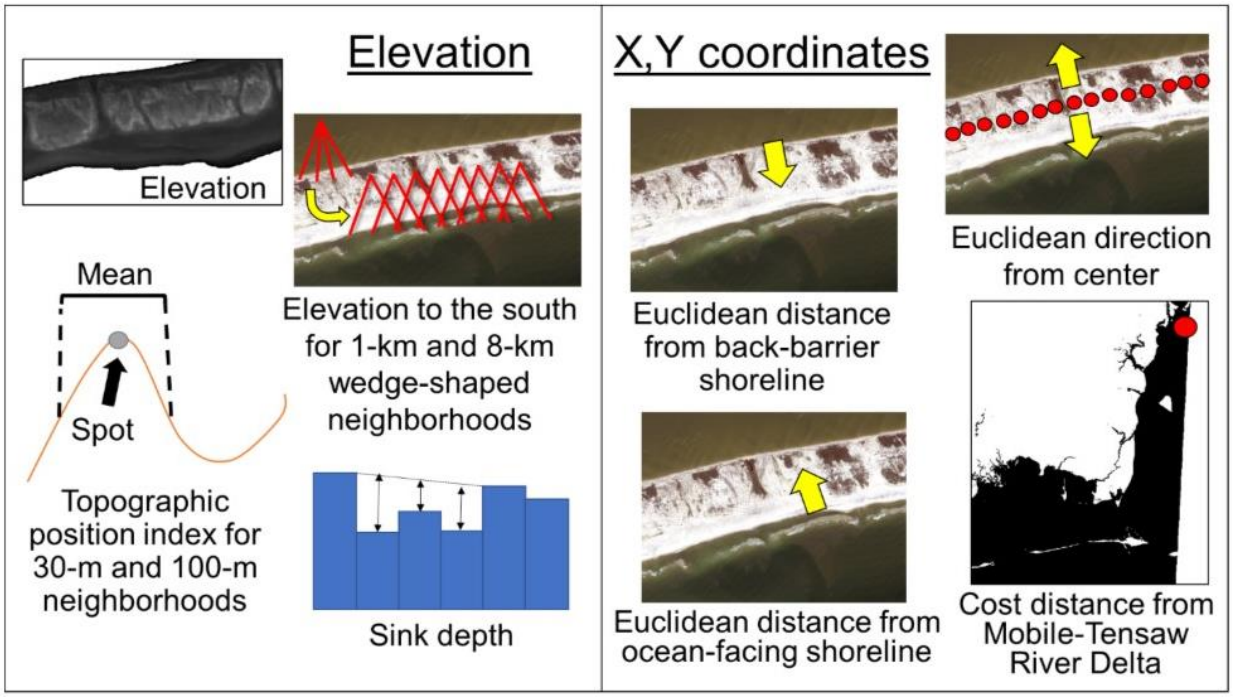

Figure 4.4. Landscape position predictor variables for the barrier island habitat modeling effort on Dauphin Island, Alabama, USA. The imagery source data is 0.3-m color-infrared orthophotography acquired in December 2015 and the elevation data source data is a 1-m digital elevation model from January 2015. Both of these data were collected by Digital Aerial Solutions, LLC (Riverview, FL, USA) and the U.S. Geological Survey.

4.2.7. Habitat Modeling

The first step in the modeling process was to develop a habitat model for each tidal zone from contemporary data (Figure 4.5). I used the 2015 habitat map (solid outline in Figure 4.2; Enwright et al., in press) to develop training and validation datasets. These data were stratified among tidal zones and by habitat types within tidal zones to be proportional of the habitat strata from the 2015 habitat map (Table 4.2; Enwright et al., in press). With a minimum of 42 training points, I ensured that I had at least 30 training points for each class for training datasets made from 70% random permutations. To limit spatial autocorrelation issues with training data, I created random points per class through an iterative process aimed at maximizing the minimum distance between points. I used a similar approach to control the minimum sample distance per

habitat class for all random samples developed in this effort (i.e., training data and validation data for the contemporary and hindcast outputs). The validation dataset included 1,000 points per tidal zone stratified by the areal coverage of habitat classes predicted per tidal zone. Areas within 10 m of the training samples were excluded from the validation set. Furthermore, to avoid the influence from human constructions, I buffered developed areas from the 2015 habitat map by 10 m and excluded these areas from the validation sampling frame. Mapping intertidal areas from aerial orthophotography can be difficult since the imagery just shows water levels from a single snapshot. Thus, I excluded intertidal areas that were below MSL in the contemporary TBDEM (Enwright et al., in press) from the contemporary validation assessment. Following guidelines from Congalton and Green (2009) for accuracy assessment, I attempted to include at least 50 points per class, but I was only able to include around 30 points in woody wetland and water-fresh habitats because of the limited areal coverage of these habitats and the constraint of the minimum distance criterion.

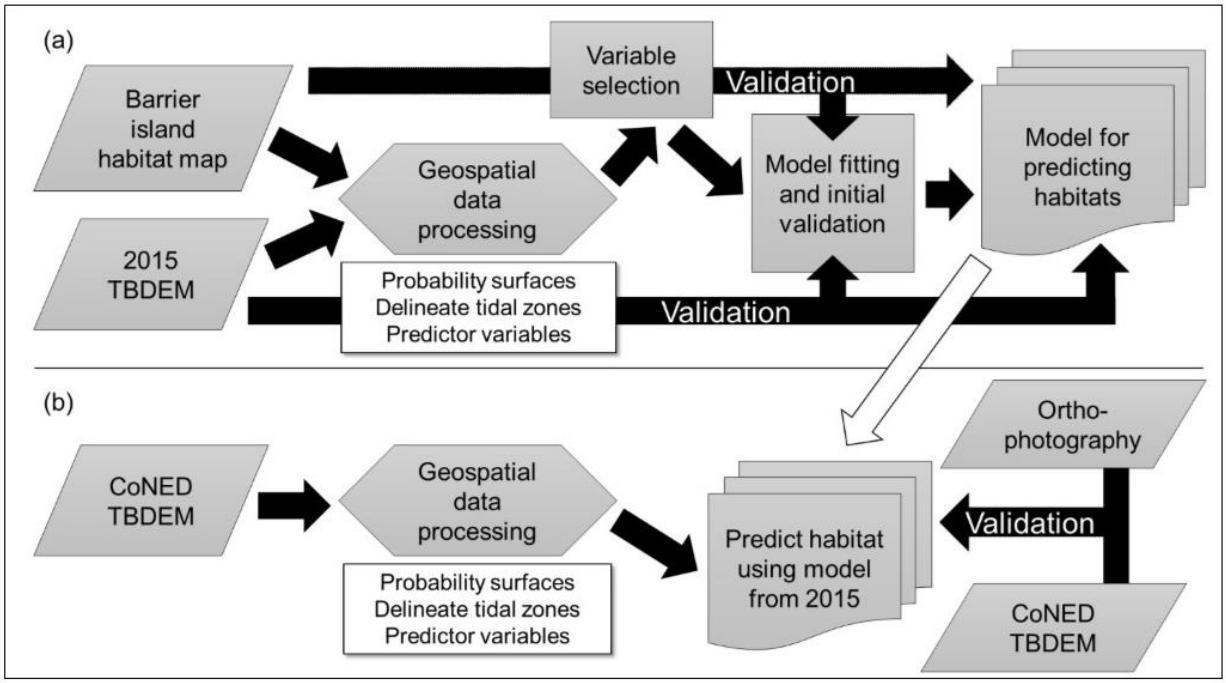

Figure 4.5. Workflow for the barrier island habitat model development for Dauphin Island, Alabama, USA. (a) Overview of process for developing and validating the contemporary model for predicting barrier island habitats using a habitat map and a topobathymetric (TBDEM) from 2015; (b) Overview of the process for predicting barrier island habitats using historical data from the USGS Coastal National Elevation Dataset (CoNED) TBDEM using the model fitted with contemporary data (i.e., hindcast).

I used MathWorks® MATLAB 2016b (Natick, Massachusetts, USA) for model fitting and prediction. I used the MATLAB Classification Learner application in the Statistics and Machine Learning Toolbox to fit and assess KNN, SVM, and RF models for several MATLAB model presets, such as various neighborhood sizes, weights, and distance metrics for KNN models, and kernel scale and kernel function for SVM models (Appendix C). I opted to use standard MATLAB model presets since this model was developed from a single snapshot of barrier island habitat data and barrier islands are dynamic ecosystems that can change gradually from coastal processes, including currents and tides or rapidly from episodic events, such as storms. Based on five permutations of the training data, I selected the best performing KNN, SVM models using five-fold cross-validation for each tidal zone (Tables C.1–C.3). These models

were combined with the RF models for further validation. For KNN and SVM models, I followed general recommendations to standardize the predictor variables to scale the feature space distance for these models (James et al., 2013). Table 4.2 lists the variables used per model with rationale. To illustrate how landscape position can influence barrier island habitats, I used the MATLAB Distribution Fitting application in the Statistics and Machine Learning Toolbox to plot univariate probability density functions for elevation and distance from the ocean-facing shoreline for the supratidal/upland habitats. For the probability density plots, I used non-parametric curves with bandwidths that best fit the data based on visual inspection.

Table 4.2. Response variables (i.e., habitat classes) and predictor variables per tidal zone for the habitat model for Dauphin Island, Alabama, USA.

Tidal zone	Habitat (number of training points)	Predictor variables and source	Source
Subtidal	Water-estuarine (1,000) Water-marine (1,000)	(1) Distance from Mobile-Tensaw River Delta (2) Direction from center	(1–2) Cowardin et al. (1979)
Intertidal	Intertidal flat (252) Intertidal beach (50) Intertidal marsh (121)	(1) Elevation (2) Elevation to the south (8-km) (3) Distance from ocean-facing shoreline (4) Distance from back-barrier shoreline	(1) Cowardin et al. (1979); Foster et al. (2017); Young et al. (2011); Anderson et al. (2016); Zinnert et al. (2017) (3–4) Young et al. (2011)
Supratidal /upland	Barrier flat (484) Beach (99) Dune (184) Water-fresh (43) Woody vegetation (327) Woody wetland (43)	(1) Elevation (2) Elevation to the south (1-km) (3) Topographic position index (30-m) (4) Topographic position index (100-m) (5) Distance from ocean-facing shoreline (6) Distance from back-barrier shoreline	(1) Cowardin et al. (1979); Foster et al. (2017); Young et al. (2011); Anderson et al. (2016); Zinnert et al. (2017) (3–4) Wernette et al. (2016); Halls et al. (2018); Enwright et al. (in review) (5–6) Young et al. (2011)

To avoid overfitting a single model, I trained 100 models per tidal zone from 70% of the training set selected by random permutations. For each cell, the majority habitat class of the 100 predictions was chosen as the final prediction. The intertidal zone and

the supratidal/upland zone models were applied to each cell in the 10-m raster; however, to increase efficiency of the subtidal zone models, I made predictions for a 100-m raster and then converted these data to a 10-m raster using inverse distance weighted interpolation.

I used the validation points to conduct an accuracy assessment and quantify the overall accuracy and the producer's accuracy and user's accuracy for each class. For each assessment, I calculated a deterministic and fuzzy estimate for all accuracy statistics following guidelines by Congalton and Green (2009) and Woodcock and Gopal (2000). The fuzzy accuracy estimate allows classification of: (1) exact match (e.g., woody vegetation in model results and orthophotography); (2) acceptable match due to landscape position and geomorphic setting (e.g., calling a location Intertidal beach or water-marine along ocean-facing shoreline); and (3) unacceptable/error (e.g., intertidal marsh located on the high energy, ocean-facing shoreline). Fuzzy accuracy is well suited for assessing barrier island habitats due to dynamic transitions like open water classes and intertidal classes, which are dependent on water level.

To determine the best model per tidal zone (i.e., from the subset of models, which included the RF models and the top-performing KNN and SVM models), I used the tidal zone delineations from the contemporary 10-m TBDEM to extract the validation points that fall within the tidal zone. However, because the validation data was from the 1-m 2015 habitat map, there may be some discrepancies between the reference labels within a tidal zone due to temporal lag and spatial resolution differences. Thus, I omitted validation points that have a reference label other than what would be expected in the

tidal zone being assessed (e.g., I omitted points that had a reference label of intertidal beach from the supratidal/upland zone).

Next, I combined the best model per tidal zone and tested whether the application of a suite of post-processing routines enhanced the model results. These included the application of a majority filter to reduce noise along with several user-defined constraints based on the theoretical understanding of barrier island habitats from the literature regarding elevation and X,Y coordinates (Table 4.3; Cowardin et al., 1979; Leatherman, 1979; Young et al., 2011). For example, on non-fetch-limited barrier islands, emergent marsh vegetation typically occurs where wave energy is lower, whereas unvegetated intertidal mudflats or intertidal beach habitats are more common where wave energy is higher (Roland & Douglass, 2005). Therefore, intertidal marsh habitat found along the ocean-facing shore were changed to intertidal beach habitat. An additional example is that dunes are not expected to be sustainable at low-lying elevations, such as those below a common extreme storm water level (Sallenger, 2000). Therefore, dune habitat that had a probability less than 0.5 for being above the extreme storm water level were recoded to barrier flat (Enwright et al., in press). These rules were applied in a step-wise fashion (Table 4.3). Some of the thresholds used are directly related to tidal datums (e.g., EHWS), whereas others, such as sink depth, were determined by trial-and-error with the final value being selected by visual inspection. I also explored whether the use of a four-pixel minimum mapping unit (MMU) impacted model performance. I selected four pixels as the maximum MMU based on visual inspection of results (i.e., small habitat areas can be lost if the MMU is too high).

Table 4.3. The type, condition, and order for user-defined rules applied to model results via post-processing by habitat class for the habitat model for Dauphin Island, Alabama, USA.

Type of correction	Habitat	Condition	Order
Elevation	Dune	Dune areas that had a probability less than 0.5 for being above the extreme storm water level were changed to barrier flat.	2
Elevation - depressional habitats	Barrier flat	Barrier flat areas that had a sink depth greater than or equal to 0.5 m were changed to water-fresh.	11
	Intertidal beach	Intertidal beach areas that had a sink depth greater than or equal to 0.01 m should be commonly inundated with standing water and were changed to water-marine.	7
	Intertidal flat	Intertidal flat areas that had a sink depth greater than or equal to 0.01 m should be commonly inundated with standing water and were changed to water-estuarine.	8
	Water-fresh	Water-fresh areas that did not have a sink depth greater than or equal to 0.5 m were changed to barrier flat.	10
	Woody wetland	Woody wetland areas that did not have a sink depth greater than or equal to 0.1 m were recoded to be woody vegetation.	1
X,Y coordinates	Intertidal beach	Intertidal beach areas that were found to be closer to the back-barrier shoreline than the ocean-facing shoreline were changed to intertidal flat.	3
	Barrier flat	Barrier flat areas that had intertidal beach within a 5-by-5 pixel neighborhood were changed to beach due to the proximity to the ocean-facing shoreline.	9
	Intertidal beach	Intertidal beach areas that are located behind supratidal areas with an elevation to the south for 1 km greater than or equal to 0.6 m were changed to intertidal flat.	5
	Intertidal flat	Intertidal flat areas that were closer to water-marine than water-estuarine were changed to intertidal flat.	6
	Intertidal marsh/Intertidal flat	Intertidal marsh areas should be sheltered from high energy areas (Roland & Douglass, 2005). These areas that did not have an elevation to the south for 8 km greater than or equal to 0.448 m (i.e., EHWS) were changed to intertidal beach. This rule was also applied to intertidal flat.	4

Lastly, I applied the final model to hindcast habitats based on the predictor variables developed from the CoNED TBDEM (Figure 4.5). To validate the hindcast results, I developed a hindcast validation dataset with about 300 points per zone (*n* = 1,029). These data consisted of stratified random points within each habitat model class. I assigned reference labels to the hindcast validation points through

photointerpretation of the orthophotography and inspection of the TBDEM and probability surfaces and assessed deterministic and fuzzy map accuracies.

4.3. Results

Similar to Young et al. (2011), I found that habitats on Dauphin Island are related to landscape position (Figure 4.6). For example, these plots show that beach habitat tended to be located near the ocean-facing shore and had a mode for elevation of around 1 m relative to MSL, whereas woody vegetation had a mode for elevation of just under 2 m relative to MSL and was further away from the ocean-facing shoreline. Collectively, these plots confirmed that landscape position variables are important predictors for supratidal/upland habitats on Dauphin Island.

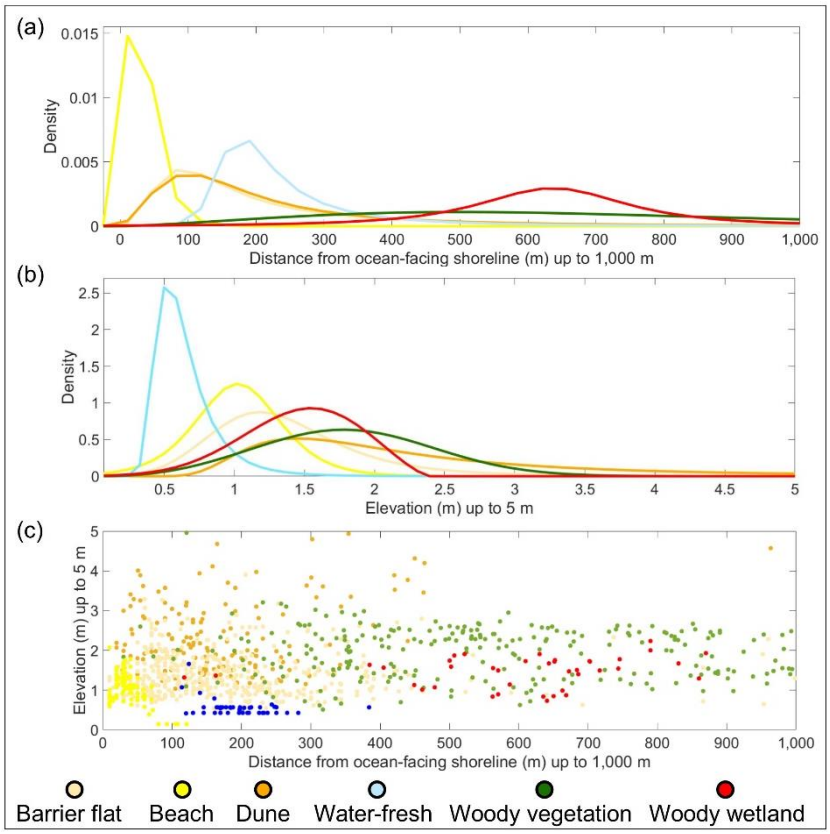

Figure 4.6. Probability density functions developed from the training data for the supratidal/upland zone from the contemporary (i.e., 2015) habitat model for Dauphin Island, Alabama, USA. (a) Distance (m) from the ocean-facing shoreline up to 1,000 m; (b) Elevation (m) up to 5 m; and (c) a bivariate plot for these two variables.

The top performing models for the subtidal zone using five-fold cross validation were coarse KNN, fine gaussian SVM, and RF (Table C.1). For the intertidal zone, the top performing models using five-fold cross validation were weighted KNN, cubic SVM, and RF (Table C.2). Lastly, the top performing models for the supratidal/upland zone using five-fold cross validation were weighted KNN, quadratic SVM, and RF (Table C.3). With more robust model development (i.e., using 100 random permutations of the training data) and assessment using the validation data from the 2015 habitat map, the performance of all of the models was similar for the subtidal zone (Figure C.1a); however, the coarse KNN model was selected for the subtidal zone based on visual inspection of the results. I found that RF performed the best for the intertidal and supratidal/upland zones (Figure C.1b–c).

As previously mentioned, these models were combined to create the contemporary model results. The combined contemporary model had a deterministic overall accuracy of 66.9% and a fuzzy overall accuracy of 80.3% (Figure 4.7a–b; Table C.4). The application of post-processing yielded a slight enhancement to the deterministic and fuzzy overall accuracy (Figure 4.7c–d; Table C.5). I selected the model with post-processing and a four-pixel MMU as the final model. This model had a deterministic overall accuracy of 67.5% and a fuzzy overall accuracy of 82.1% (Figure 4.7e–f; Table 4.4). However, I did not find that the application of the MMU led to a negative impact on the results (Figure 4.7c–f; Table C.4–5).

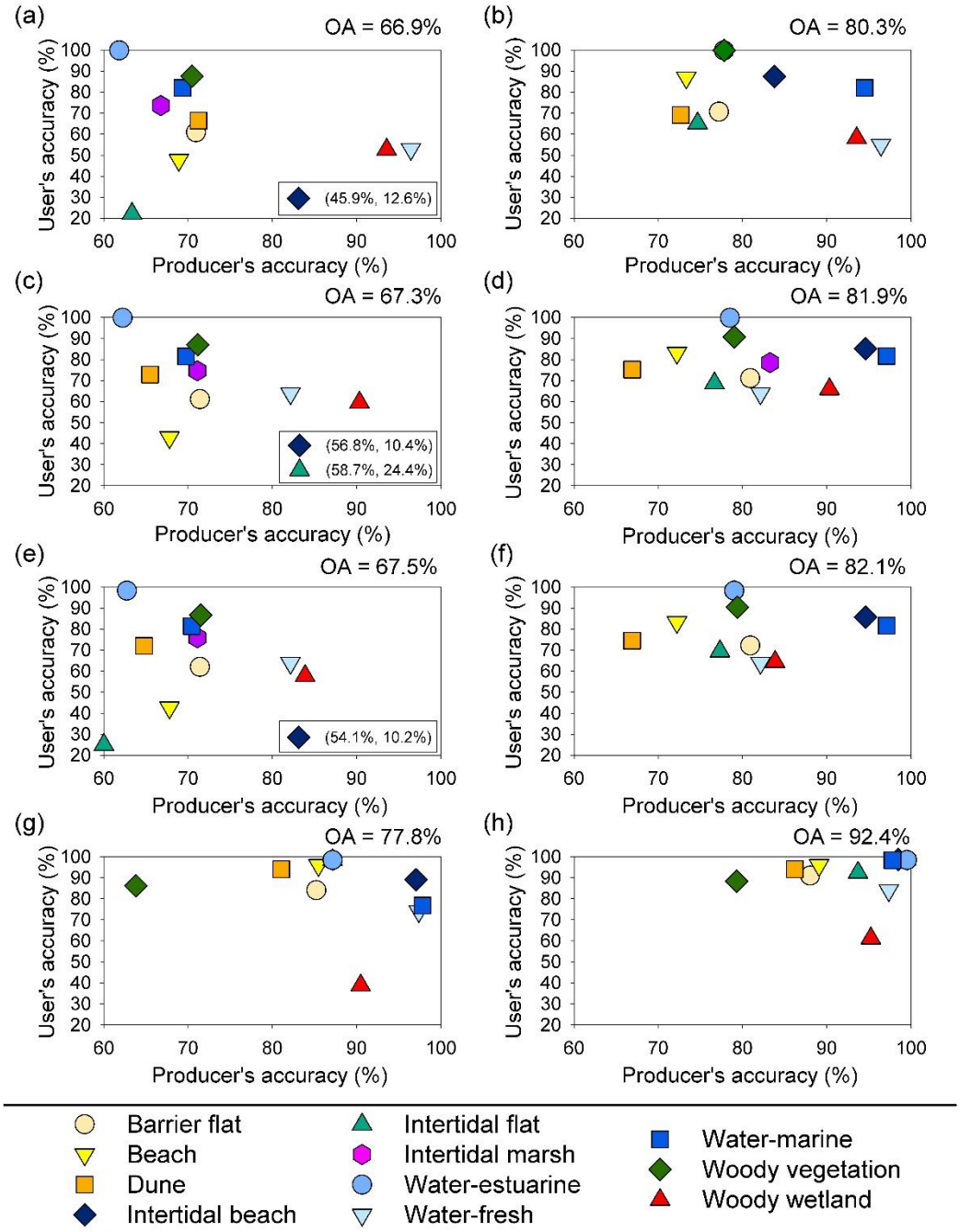

Figure 4.7. Producer's and user's accuracy results for the barrier island habitat model effort for Dauphin Island, Alabama, USA. (a–b) Deterministic accuracies (a) and fuzzy accuracies (b) for the final contemporary model without post-processing; (c–d) Deterministic accuracies (c) and fuzzy accuracies (d) for the final contemporary model with post-processing, but no minimum mapping unit (MMU); (e–f) Deterministic accuracies (e) and fuzzy accuracies (f) for the final contemporary model with post-processing and a four-pixel MMU; (g–h) Deterministic accuracies (g) and fuzzy accuracies (h) for the hindcast model with post-processing and a four-pixel MMU. OA: Overall accuracy of the model results.

Table 4.4. Error matrix with deterministic and fuzzy accuracies for the final contemporary model results (i.e., with post-processing and a four-pixel minimum mapping unit) for Dauphin Island, Alabama, USA. For the off-diagonal cells, the first value indicates deterministic count and the second value indicates the fuzzy count. BF: Barrier flat; B: Beach; CT: Column total; D: Dune; DPA: Deterministic producer's accuracy; DOA: Deterministic overall accuracy; DUA: Deterministic user's accuracy; FOA: Fuzzy overall accuracy; FPA: Fuzzy producer's accuracy; FUA: Fuzzy user's accuracy; IB: Intertidal beach; IF: Intertidal flat; IM: Intertidal marsh; RT: Row total; WE: Water-estuarine; WF: Water-fresh; WM: Water-marine; WV: Woody vegetation; WW: Woody wetland.

		Reference data													
	Class	BF	B	D	IB	IF	IM	WE	WF	WM	WV	WW	RT	DUA (%)	FUA (%)
Model data	BF	**307**	4;2	43;2	0;0	14;7	23;2	13;0	4;0	1;1	36;16	0;0	495	62.0	72.1
	B	9;9	**61**	1;1	1;15	1;4	4;0	1;0	0;0	7;28	0;1	0;0	143	42.7	83.2
	D	27;1	0;1	**90**	0;0	0;2	0;0	0;0	0;0	0;0	3;1	0;0	125	72.0	74.4
	IB	0;7	17;1	0;0	**20**	0;11	5;0	2;38	0;0	4;92	0;0	0;0	197	10.2	85.8
	IF	9;6	0;0	1;0	0;0	**90**	35;35	62;118	0;0	0;0	3;1	0;0	360	25.0	69.4
	IM	14;9	2;0	1;0	0;0	16;4	**327**	53;3	0;0	1;0	0;1	0;0	431	75.9	79.8
	WE	4;0	0;0	0;0	0;0	1;0	6;0	**616**	0;0	0;0	0;0	0;0	627	98.3	98.3
	WF	5;0	0;0	0;0	0;0	0;0	0;0	6;0	**23**	0;0	2;0	0;0	36	63.9	63.9
	WM	0;0	2;0	0;0	1;0	0;0	0;0	69;1	0;0	**319**	0;0	0;0	392	81.4	81.6
	WV	14;9	0;0	0;0	0;0	0;0	3;0	0;0	1;0	0;0	**208**	5;0	240	86.7	90.4
	WW	0;0	0;0	0;0	0;0	0;0	0;0	0;0	0;0	0;0	16;3	**26**	45	57.8	64.4
	CT	430	90	139	37	150	460	982	28	453	291	31	**3,091**		
	DPA (%)	71.4	67.8	64.8	54.1	60.0	71.4	62.7	82.1	70.4	71.5	83.9			
	FPA (%)	80.9	72.2	66.9	94.6	77.3	83.5	79.0	82.1	97.1	79.4	83.9			
		DOA (%): 67.5; FOA (%): 82.1													

While overall accuracy is a helpful measure, it is also important to assess class-specific performance reported by producer's and user's accuracy. For the final contemporary model, the top three classes with regard to deterministic producer's accuracy were woody wetland (83.9%), water-fresh (82.1%), and woody vegetation (71.5%). The three classes with the highest fuzzy producer's accuracy were water-marine (97.1%), intertidal beach (94.6%), and woody wetland (83.9%). The classes with the lowest deterministic and fuzzy producer's accuracy were intertidal flat (60.0%) and dune (66.9%), respectively. The three classes with the highest deterministic user's accuracy were water-estuarine (98.3%), woody vegetation (86.7%), and water-marine

(81.4%). The three classes with the highest fuzzy user's accuracy were water-estuarine (98.3%), woody vegetation (90.4%), and intertidal beach (85.8%). The classes with the lowest deterministic and fuzzy user's accuracy were intertidal beach (10.2%) and water-fresh (63.9%), respectively.

Figure 4.7a–f highlights the change in accuracy as a result from the use of fuzzy accuracy. For the final model, the use of fuzzy accuracy led to a median increase of producer's accuracy of 9.5% with an interquartile range of 15.2% (Figure 4.7e–f), while the user's accuracy was more variable with a median increase of user's accuracy of 3.9% with an interquartile range of 40.3%. In addition to the use of fuzzy accuracy, I found that the model results were often enhanced when post-processing routines were applied. Compared to the original model results, the three highest magnitude changes in deterministic producer's accuracy as a result of the user-defined rules were water-fresh (-14.3%), intertidal beach (+10.8%) and dune (-5.7%). As a result of the user-defined rules, the three highest magnitude changes in deterministic user's accuracy were water-fresh (+11.0%), woody wetland (+6.9%) and dune (+6.4%). Figure 4.8 shows additional evidence to support the use of post-processing by contrasting the western tip of Dauphin Island without post-processing (Figure 4.8a) and with post-processing (Figure 4.8b). Besides the reduction in dune habitat, a few notable differences include the reduction of intertidal beach areas that are found behind beach habitat, introduction of estuarine ponds within intertidal marsh, and the reduction in the salt-and-pepper effect. When comparing the areal coverage per supratidal/upland habitat, I found the overall comparison of percent difference per habitat class more closely matches the 2015 habitat map (Enwright et al., in press).

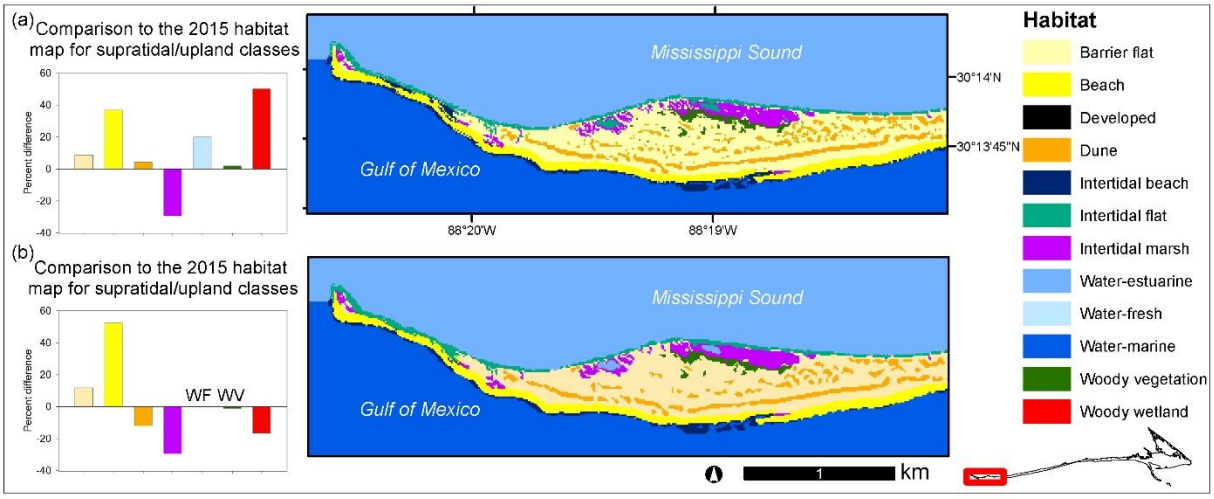

Figure 4.8. Barrier island habitat contemporary (i.e., 2015) habitat model outputs and percent difference comparison for supratidal/upland habitat compared to the 2015 habitat map (Enwright et al., in press), Dauphin Island, Alabama, USA. (a) Contemporary model without post-processing; (b) Contemporary model with post-processing and four-pixel minimum mapping unit.

Overall, the model did generalize well for the hindcast with a deterministic overall accuracy of 77.8% and a fuzzy overall accuracy of 92.4% (Table 4.5; Figure 4.7g–h). With regard to deterministic producer's accuracy, the top three classes were water-marine (97.8%), water-fresh (97.4%), and intertidal beach (97.0%). The three classes with the highest fuzzy producer's accuracy were water-estuarine (99.5%), intertidal beach (98.5%), and water-marine (97.8%). The classes with the lowest deterministic and fuzzy producer's accuracy were intertidal flat (35.9%) and woody vegetation (79.3%), respectively. The three classes with the highest deterministic user's accuracy were water-estuarine (98.4%), beach (95.9%), and dune (94.0%). The three classes with the highest fuzzy user's accuracy were water-estuarine (98.4%), water-marine (98.4%), and beach (95.9%). The classes with the lowest deterministic and fuzzy user's accuracy were woody wetland/intertidal marsh (38.8%) and woody wetland (61.2%), respectively.

Table 4.5. Error matrix with deterministic and fuzzy accuracies for the hindcast model results (i.e., with post-processing and a four-pixel minimum mapping unit) for Dauphin Island, Alabama, USA. For the off-diagonal cells, the first value indicates deterministic count and the second value indicates the fuzzy count. BF: Barrier flat; B: Beach; CT: Column total; D: Dune; DPA: Deterministic producer's accuracy; DOA: Deterministic overall accuracy; DUA: Deterministic user's accuracy; FOA: Fuzzy overall accuracy; FPA: Fuzzy producer's accuracy; FUA: Fuzzy user's accuracy; IB: Intertidal beach; IF: Intertidal flat; IM: Intertidal marsh; RT: Row total; WE: Water-estuarine; WF: Water-fresh; WM: Water-marine; WV: Woody vegetation; WW: Woody wetland.

		Reference data													
	Class	BF	B	D	IB	IF	IM	WE	WF	WM	WV	WW	RT	DUA (%)	FUA (%)
Model data	BF	**121**	5;2	5;3	0;0	0;0	0;0	1;0	1;0	0;0	1;5	0;0	144	84.0	91.0
	B	1;0	**47**	1;0	0;0	0;0	0;0	0;0	0;0	0;0	0;0	0;0	49	95.9	95.9
	D	2;0	0;0	**47**	0;0	0;0	0;0	0;0	0;0	0;0	1;0	0;0	50	94.0	94.0
	IB	0;0	0;0	0;0	**65**	1;7	0;0	0;0	0;0	0;0	0;0	0;0	73	89.0	98.6
	IF	0;0	0;0	0;0	0;1	**57**	5;3	0;0	0;0	0;0	0;0	0;0	66	86.4	92.4
	IM	3;1	0;0	0;0	1;0	7;85	**62**	0;0	0;0	0;0	1;0	0;0	160	38.8	92.5
	WE	0;0	0;0	0;0	0;0	1;0	0;0	**183**	0;0	2;0	0;0	0;0	186	98.4	98.4
	WF	6;2	0;0	0;0	0;0	0;0	0;0	0;1	**37**	0;0	2;2	0;0	50	74.0	84.0
	WM	0;0	1;0	0;0	0;0	1;0	0;0	0;25	0;0	**89**	0;0	0;0	116	76.7	98.4
	WV	5;1	0;0	2;0	0;0	0;0	2;0	0;0	0;0	0;0	**74**	1;1	86	86.1	88.4
	WW	0;0	0;0	0;0	0;0	0;0	0;0	0;0	0;0	0;0	19;11	**19**	49	38.8	61.2
	CT	142	55	58	67	159	72	210	38	91	116	21	**1,029**		
	DPA (%)	85.2	85.5	81.0	97.0	35.9	86.1	87.1	97.4	97.8	63.8	90.5			
	FPA (%)	88.0	89.1	86.2	98.5	93.7	90.3	99.5	97.4	97.8	79.3	95.2			
		DOA (%): 77.8; FOA (%): 92.4													

4.4. Discussion

This effort builds on the work of Young et al. (2011) and Foster et al. (2017) by using machine learning algorithms to develop spatially explicit predictions of barrier island habitat based on landscape position information. I found that the flexibility of machine learning algorithms makes them well suited to predict barrier island habitats. In some cases, the individual parameters followed Gaussian distributions for particular habitats (Figure 4.6a–b); however, the distributions can become complex in the n-dimensional space (Figure 4.6c). Furthermore, machine learning algorithms are not concerned with multicollinearity from the predictor variables that could be problematic

for traditional models, such as multinomial logistic regression, but instead the main concern with machine learning is how well the model can generalize to new data (James et al., 2013; Shmueli, 2010). The deterministic overall accuracy for the contemporary model was just under 70% and the fuzzy overall accuracy was just over 80%, whereas the hindcast deterministic overall accuracy was just under 80% and the fuzzy overall accuracy was over 90%.

One challenge with the use of data-driven machine learning algorithms is that the algorithm can only learn relationships that are present in the training dataset. This can be problematic for a dynamic environment, such as barrier islands, where habitat transition zones can change rapidly from the impact of an episodic event, such as a storm. The data-driven nature of machine learning algorithms underscores the need for a theoretical basis in the selection of predictor variables, as done with this study. Similarly, the results of a model can be assessed to ensure they comply with theoretical understanding of barrier island habitats through post-processing routines similar to the ones I utilized. While the post-processing routines I used reduced the accuracies of some classes, the reduction was often associated with a minor increase in omission error. This tradeoff was justified by the overall positive increase in performance (Figure 4.7) and overall comparison with habitat coverage (i.e., supratidal) in the 2015 habitat map (Figure 4.8). In order to reduce issues associated with the data-driven approach, future efforts could aim to augment time for space by developing additional training data from historical habitat maps paired with landscape position information. Additionally, details regarding precedent conditions relating to storminess could be added to such a training dataset using an approach similar to Mickey, Long, Plant, Thompson, and

Dalyander (2017) to characterize storminess for a period. While I used standard presets, a more robust training dataset would allow for model preset optimization. Additionally, variables that pertain to longer-term, larger-scale variables similar to the ones used by Gutierrez et al. (2015), such as island width and historical shoreline erosion rates, could also provide valuable information to improve barrier island habitat models.

In addition to utilizing post-processing to refine the models results, the use of fuzzy accuracy also helped better evaluate the performance of a model due to flexibility to note uncertainties regarding the vegetative state of areas for a given time. For example, some areas were predicted to be intertidal marsh based on landscape position in the hindcast results, yet these areas only had sparse vegetation in the orthophotography used for validation and, at that time, may be more appropriately predicted as intertidal flat instead of intertidal marsh. In other words, an area could be predicted to be intertidal marsh based on landscape position, yet it may not be intertidal marsh at the time of assessment because it often takes time for habitat succession necessary for a marsh to develop (Mitsch & Wilson, 1996). Additionally, due to data availability there can be a temporal lag between the acquisitions of lidar data used for model development and orthophotography used for model validation. Similarly, moving from a detailed habitat map (Enwright et al., in press) to a general model based on landscape position information required some generalizations for habitat classes. For instance, the barrier flat habitat model class (Figure 4.3; Table 4.1) includes a wide spectrum of vegetation levels from densely vegetated meadow habitat to sparsely vegetated barrier flat (Enwright et al., in press). The reason for this type of

generalization was due to the difficulty of predicting vegetation succession from a model with landscape position alone as the vegetation state is largely controlled by exposure to abiotic factors, such as inundation and overwash from storm surges. Future research is needed to explore how landscape position and temporal lag from disturbances impact the probability of an area being vegetated.

While there are developed areas on Dauphin Island, I did not incorporate urban growth into the model. I assumed development was constant and excluded these areas from validation. Alternatively, this model framework could be used to predict potential habitat for developed areas based on landscape position. If a researcher is interested in integrating urban growth into this type of model framework, then utilizing or calibrating an existing urban growth model such as the SLEUTH model (Slope, Land cover, Exclusion, Urbanization, Transportation, and Hillshade; Terando et al., 2014) may be desirable.

While the model predictor variables were developed from high-resolution lidar DEMs (i.e., 1-m to 3-m spatial resolution), I opted to use 10 m as the spatial resolution to show how a model could be applied to forecast applications, which can have variable cross-shore and alongshore resolutions (Passeri et al., 2018). I expect that using a higher resolution model grid would increase the prediction performance for the dune class based on the increased ability to resolve relative topography from higher resolution data. If I was not focused on forecasting, the model framework outlined in this effort could be calibrated with high-resolution data. Similarly, while this effort focused on developing a model to predict habitats from a DEM alone, the landscape position information used in this study could be applied to machine learning algorithms for

producing contemporary or historical barrier islands habitat maps with remotely sensed imagery and lidar data.

The model framework presented here can be calibrated and extended to other islands. While this effort developed a single global model for Dauphin Island, future efforts may explore the utility of developing local models based on wave energy settings and habitat composition. For instance, the orientation of an island could be used as an indicator of the need for a separate model. Dauphin Island is generally parallel to the mainland (i.e., generally east to west), whereas portions of the island run from the northwest to the southeast (Figure 4.2). Likewise, topographic state metrics could be used to develop meaningful model zones (Zinnert et al., 2017) using methods similar to that of Monge and Stallins (2016).

The advantage of developing a model largely based on information that could be extracted from a TBDEM is that these models can be calibrated and used with numerical models for forecasting alternative future states of an island with accelerated sea-level rise and simulated storms. Landscape position-based habitat models can be coupled with hydrodynamic geomorphology models (Passeri et al., 2018) that incorporate coastal morphodynamics and dune evolution (Dalyander, Mickey, Passeri, & Plant, in review). Collectively, these types of models can provide natural resource managers with tools for predicting the potential future states of these ecosystems with and without management actions (e.g., beach nourishment, dune creation or restoration, marsh creation or restoration).

4.5. Conclusion

In this effort, I explored whether machine learning algorithms could be used to predict habitat on barrier islands based on landscape position information. The model performance among the KNN, SVM, and RF models was similar for the subtidal zone, but I opted for the KNN model based on a smoother transition from water-estuarine to water-marine. I found that RF was the best model for the intertidal and supratidal/upland zones. The deterministic overall accuracy for the contemporary model was just under 70% and the fuzzy overall accuracy was just over 80%. I tested whether model performance was enhanced using post-processing routines. While this process introduced some omission error in certain classes, such as water-fresh and dune classes, the post-processing routines, collectively, tended to enhance the model results via increases in accuracy and overall comparison with habitat coverage from the source map used for training data development. I found that the model did generalize well to new data. The hindcast deterministic overall accuracy was just under 80% and the fuzzy overall accuracy was over 90%. This model framework could be coupled with hydrodynamic geomorphology models that can incorporate coastal morphodynamics and dune evolution for forecasting alternative states of barrier islands with and without various management actions or for producing contemporary or historical detailed barrier island habitat maps using remotely sensed imagery and lidar.

CHAPTER 5. CONCLUSION

Barrier islands provide important ecosystem services, including storm protection and erosion control to the mainland, habitat for fish and wildlife, and tourism (Barbier et al., 2011; Feagin et al., 2010; Sallenger, 2000). Barrier islands tend to be dynamic due to their location along the estuarine-marine interface. Besides gradual changes caused by constant forces, such as currents and tides, barrier islands face numerous threats including hurricanes, accelerated sea-level rise, oil spills, and anthropogenic impacts (Pilkey & Cooper, 2014). These threats are likely to influence the future of barrier islands in the latter part of the 21st century, especially as climate-related threats to coastal areas are expected to increase in the future (Knutson et al., 2010; Hansen et al., 2016). As a result, natural resource managers are concerned with monitoring changes to these islands and modeling future states of these environments. In this dissertation, I outlined how barrier island habitat mapping and modeling can be enhanced using landscape position information and elevation uncertainty. While this dissertation is focused on barrier islands, this research includes many important concepts in the fields of geographical information science and remote sensing, including management of uncertainty, data fusion, object-based analyses, spatial scale, temporal scale, fuzzy logic, and geocomputational modeling. The remainder of this chapter includes a summary of each research objective along with limitations to the research and next steps. This section concludes with a discussion of how this dissertation fits in the context of a comprehensive barrier island habitat research agenda.

Natural resource managers are concerned with monitoring the extent and distribution of intertidal wetlands due to the numerous valuable ecosystem goods and

services that these ecosystems provide (Barbier et al., 2011). For the first research objective of this dissertation, I applied a simple approach to enhance the results of automated intertidal area mapping using light detection and ranging (lidar) data. The level of uncertainty from data collected with conventional aerial topographic lidar systems is considerable within intertidal areas and can be as high as 60 cm in densely vegetated emergent wetlands (Buffington et al., 2016; Medeiros et al., 2015). Due to the lack of detailed error information, the uncertainty of lidar-based digital elevation models (DEMs) is often left unaddressed for habitat mapping efforts, yet the level of uncertainty becomes critical when studying low-relief environments, such as barrier islands, where centimeters can make a difference in the exposure to physically demanding abiotic conditions (e.g., inundation, salt spray, and wave energy) (Anderson et al., 2016; Young et al., 2011). To address this issue, I assumed two estimates of elevation data uncertainty, which included uncertainty estimated from relative accuracy assessments using in situ Real-Time Kinematic Global Position System (RTK GPS) data and an estimate included in a metadata report that followed the American Society of Photogrammetry and Remote Sensing's (ASPRS) standards that accompanied the lidar data product. These data were used to simulate the propagation of elevation uncertainty into a DEM using Monte Carlo simulations for Dauphin Island, a barrier island along the coast of Alabama, USA. I extracted low-lying lands and intertidal areas from probabilistic outputs from the Monte Carlo simulations using a tidally relevant elevation threshold. These data were compared to low-lying lands and intertidal areas that were extracted from a DEM without any management of uncertainty. I found that the DEMs with the treatment of elevation uncertainty had higher producer's accuracy and user's

accuracy for identifying low-lying areas. For the entire island, the percentage of intertidal areas delineated through an automated extraction increased by up to 80% when using Monte Carlo analyses to treat elevation uncertainty of the lidar data. Results from a sensitivity analysis suggest that it could be reasonable to use error and bias values from literature for similar environments, conditions, and lidar acquisition characteristics in the event that collection of site-specific data is not feasible and/or information in the lidar metadata is insufficient. In this event, I found that bias values may be less sensitive than error, although it is critical to select a positive bias (i.e., DEM elevation overestimates actual elevation) value greater than 50% if the study area has abundant vegetation cover. These results confirmed the findings of others, which suggest that lidar DEMs can have a substantial level of vertical uncertainty within intertidal areas (Buffington et al., 2016; Medeiros et al., 2105; Schmid et al., 2011), and elevation uncertainty should be treated prior to conducting automated extraction of elevation-dependent habitats (Kidwell et al., 2017). The simple probabilistic approach presented in this research should provide insights to researchers for increasing the repeatability, accuracy, and efficiency of the delineation of tidal zones in coastal settings using lidar data. Furthermore, the results from the sensitivity analysis highlight how minor adjustments to the error and bias affect the results of delineating low-lying lands. Researchers can use this information to gauge whether it would be reasonable to use literature-derived error and bias values for similar environments, which could be helpful for instances where the collection of site-specific RTK GPS data is not feasible due to budget constraints or site accessibility. The methodology utilized in this study could be used to develop stand-alone products with the aim of providing land managers with accurate areal coverage of

intertidal areas or to serve as a foundation for the identification of tidal regimes for detailed habitat mapping efforts. The approach outlined in this study should be applicable, with certain calibration, to future technological advancements, such as next-generation lidar sensors and on-demand lidar via unmanned aerial systems (UASs). A byproduct of delineating the upper intertidal boundary is information on the areal coverage of the supratidal/upland zone. On barrier islands, supratidal/upland areas include habitats such as beach, dune, and barrier flat (e.g., meadow, nonvegetated barrier flat, and forest). Monitoring these areas is equally important to resource managers (Zinnert et al., 2016) because they provide important habitats for resident and migratory shorebirds (Galbraith et al., 2014), neotropical migrants (Lester et al., 2016), and sea turtles (Katselidis et al., 2014). A limitation of this effort was that the field data used for the site-specific RTK GPS was collected with a sample design for the validation of a habitat map instead of being customized for elevation uncertainty analyses. Future research could build on this work by collecting data with a sampling design that is more targeted for elevation uncertainty analyses, including sampling vegetated and unvegetated areas proportionally and using systematic transects to capture a gradient of vegetation densities. Lidar intensity data has been shown to enhance habitat classifications in coastal environments (Brennan & Webster, 2006; Chust et al., 2008). Thus, future efforts could also explore how the application of spatially variable error and bias based on lidar intensity enhances this framework.

Barrier islands are dynamic environments that change over time via gradual processes including waves, currents, and tides or rapidly via extreme episodic events, such as storms. Thus, natural resource managers need repeat remote sensing-based

assessments of habitats for monitoring and managing these resources (Kindinger et al., 2013). For the second research objective of this dissertation, I showed how elevation uncertainty and relative topography can be integrated into a methodology for mapping barrier island habitats. I developed a custom 17-class habitat classification scheme for Dauphin Island, Alabama through the review of existing barrier island habitat mapping efforts. This study built on the work of Halls et al. (2018) and Wernette et al. (2016) by integrating the use of relative topography for delineating dunes into a barrier island habitat mapping effort. Storms can shape dune morphology (Sallenger, 2000), thus extreme water levels associated with storms can serve as a reasonable dune elevation threshold. Thus, dunes are also elevation-dependent habitats. In addition to adding the tidal zone delineation from the first research objective, I also used storm water level observations (Zervas, 2013) to produce a probabilistic map with regard to elevations above an extreme water level. This research highlighted the use of elevation uncertainty and landscape position information for semi-automated dune habitat extraction. The probabilistic map with regard to elevations above an extreme water level was used to remove upper slopes and ridges that were identified by the topographic position index (TPI; Weiss, 2001) that were located in low-lying areas, such as a beach berm. This refinement led to an 18% decrease in the areal coverage of potential dune habitat. Next, the potential dune area was refined with manual edits from visual inspection. Collectively all of the dune refinement steps led to a 49% reduction from the original TPI-based potential dunes (i.e., upper slopes and ridges). These findings underscore the importance of refining dunes extracted from relative topography alone. The final habitat map had an overall accuracy of 79.2% and a Kappa statistic of 0.77. Most of the

confusion was associated with hummock dune areas being misclassified as meadow or unvegetated barrier flat. Future efforts should explore if a finer-scaled TPI and visual inspection enhance hummock dune mapping. Another potential opportunity is the use of UASs, which can provide elevation data through structure-from-motion or via onboard lidar (Jaakkola et al., 2010; Lin et al., 2011). Researchers are already using digital surface models created via structure-from-motion for geomorphic feature extraction and habitat classification for coastal beach-dune systems (Sturdivant et al., 2017). Two advantages of using UAS data are the temporal alignment of elevation and imagery data and the ability to collect data with a very high spatial resolution (e.g., spatial resolutions are commonly 15 centimeters or higher). This very high spatial resolution may increase the ability to detect less well-defined dunes, such as hummock dunes, in geospatial data. A few disadvantages of this type of data collection could include limitations with regard to data collection feasibility (i.e., limitations to spatial extent of the data collection and site accessibility) and outliers introduced from the very high spatial resolution data (e.g., increased detection of vegetation canopy shadow). The framework outlined in this work utilized object-based image analysis, which performs well with very high resolution geospatial data (Blaschke et al., 2014). I expect that advancements in sensor technology, such as single photon and Geiger-mode lidar sensors (Stoker et al., 2016) and UAS-based lidar data collection (Jaakkola et al., 2010; Lin et al., 2011), should lead to a greater frequency and coverage of high-quality elevation data for use by scientists and natural resource managers. The Monte Carlo and mapping framework outlined in this study provide a repeatable and more accurate method for automated extraction of elevation-dependent habitats and could be implemented with these data as

well as the orthophotography and airborne topographic lidar used in this study. Collectively, this approach should allow geographers and remote sensing analysts to make better use of the increasingly available high-quality geospatial data for mapping and monitoring barrier island habitats while reducing subjectivity in classes, such as dunes and intertidal habitats. These methods also should increase the overall accuracy of tidal regime information through the treatment of elevation uncertainty.

To make more informed decisions today, natural resource managers rely on models for predictions of likely future alternative states of an area. For the third research objective of this dissertation, I integrated methods and data from my prior research objectives to predict barrier island habitats based on landscape position-habitat linkages identified in the literature (Anderson et al. 2016; Foster et al. 2017; Halls et al., 2018; Young et al. 2011). In this effort, I explored whether machine learning algorithms (i.e., K-nearest neighbor (KNN), support vector machine (SVM), and random forest (RF)) could be used to predict barrier island habitats based on landscape position information for Dauphin Island, Alabama. I used a contemporary habitat map to identify landscape position linkages for habitats, such as beach, dune, woody vegetation, and marsh. I used deterministic accuracy, fuzzy accuracy, and hindcasting to validate the model. Because barrier island habitats can be separated by tidal zones, I developed separate models per tidal zone (i.e., subtidal, intertidal, and supratidal/upland). I found machine learning algorithms were well suited for predicting barrier island habitats using landscape position. The model performance among the KNN, SVM, and RF models was similar for the subtidal zone, but I opted for the KNN model based on a smoother transition from water-estuarine to water-marine. I found that RF was the best model for

the intertidal and supratidal/upland zones. The deterministic overall accuracy for the contemporary model was just under 70% and the fuzzy overall accuracy was just over 80%. I tested whether the model performance was enhanced using post-processing routines, which included noise reduction and the posteriori application of expert rules based on my theoretical understanding of barrier island habitats. While this process introduced some omission error in certain classes, such as water-fresh and dune, the post-processing routines, collectively, tended to enhance the model results. The rationale for this was based on a slight increase in overall accuracy, increases in user's accuracies, and the overall comparison with habitat coverage from the source map used for the training data development. I found that the model was able to generalize well when predicting habitats from historical data (i.e., hindcast). The hindcast deterministic overall accuracy was just under 80% and the fuzzy overall accuracy was over 90%. Engineers and coastal researchers could use a similar approach as the one outlined here to develop landscape position-based habitat models that could be coupled with morphological models to make predictions of future conditions on barrier islands. The models developed in this effort could be applied to future morphology predictions with and without restoration actions to provide important information to natural resource managers for making future-focused management decisions. This could allow planners to utilize a structured decision-making process, such as the one used by Dalyander et al. (2016) to gauge how restoration actions (i.e., including a no-action alternative) could positively or negatively impact habitat resources over time. This information could provide insights to natural resource managers and planners on how a restoration project and even the restoration project placement location may allow or impede natural coastal

processes and provide information critical for making decisions regarding barrier island restoration. The model framework presented here can be calibrated and extended to other islands. While this effort developed a single global model for Dauphin Island, future efforts may explore the utility of developing more localized models based on wave energy settings and morphology. For instance, the orientation of an island could be used as an indicator of the need for a separate model. Additionally, topographic state metrics could be used to develop meaningful model zones (Zinnert et al., 2017) using methods similar to that of Monge and Stallins (2016). Data-driven, machine learning algorithms are powerful tools for teasing out patterns and relationships in data; however, one potential issue is that they require the assumption that the data used to train the model is representative of the phenomena being modeled. To develop a more robust training dataset, future efforts could aim to augment time for space by developing additional training data from historical habitat maps paired with landscape position information from that time. Additionally, details regarding precedent conditions relating to storminess (e.g., magnitude, frequency, and temporal lag) could be added to such a training dataset using an approach similar to Mickey et al. (2017) to characterize storminess for a period. While this research used default MATLAB algorithm presets, a more robust training dataset may allow for meaningful optimization of model tuning parameters. Researchers could also evaluate whether the use of longer-term, larger-scale variables similar to the ones used by Gutierrez et al. (2015), such as island width and historical shoreline erosion rates, enhances barrier island habitat model predictions. Finally, more research is needed to explore how landscape position and temporal lag from disturbances impact the probability of an area being vegetated. This would provide

information that could be combined with the general habitat predictions from this research to enhance geomorphic models, such as for refining friction coefficients that are used in morphological modeling of barrier island environments (Feagin et al., 2015; Mendoza et al., 2017; Passeri et al., 2018).

In conclusion, barrier islands are important environments due to the numerous ecosystems goods and services they provide (Barbier et al., 2011). These islands are unique coastal systems due to their dynamic nature resulting from many abiotic factors operating at a wide range of spatiotemporal scales (Young et al., 2011; Zinnert et al., 2017). For instance, barrier island geomorphology and habitat coverage can change rapidly because of storms or gradually from tides and currents. Additionally, wave-dominated barrier islands, such as Dauphin Island, are often long and narrow (McBride et al., 2013), which influences the importance of spatial scale of geospatial data in both the cross-shore and alongshore directions. Collectively, these traits make barrier islands both a challenging and fascinating research setting. Barrier island geomorphology and habitat configuration are an expression of abiotic forcings on a barrier island (Young et al., 2011; Zinnert et al., 2017). Additionally, wildlife utilize barrier island habitats for important portions of their life cycle, including resident and migratory shorebirds (Galbraith et al., 2014), neotropical migrants (Lester et al., 2016), and sea turtles (Katselidis et al., 2014). Thus, natural resource managers are concerned with understanding how habitats on barrier islands are changing over time in addition to insights on potential future alternative states of these systems. Collectively, this dissertation highlighted how the incorporation of landscape position information and elevation uncertainty can be used to enhance barrier island habitat mapping and

modeling. The habitat mapping components outlined in Chapters 2 and 3 provide a roadmap for efficiently processing remote sensing data while also enhancing the semantics of barrier island habitat maps through the use of landscape position information and treatment of elevation uncertainty. Together these frameworks can help enhance map comparison through time and map conflation for regional analyses. The habitat model framework outlined in Chapter 4 showed how landscape position information extracted from lidar data can be used to model barrier island habitats using machine learning algorithms. This framework can be calibrated for other barrier islands and data including, hydrodynamic geomorphologic model outputs. When coupled with hydrodynamic geomorphologic model outputs, researchers could use this habitat model framework to forecast barrier island habitats under alternative scenarios with regard to sea-level rise, storminess, and restoration actions. In order to create a comprehensive research agenda for barrier island habitats, it is important to address the unique spatiotemporal scales of barrier island evolution, which requires the inclusion of a range of temporal scales (e.g., every few weeks to 10 or more years) and spatial scales (e.g., very high to moderate spatial resolutions). Building on the work outlined in this dissertation, my future research will focus on: (1) extending the barrier island habitat model framework to forecast habitats based on landscape position information extracted from hydrodynamic geomorphic model outputs; (2) exploring the tradeoffs and opportunities of using high-resolution UAS data for barrier island habitat mapping; and (3) studying overwash impacts to dune and barrier flat habitats to develop a predictive model for estimating vegetation cover in these habitats.

REFERENCES

Acosta, A., Blasi, C., Carranza, M. L., Di Martino, P., Paura, B., & Tolve, E. (2003). Il programma CORINE Land-Cover: un esempio per il bacino del F. Biferno (Molise). *Informatore Botanico Italiano, 35*, 21-29.

Acosta, A., Carranza, M. L., & Izzi, C. F. (2005). Combining land cover mapping of coastal dunes with vegetation analysis. *Applied Vegetation Science, 8*(2), 133-138. doi:10.1111/j.1654-109X.2005.tb00638.x

Alizad, K., Hagen, S. C., Morris, J. T., Medeiros, S. C., Bilskie, M. V., & Weishampel, J. F. (2016). Coastal wetland response to sea-level rise in a fluvial estuarine system. *Earth's Future, 4*, 483-497. doi:10.1002/2016EF000385

American Society for Photogrammetry and Remote Sensing. (2015). ASPRS positional Accuracy Standards for Digital Geospatial Data, November 2014. *Photogrammetric Engineering & Remote Sensing, 81*(3), A1-A26. doi:10.14358/PERS.81.3.A1-A26

Anderson, C. P., Carter, G. A., & Funderburk, W. R. (2016). The Use of Aerial RGB Imagery and LIDAR in Comparing Ecological Habitats and Geomorphic Features on a Natural Versus Man-Made Barrier Island. *Remote Sensing, 8*, 602. doi:10.3390/rs8070602

Arundel, S. T., Archuleta, C. M., Philips, L. A., Roche, B. L., & Constance, E. W. (2015). 1-M Digital Elevation Model Specification. In H. K. Heidemann (Ed.), *U.S. Geological Survey Techniques and Methods*. Reston, VA: U.S. Geological Survey. Retrieved from U.S. Geological Survey website: https://pubs.er.usgs.gov/publication/tm11B7

Bachmann, C. M., Donato, T. F., Lamela, G. M., Rhea, W. J., Bettenhausen, M. H., Fusina, R. A., . . . Truitt, B. R. (2002). Automatic Classification of Land Cover on Smith Island, VA, using HyMAP imagery. *IEEE Transactions on Geoscience and Remote Sensing, 40*(10), 2313-2330. doi:10.1109/TGRS.2002.804834

Ball, G. H., & Hall, D. J. (1965). ISODATA, a novel method of data anlysis and pattern classification (Tech. rept. NTIS AD 699616). Stanford, CA: Stanford Research Institute.

Barandela, R., & Juarez, M. (2002). Supervised classification of remotely sensed data with ongoing learning capability. *International Journal of Remote Sensing, 23*(22), 4965-4970. doi:10.1080/01431160110087944

Barbier, E. B., Hacker, S. D., Kennedy, C., Koch, E. W., Stier, A. C., & Silliman, B. R. (2011). The value of estuarine and coastal ecosystem services. *Ecological Monographs, 81*(2), 169-193. doi:10.1890/10-1510.1

Blaschke, T., Hay, G. J., Kelly, M., Lang, S., Hofmann, P., Addink, E., . . . Tiede, D. (2014). Geographic Object-Based Image Analysis – Towards a new paradigm. *ISPRS Journal of Photogrammetry and Remote Sensing of Environment, 87*, 180-191. doi:10.1016/j.isprsjprs.2013.09.014

Bonisteel, J. M., Nayegandhi, A., Wright, C. W., Brock, J. C., & Nagle, D. B. (2009). *Experimental Advanced Airborne Research Lidar (EAARL) Data Processing Manual* (Open-File Report 2009-1078). Retrieved from U.S. Geological Survey website: https://pubs.usgs.gov/of/2009/1078/pdf/OFR2009-1078.pdf

Breiman, L. (2001). Statistical Modeling: The Two Cultures. *Statistical Science, 16*(3), 199-231. doi:10.1214/ss/1009213726

Brennan, R., & Webster, T. L. (2006). Object-oriented land cover classification of lidar-derived surfaces. *Canadian Journal or Remote Sensing, 32*, 162-172. doi:10.5589/m06-015

Brock, J. C., Krabill, W. B., & Sallenger, A. H. (2004). Barrier Island Morphodynamic Classification Based on Lidar Metrics for North Assateague Island, Maryland. *Journal of Coastal Research, 20*(2), 498-509. doi:10.2112/1551-5036(2004)020[0498:BIMCBO]2.0.CO;2

Brock, J. C., & Purkis, S. J. (2009). The Emerging Role of Lidar Remote Sensing in Coastal Research and Resource Management. *Journal of Coastal Research, SI53*, 1-5. doi:10.2112/SI53-001.1

Brownett, J. M., & Mills, R. S. (2017). The development and application of remote sensing to monitor sand dune habitats. *Journal of Coastal Conservation, 21*(5), 643-656. doi:10.1007/s11852-017-0504-x

Buffington, K. J., Dugger, B. D., Thorne, K. M., & Takekawa, J. Y. (2016). Statistical correction of lidar-derived digital elevation models with multispectral airborne imagery in tidal marshes. *Remote Sensing of Environment, 186*, 616-625. doi:10.1016/j.rse.2016.09.020

Byrnes, M. R., Baker, J. L., & Li, F. (2002). *Quantifying potential measurement errors and uncertainties associated with bathymetric change analysis* (ERDC/CHL CHETN-IV-50). Vicksburg, MS: U.S. Army Corps of Engineers, Engineer Research and Development Center, Coastal and Hydraulics Laboratory. Retrieved from U.S. Army Corps of Engineers website: https://apps.dtic.mil/dtic/tr/fulltext/u2/a588888.pdf

Campbell, A., & Wang, Y. (2018). Examining the Influence of Tidal Stage on Salt Marsh Mapping Using High-Spatial-Resolution Satellite Remote Sensing and Topobathymetric LiDAR. *IEEE Transactions on Geoscience and Remote Sensing*, *56*(9), 1-8. doi:10.1109/TGRS.2018.2810503

Campbell, A., Wang, Y., Christiano, M., & Stevens, S. (2017). Salt Marsh Monitoring in Jamaica Bay, New York from 2003 to 2013: A Decade of Change from Restoration to Hurricane Sandy. *Remote Sensing*, *9*(2), 131. doi:10.3390/rs9020131

Carruthers, T. J. B., Berkert, K., Schupp, C. A., Saxby, T., Kumer, J. P., Thomas, J., . . . Zimmerman, C. S. (2013). Improving management of a mid-Atlantic coastal barrier island through assessment of habitat condition. *Estuarine Coastal and Shelf Science, 116*, 74-86. doi:10.1016/j.ecss.2012.08.012

Chust, G., Galparsoro, I., Borja, A., Franco, J., & Uriate, A. (2008). Coastal and estuarine habitat mapping, using LIDAR height and intensity and multispectral imagery. *Estuarine, Coastal and Shelf Science, 78*(4), 633-643. doi:10.1016/j.ecss.2008.02.003

Cohen, J. (1960). A Coefficient of Agreement for Nominal Scales. *Educational and Psychological Measurement, 20*, 37-46. doi:10.1177/001316446002000104

Congalton, R. G., & Green, K. (2009). *Assessing the accuracy of remotely sensed data principles and practices* (Second ed.). Boca Raton, FL: CRC Press.

Constanza, R., de Groot, R., Sutton, P., van der Ploeg, S., Anderson, S. J., Kubiszewski, I., . . . Turner, R. K. (2014). Changes in the global value of ecosystem services. *Global Environmental Change, 26*, 152-158. doi:10.1016/j.gloenvcha.2014.04.002

Cooper, H. M., & Chen, Q. (2013). Incorporating uncertainty of future sea-level rise estimates into vulnerability assessment: A case study in Kahului, Maui. *Climatic Change, 121*(4), 635-647. doi:10.1007/s10584-013-0987-x

Cooper, H. M., Fletcher, C. H., Chen, Q., & Barbee, M. M. (2013). Sea-level rise vulnerability mapping for adaptation decisions using lidar DEMs. *Progress in Physical Geography, 37*(6), 745-766. doi:10.1177/0309133313496835

Cowardin, L. M., Carter, V., Golet, F. C., & LaRoe, E. T. (1979). *Classification of wetlands and deepwater habitats of the United States* (FWS/OBS-79/31). Washington, D.C.: U.S. Fish and Wildlife Service. Retrieved from U.S. Fish and Wildlife website: https://www.fws.gov/wetlands/Documents/Classification-of-Wetlands-and-Deepwater-Habitats-of-the-United-States.pdf

Dalyander, P. S., Meyers, M., Mattsson, B., Steyer, G., Godsey, E., McDonald, J., . . . Ford, M. (2016). Use of structured decision-making to explicitly incorporate environmental process understanding in management of coastal restoration projects: Case study on barrier islands of the northern Gulf of Mexico. *Journal of Environmental Management, 183*(3), 497-509. doi:10.1016/j.jenvman.2016.08.078

Dalyander, P. S., Mickey, R. C., Passeri, D. L., & Plant, N. G. (in review). Development of an Empirical Dune Growth Model and Use in Evaluating Barrier Island Recovery from Storms. *Coastal Engineering*.

Dayton, P. K. (1972). *Toward an understanding of community resilience and the potential effects of enrichments to the benthos at McMurdo Sound, Antarctica.* Proceedings from the '72 Colloquium on Conservation Problems in Antarctica. Blacksburg, VA: Allen Press.

De Reu, J., Bourgeois, J., Bats, M., Zwertvaegher, A., Gelorini, V., De Smedt, P., . . . Crombé, P. (2013). Application of the topographic position index to heterogeneous landscapes. *Geomorphology, 186*(15), 39-49. doi:10.1016/j.geomorph.2012.12.015

DeWitt, N. T., Stalk, C. A., Flocks, J. G., Bernier, J. C., Kelso, K. W., Fredericks, J. J., & Tuten, T. (2015). *Single-beam bathymetry data collected in 2015 nearshore Dauphin Island, Alabama* [Data file]. doi:10.5066/f7bz648w

Dobson, J. E., Bright, E. A., Ferguson, R. L., Field, D. W., Wood, L. L., Haddad, K. D., . . . Thomas, J. P. (1995). *NOAA Coastal Change Analysis Program (C-CAP): Guidance for Regional Implementation* (NOAA Technical Report NMFS 123). Washington, D.C.: National Oceanic and Atmospheric Administration. Retrieved from National Oceanic and Atmospheric Administration website: https://repository.library.noaa.gov/view/noaa/6204

Dronova, I. (2015). Object-Based Image Analysis in Wetland Research: A Review. *Remote Sensing*,*7*(5), 6380-6413. doi:10.3390/rs70506380

Enwright, N. M., Borchert, S. M., Day, R. H., Feher, L. C., Osland, M. J., Wang, L., & Wang, H. (2017). *Barrier Island Habitat Map and Vegetation Survey—Dauphin Island, Alabama, 2015* (U.S. Geological Survey Open-File Report 2017–1083). Reston, VA: U.S. Geological Survey. doi:10.3133/ofr20171083

Enwright, N. M., Griffith, K. T., & Osland, M. J. (2016). Barriers to and opportunities for landward migration of coastal wetlands with sea-level rise. *Frontiers in Ecology and the Environment, 14*(6), 307-316. doi:10.1002/fee.1282

Enwright, N. M., SooHoo, W. M., Dugas, J. L., Lee, D. M., & Borrok, P. S. (2018a). *Louisiana Barrier Island Comprehensive Monitoring Program – habitat mapping* [Data file]. doi:10.5066/F7XP7440.

Enwright, N. M., Wang, L., Borchert, S. M., Day, R. H., Feher, L. C., & Osland, M. J. (2018b). The Impact of Lidar Elevation Uncertainty on Mapping Intertidal Habitats on Barrier Islands. *Remote Sensing, 10*(1), 5. doi:10.3390/rs10010005

Enwright, N. M., Wang, L., Borchert, S. M., Day, R. H., Feher, L. C., & Osland, M. J. (in press). Advancing barrier island habitat mapping using landscape position information and elevation uncertainty. *Progress in Physical Geography*.

Feagin, R. A., Figlus, J., Zinnert, J. C., Sigren, J., Martínez, M. L., Silva, R., . . . Carter, G. (2015). Going with the flow or against the grain? The promise of vegetation for protecting beaches, dunes, and barrier islands from erosion. *Frontiers in Ecology and the Environment, 13*(4), 203-210. doi:10.1890/140218

Feagin, R. A., Smith, W. K., Psuty, N. P., Young, D. R., Martínez, L. M., Carter, G. A., . . . Koske, R. E. (2010). Barrier Islands: Coupling Anthropogenic Stability with Ecological Sustainability. *Journal of Coastal Research, 26*(6), 987-992. doi:10.2112/09-1185.1

Fearnley, S., Brien, L., Martinez, L., Miner, M., Kulp, M., & Penland, S. (2009). *Louisiana Barrier Island Comprehensive Monitoring Program (BICM), Volume 5: Chenier Plain, South-Central Louisiana, and Chandeleur Islands, Habitat mapping and change analysis 1996 to 2005, Part 1: Methods for habitat mapping and change analysis 1996 to 2005.* Retrieved from Louisiana Coastal Protection and Restoration Authority website: https://www.lacoast.gov/reports/project/BICM5_part1_habitat%20methods.pdf

Feranec, J., Solin, L., Kopecka, M., Otahel, J., Kupkova, L., Stych, P., . . . Brodsky, L. (2014). Analysis and expert assessment of the semantic similarity between land cover classes. *Progress in Physical Geography, 38*(3), 301-327. doi:10.1177%2F0309133314532001

Foster, T. E., Stolen, E. D., Hall, C. R., Schaub, R., Duncan, B. W., Hunt, D. K., & Drese, J. H. (2017). Modeling vegetation community responses to sea-level rise on barrier island systems: A case study on the Cape Canaveral barrier island complex, Florida, USA. *PLoS ONE, 12*(8), e0182605. doi:10.1371/journal.pone.0182605

Galbraith, H., DesRochers, D. W., Brown, S., & Reed, J. M. (2014). Predicting Vulnerabilities of North American Shorebirds to Climate Change. *PLoS ONE, 9*(9), e108899. doi:10.1371/journal.pone.0108899

Gao, J., Chen, H., Zhang, Y., & Zha, Y. (2004). Knowledge-Based Approaches to Accurate Mapping of Mangroves from Satellite Data. *Photogrammetric Engineering & Remote Sensing, 70*(11), 1241-1248. doi:10.14358/PERS.70.11.1241

Gibson, D. J., & Looney, P. B. (1992). Variation in Vegetation Classification on Perdido Key, a Barrier Island off the Coast of the Florida Panhandle. *Journal of Coastal Research, 8*(4), 943-956.

Gieder, K. D., Karpanty, S. M., Fraser, J. D., Catlin, D. H., Gutierrez, B. T., Plant, N. G., . . . Thieler, E. R. (2014). A Bayesian network approach to predicting nest presence of the federally-threatened piping plover (*Charadrius melodus*) using barrier island features. *Ecological Modelling, 276*, 38-50. doi:10.1016/j.ecolmodel.2014.01.005

Guo, Q., Kelly, M., & Graham, C. H. (2005). Support vector machines for predicting distribution of Sudden Oak Death in California. *Ecological Modelling, 182*(1), 75-90. doi:10.1016/j.ecolmodel.2004.07.012

Gutierrez, B. T., Plant, N. G., Thieler, E. R., & Tureck, A. (2015). Using a Bayesian network to predict barrier island geomorphologic characteristics. *Journal of Geophysical Research: Earth Surface, 120*(12), 2452-2475. doi:10.1002/2015JF003671

Guy, K. K. (2015). *Barrier island shorelines extracted from Landsat imagery* (U.S. Geological Survey Open-File Report 2015-1179). Reston, VA: U.S. Geological Survey. doi:10.3133/ofr20151179

Halls, J. N., Frishman, M. A., & Hawkes, A. D. (2018). An Automated Model to Classify Barrier Island Geomorphology Using Lidar Data and Change Analysis. *Remote Sensing, 10*(7), 1109. doi:10.3390/rs10071109

Hansen, J., Sato, M., Hearty, P., Ruedy, R., Kelley, M., Masson-Delmotte, V., . . . Lo, K.-W. (2016). Ice melt, sea level rise and superstorms: evidence from paleoclimate data, climate modeling, and modern observations that 2 °C global warming could be dangerous. *Atmospheric Chemistry and Physics, 16*, 3761-3812. doi:10.5194/acp-16-3761-2016

Hantson, W., Kooistra, L., & Slim, P. A. (2012). Mapping invasive woody species in coastal dunes in the Netherlands: a remote sensing approach using LIDAR and high-resolution aerial photographs. *Applied Vegetation Science, 15*(4), 536-547. doi:10.1111/j.1654-109X.2012.01194.x

Heidemann, H. K. (2014). Lidar base specification (ver. 1.3, February 2018). In H. K. Heidemann (Ed.), *U.S. Geological Survey Techniques and Methods*. Reston, VA: U.S. Geological Survey. Retrieved from U.S. Geological Survey website: https://pubs.er.usgs.gov/publication/tm11B4

Henderson, R. E., Nelson, P. R., Long, J. W., & Smith, C. G. (2017). *Vector Shorelines and Associated Shoreline Change Rates Derived from Lidar and Aerial Imagery for Dauphin Island, Alabama: 1940-2015* [Data file]. doi:10.5066/F7T43RB5

Heumann, B. W. (2011). An Object-Based Classification of Mangroves Using a Hybrid Decision Tree—Support Vector Machine Approach. *Remote Sensing, 3*(11), 2440-2460. doi:10.3390/rs3112440

Hodgson, M. E., & Bresnahan, P. (2004). Accuracy of Airborne Lidar-Derived Elevation: Empirical Assessment and Error Budget. *Photogrammetric Engineering & Remote Sensing, 70*(3), 331-339. doi:10.14358/PERS.70.3.331

Homer, C. G., Dewitz, J. A., Yang, L., Jin, S., Danielson, P., Xian, G., . . . Megown, K. (2015). Completion of the 2011 National Land Cover Database for the conterminous United States – Representing a decade of land cover change information. *Photogrammetric Engineering and Remote Sensing, 81*(5), 345-354. doi:10.14358/PERS.81.5.345

Hudak, A. T., Evans, J. S., & Smith, A. M. S. (2009). LiDAR Utility for Natural Resource Managers. *Remote Sensing, 1*(4), 934-951. doi:10.3390/rs1040934

Hugenholtz, C. H., Levin, N., Barchyn, T. E., & Baddock, M.C. (2012). Remote sensing and spatial analysis of aeolian sand dunes: A review and outlook. *Earth-Science Reviews, 111*(3-4), 319-334. doi:10.1016/j.earscirev.2011.11.006

Hunter, G. J., & Goodchild, M. F. (1995). Dealing with error in spatial databases: A simple case study. *Photogrammetric Engineering & Remote Sensing, 61*(5), 529-537.

Jaakkola, A., Hyyppä, J., Kukko, A., Yu, X., Kaartinen, H., Lehtomäki, M., & Lin, Y. (2010). A low-cost multi-sensoral mobile mapping system and its feasibility for tree measurements. *ISPRS International Journal of Photogrammetry and Remote Sensing, 65*(6), 514-522. doi:10.1016/j.isprsjprs.2010.08.002

James, G., Witten, D., Hastie, T., & Tibshirani, R. (2013). *An Introduction to Statistical Learning: with Applications in R*. New York, NY: Springer-Verlag New York.

Jeter, G. W., Jr., & Carter, G. A. (2015). Habitat change on Horn Island, Mississippi, 1940-2010, determined from textural features in panchromatic vertical aerial imagery. *Geocarto International, 31*(9), 1-10. doi:10.1080/10106049.2015.1094527

Katselidis, K. A., Schofield, G. S., Stamou, G., Dimopoulos, P., & Pantis, J. D. (2014). Employing sea-level rise scenarios to strategically select sea turtle nesting habitat important for long-term management at a temperate breeding area. *Journal of Experimental Marine Biology and Ecology, 450*, 47-54. doi:10.1016/j.jembe.2013.10.017

Kidwell, D. M., Dietrich, J. C., Hagen, S. C., & Medeiros, S. C. (2017). An earth's future special collection: Impacts of the coastal dynamics of sea level rise on low-gradient coastal landscapes. *Earth's Future, 5*(1), 2-9. doi:10.1002/2016EF000493

Kindinger, J. L., Buster, N. A., Flocks, J. G., Bernier, J. C., & Kulp, M. A. (2013). *Louisiana Barrier Island Comprehensive Monitoring (BICM) Program Summary Report: Data and Analyses 2006 through 2010* (U.S. Geological Survey Open-File Report 2013-1083). Reston, VA: U.S. Geological Survey. Retrieved from U.S. Geological Survey website: https://pubs.usgs.gov/of/2013/1083/pdf/ofr2013-1083.pdf

Klemas, V. (2013). Remote sensing of emergent and submerged wetlands: An overview. *International Journal of Remote Sensing, 34*(18), 6286-6320. doi:10.1080/01431161.2013.800656

Knutson, T. R., McBride, J. L., Chan, J., Emanuel, K., Holland, G., Landsea, C., . . . Sugi, M. (2010). Tropical cyclones and climate change. *Nature Geoscience, 3*, 157-163. doi:10.1038/ngeo779

Lea, C., & Curtis, A. C. (2010). *Thematic Accuracy Assessment Procedures, National Park Service Vegetation Inventory, Version 2.0* (Natural Resource Report NPS/NRPC/NRR—2010/204). Fort Collins, CO: U.S. National Park Service. Retrieved from U.S. Geological Survey website: https://www1.usgs.gov/vip/standards/NPSVI_Accuracy_Assessment_Guidelines_ver2.pdf

Leatherman, S. P. (1979). *Barrier Island Handbook*. Amherst, MA: National Park Service.

Leon, J. X., Heuvelink, G. B. M., & Phinn, S. R. (2014). Incorporating DEM Uncertainty in Coastal Inundation Mapping. *PLoS ONE, 9*(9), e108727. doi:10.1371/journal.pone.0108727

Lester, L. A., Ramierez, M. G., Kneidel, A. H., & Heckscher, C. M. (2016). Use of a Florida Gulf Coast Barrier Island by Spring Trans-Gulf Migrants and the Projected Effects of Sea Level Rise on Habitat Availability. *PLoS ONE, 11*(3), e0148975. doi:10.1371/journal.pone.0148975

Lin, Y., Hyyppä, J., & Jaakkola, A. (2011). Mini-UAV-Borne LIDAR for Fine-Scale Mapping. *IEEE Geoscience and Remote Sensing Letters, 8*(3), 426-430. doi:10.1109/LGRS.2010.2079913

Liu, H., Sherman, D., & Gu, S. (2007). Automated Extraction of Shorelines from Airborne Light Detection and Ranging Data and Accuracy Assessment Based on Monte Carlo Simulation. *Journal of Coastal Research, 23*(6), 1359-1369. doi:10.2112/05-0580.1

Lucas, K. L., & Carter, G. A. (2010). Decadal Changes in Habitat-Type Coverage on Horn Island, Mississippi, U.S.A. *Journal of Coastal Research, 26*, 1142-1149. doi:10.2112/JCOASTRES-D-09-00018.1

Lucas, K. L., & Carter, G. A. (2013). Change in distribution and composition of vegetated habitats on Horn Island, Mississippi, northern Gulf of Mexico, in the initial five years following Hurricane Katrina. *Geomorphology, 199*, 129-137. doi:10.1016/j.geomorph.2012.11.010

Ma, L., Manchun, L., Xiaoxue, M., Cheng, L., Du, P., & Liu, Y. (2017). A review of supervised object-based land-cover image classification. *ISPRS Journal of Photogrammetry and Remote Sensing, 130*, 277-293. doi:10.1016/j.isprsjprs.2017.06.001

Madden, M., Jones, D., & Vilcheck, L. (1999). Photointerpretation key for the Everglades vegetation classification system. *Photogrammetry Engineering & Remote Sensing, 65*(2), 171-177.

Manton, M. G., Angelstam, P., & Mikusiński, G. (2005). Modelling habitat suitability for deciduous forest focal species – A sensitivity analysis using different satellite land cover data. *Landscape Ecology, 20*(7), 827-839. doi:10.1007/s10980-005-3703-z

Maxa, M., & Bolstad, P. (2009). Mapping northern wetlands with high resolution satelite images and lidar. *Wetlands, 29*, 248-260. doi:10.1672/08-91.1

Mcbride, R. A., Anderson, J. B., Buynevich, I. V., Cleary, W., Fenster, M. S., Fitzgerald, D. M., . . . Wang, P. (2013). Morphodynamics of Barrier Systems: A Synthesis. In D. J. Sherman (Ed.), *Treatise on Geomorphology* (Vol. Coastal Geomorphology, pp. 166-244). San Diego: Academic Press. doi:10.1016/B978-0-12-374739-6.00279-7

McCarthy, M. J., & Halls, J. N. (2014). Habitat Mapping and Change Assessment of Coastal Environments: An Examination of WorldView-2, QuickBird, and IKONOS Satellite Imagery and Airborne LiDAR for Mapping Barrier Island Habitats. *ISPRS International Journal of Geo-Information, 3*(1), 297-325. doi:10.3390/ijgi3010297

Medeiros, S., Hagen, S., Weishampel, J., & Angelo, J. (2015). Adjusting Lidar-Derived Digital Terrain Models in Coastal Marshes Based on Estimated Aboveground Biomass Density. *Remote Sensing, 7*(4), 3507-3525. doi:10.3390/rs70403507

Mendoza, E., Odériz, I., Martínez, M. L., & Silva, R. (2017). Measurements and Modelling of Small Scale Processes of Vegetation Preventing Dune Erosion. *Journal of Coastal Research, SI77*, 19-28. doi:10.2112/SI77-003.1

Meng, X., Currit, N., & Zhao, K. (2010). Ground Filtering Algorithims for Airborne LiDAR Data: A Review of Critical Issues. *Remote Sensing, 2*(3): 833-860. doi:10.3390/rs2030833

Meng, X., Wang, L., & Currit, N. (2009). Morphology-based Building Detection from Airborne Lidar Data. *Photogrammetric Engineering & Remote Sensing, 75*(4), 437-442. doi:10.14358/PERS.75.4.437

Mickey, R. C., Long, J. W., Plant, N. G., Thompson, D. M., & Dalyander, P. S. (2017). *A Methodology for Modeling Barrier Island Storm-Impact Scenarios* (U.S. Geological Survey Open-File Report 2017-1009). Reston, VA: U.S. Geological Survey. doi:10.3133/ofr20171009

Mitsch, W. J., & Wilson, R. F. (1996). Improving the Success of Wetland Creation and Restoration with Know-How, Time, and Self-Design. *Ecological Applications, 6*(1), 77-83.

Monge, J. A., & Stallins, J. A. (2016). Properties of dune topographic state space for six barrier islands of the U.S. Southeastern Atlantic Coast. *Physical Geography, 37*(6), 452-475. doi:10.1080/02723646.2016.1230041

Morton, R. A. (2008). Historical changes in the Mississippi-Alabama barrier-island chain and the roles of extreme storms, sea level, and human activities. *Journal of Coastal Research, 24*(6), 1587-1600. doi:10.2112/07-0953.1

Myint, S. W., Gober, P., Brazel, A., Grossman-Clarke, S., & Weng, Q. (2011). Per-pixel vs. object-based classification of urban land cover extraction using high spatial resolution imagery. *Remote Sensing of Environment, 115*(5), 1145-1161. doi:10.1016/j.rse.2010.12.017

NOAA. (2013). Extreme Water Levels 8735180 Dauphin Island, AL webpage. Retrieved from https://tidesandcurrents.noaa.gov/est/est_station.shtml?stnid=8735180

Oertel, G. F. (1985). The barrier island system. *Marine Geology, 63*(1-4), 1-18. doi:10.1016/0025-3227(85)90077-5

O'Neil-Dunne, J., MacFaden, S., & Royar, A. (2014). A Versatile, Production-Oriented Approach to High-Resolution Tree-Canopy Mapping in Urban and Suburban Landscapes Using GEOBIA and Data Fusion. *Remote Sensing, 6*(12), 12837–12865. doi:10.3390/rs61212837

Otvos, E. G., & Carter, G. A. (2008). Hurricane Degradation—Barrier Development Cycles, Northeastern Gulf of Mexico: Landform Evolution and Island Chain History. *Journal of Coastal Research, 24*(2), 463-479. doi:10.2112/06-0820.1

Parker, B. B. (2003). The Difficulties in Measuring a Consistently Defined Shoreline—The Problem of Vertical Referencing. *Journal of Coastal Research, SI38*, 44-56.

Passeri, D. L., Long, J. W., Plant, N. G., Bilskie, M. V., & Hagen, S. C. (2018). The influence of bed friction variability due to land cover on storm-driven barrier island morphodynamics. *Coastal Engineering, 132*, 82-94. doi:10.1016/j.coastaleng.2017.11.005

Pilkey, O. H. J., & Cooper, J. A. G. (2014). *The Last Beach*. Durham, NC: Duke University Press Books.

Plant, N. G., Thieler, E. R., & Passeri, D. L. (2016). Coupling centennial-scale shoreline change to sea-level rise and coastal morphology in the Gulf of Mexico using a Bayesian network. *Earth's Future, 4*(5), 143-158. doi:10.1002/2015EF000331

Poulter, B., & Halpin, P. N. (2008). Raster modelling of coastal flooding from sea-level rise. *International Journal of Geographical Information Science, 22*(2), 167-182. doi:10.1080/13658810701371858

Prasad, A. M., Iverson, L. R., & Liaw, A. (2006). Newer Classification and Regression Tree Techniques: Bagging and Random Forests for Ecological Prediction. *Ecosystems, 9*(2), 181-199. doi:10.1007/s10021-005-0054-1

Rogan, J., Franklin, J., & Roberts, D. A. (2002). A comparison of methods for monitoring multitemporal vegetation change using Thematic Mapper imagery. *Remote Sensing of Environment, 80*(1), 143-156. doi:10.1016/S0034-4257(01)00296-6

Roland, R. M., & Douglass, S. L. (2005). Estimating wave tolerance of *Spartina alterniflora* in coastal Alabama. *Journal of Coastal Research, 21*(3), 453-463. doi:10.2112/03-0079.1

Sallenger, A. H. (2000). Storm impact scale for barrier islands. *Journal of Coastal Research, 16*(3), 890-895.

Schile, L. M., Callaway, J. C., Morris, J. T., Stralberg, D., Parker, V. T., & Kelly, M. (2014). Modeling Tidal Marsh Distribution with Sea-Level Rise: Evaluating the Role of Vegetation, Sediment, and Upland Habitat in Marsh Resliency. *PLoS ONE, 9*, e88760. doi:10.1371/journal.pone.0088760

Schmid, K. A., Hadley, B. C., & Wijekoon, N. (2011). Vertical Accuracy and Use of Topographic Lidar Data in Coastal Marshes. *Journal of Coastal Research, 27*(6A), 116-132. doi:10.2112/JCOASTRES-D-10-00188.1

Shumeli, G. (2010). To Explain or to Predict? *Statistical Science, 25*(3), 289-310. doi: 10.1214/10-STS330

Stockdon, H. F., Doran, K. J., Thompson, D. M., Sopkin, K. L., & Sallenger, A. H. (2012). *National Assessment of Hurricane-Induced Coastal Erosion Hazards—Gulf of Mexico* (U.S. Geological Survey Open-File Report 2012-1084). Reston, VA: U.S. Geological Survey. doi:10.3133/ofr20121084

Stoker, J. M., Abdullah, Q. A., Nayegandhi, A., & Winehouse, J. (2016). Evaluation of Single Photon and Geiger Mode Lidar for the 3D Elevation Program. *Remote Sensing, 8*(9), 767. doi:10.3390/rs8090767

Strahler, A. H. (1980). The use of prior probabilities in maximum likelihood classification of remotely sensed data. *Remote Sensing of Environment*, *10*(2), 135-163. doi:10.1016/0034-4257(80)90011-5

Sturdivant, E. J., Lentz, E. E., Thieler, E. R., Farris, A. S., Weber, K. M., Remsen, D. P., . . . Henderson, R. E. (2017). UAS-SfM for Coastal Research: Geomorphic Feature Extraction and Land Cover Classification from High-Resolution Elevation and Optical Imagery. *Remote Sensing, 9*(10), 1020. doi:10.3390/rs9101020

Stutz, M. L., & Pilkey, O. H. (2011). Open-Ocean Barrier Islands: Global Influence of Climatic, Oceanographic, and Depositional Settings. *Journal of Coastal Research, 27*(2), 207-222. doi:10.2112/09-1190.1

Su, J., & Bork, E. (2006). Influence of Vegetation, Slope, and Lidar Sampling Angle on DEM Accuracy. *Photogrammetric Engineering & Remote Sensing, 72*(11), 1265-1274. doi:10.14358/PERS.72.11.1265

Sugarbaker, L. J., Constance, E. W., Heidemann, H. K., Jason, A. L., Lukas, V., Saghy, D. L., & Stoker, J. M. (2014). *The 3D Elevation Program Initiative—A Call For Action* (U.S. Geological Survey Circular 1399). Reston, VA: U.S. Geological Survey. doi:10.3133/cir1399

Terando, A. J., Costanza, J., Belyea, C., Dunn, R. R., McKerow, A., & Collazo, J. A. (2014). The Southern Megalopolis: Using the Past to Predict the Future of Urban Sprawl in the Southeast U.S. *PLoS ONE, 9*(7), e102261. doi:10.1371/journal.pone.0102261

Thatcher, C. A., Brock, J. C., Danielson, J. J., Poppenga, S. K., Gesch, D. B., Palaseanu-Lovejoy, M. E., . . . Gibbs, A. E. (2016). Creating a Coastal National Elevation Database (CoNED) for Science and Conservation Applications. *Journal of Coastal Research, SI76*, 64-74. doi:10.2112/SI76-007

Timm, B. C., & McGarigal, K. (2012). Fine-scale remotely-sensed cover mapping of coastal dune and salt marsh ecosystems at Cape Cod National Seashore using Random Forests. *Remote Sensing of Environment, 127*, 106-117. doi:10.1016/j.rse.2012.08.033

Trimble. (2016). *Trimble eCognition Developer Version 9.2 User Guide*. Munich, Germany: Trimble Germany GmbH.

Wang, Y., Traber, M., Milstead, B., & Stevens, S. (2007). Terrestrial and Submerged Aquatic Vegetation Mapping in Fire Island National Seashore using High Spatial Resolution Remote Sensing Data. *Marine Geodesy, 30*(1-2), 77-95. doi:10.1080/01490410701296226

Wechsler, S. P., & Kroll, C. N. (2006). Quantifying DEM Uncertainty and its Effect on Topographic Parameters. *Photogrammetric Engineering & Remote Sensing, 72*(9), 1081-1090. doi:10.14358/PERS.72.9.1081

Weiss, A. D. (2001). *Topographic position and landforms analysis, poster presentation*. Paper presented at the ESRI Users Conference, San Diego, CA. Retrieved from http://www.jennessent.com/downloads/tpi-poster-tnc_18x22.pdf

Wernette, P., Houser, C., & Bishop, M. P. (2016). An automated approach for extracting Barrier Island morphology from digital elevation models. *Geomorphology, 262*(1), 1-7. doi:10.1016/j.geomorph.2016.02.024

Wernette, P., Thompson, S., Eyler, R., Taylor, H., Taube, C., Medlin, A., . . . Houser, C. (2018). Defining dunes: Evaluating how dune feature definitions affect dune interpretations from remote sensing. *Journal of Coastal Research, 34*(6), 1460 – 1470. doi:10.2112/JCOASTRES-D-17-00082.1

Woodcock, C. E., & Gopal, S. (2000). Fuzzy set theory and thematic maps: accuracy assessment and area estimation. *International Jorunal of Geographic Information Science, 14*(2), 153-172. doi:10.1080/136588100240895

Xu, C., Dai, F., Xu, X., & Lee, Y. H. (2012). GIS-based support vector machine modeling of earthquake-triggered landslide susceptibility in the Jianjiang River watershed, China. *Geomorphology, 145-146*(1), 70-80. doi:10.1016/j.geomorph.2011.12.040

Young, D. R., Brantley, S. T., o, J. C., & Vick, J. K. (2011). Landscape position and habitat polygons in a dynamic coastal environment. *Ecosphere, 2*(6), 1-15. doi:10.1890/ES10-00186.1

Yu, Q., Gong, P., Clinton, N., Biging, G., Kelly, M., & Schirokauer, D. (2006). Object-based Detailed Vegetation Classification with Airborne High Spatial Resolution Remote Sensing Imagery. *Photogrammetric Engineering & Remote Sensing, 72*(7), 799-811. doi:10.14358/PERS.72.7.799

Zervas, C. (2013). *Extreme water levels of the United States 1893–2010* (NOAA Technical Report NOS CO-OPS 67). Silver Spring, MD: National Oceanic and Atmospheric Administration. Retrieved from NOAA website: https://tidesandcurrents.noaa.gov/publications/NOAA_Technical_Report_NOS_COOPS_067a.pdf

Zhang, C. (2015). Applying data fusion techniques for benthic habitat mapping and monitoring in a coral reef ecosystem. *ISPRS Journal of Photogrammetry and Remote Sensing, 104*(1), 213-223. doi:10.1016/j.isprsjprs.2014.06.005

Zhang, C., Xie, Z., & Selch, D. (2013). Fusing lidar and digital aerial photography for object-based forest mapping in the Florida Everglades. *GIScience & Remote Sensing, 50*(5), 562-573. doi:10.1080/15481603.2013.836807

Zinnert, J. C., Shiflett, S. A., Via, S., Bissett, S., Dows, B., Manley, P., & Young, D. R. (2016). Spatial–Temporal Dynamics in Barrier Island Upland Vegetation: The Overlooked Coastal Landscape. *Ecosystems, 19*(4), 685-697. doi:10.1007/s10021-016-9961-6

Zinnert, J. C., Shiflett, S. A., Vick, J. K., & Young, D. R. (2011). Woody vegetative cover dynamics in response to recent climate change on an Atlantic coast barrier island: a remote sensing approach. *Geocarta International, 26*(8), 595-612. doi:10.1080/10106049.2011.621031

Zinnert, J. C., Stallins, J. A., Brantley, S. T., & Young, D. R. (2017). Crossing Scales: The Complexity of Barrier-Island Processes for Predicting Future Change. *BioScience, 67*(1), 39-52. doi:10.1093/biosci/biw154

APPENDIX A: HABITAT CLASS DEFINITIONS

Table A.1. Habitats, description, tidal regime, and description source for the barrier island habitat mapping effort for Dauphin Island, Alabama, 2015.

Habitat	Description[a]	Tidal regime	Source
Dune-bare	Dunes are supratidal features developed via Aeolian processes. Dunes are often found above storm water levels and have a well-defined relative elevation (i.e., ridge or upper slope). Dune-bare includes dunes that have less than 10% vegetation cover.	Supratidal/ upland	Acosta et al. (2005)
Dune-herbaceous	Dune-herbaceous includes low-elevation dunes with sparse to dense herbaceous vegetation coverage. Herbaceous vegetation cover should generally be greater than or equal to about 10 percent. See the dune-bare class for a general description of dune features.	Supratidal/ upland	Gibson and Looney (1992)
Dune-wooded	Dune-wooded includes relatively immobile secondary dunes that support sparse vegetation coverage by shrubs. Compared to the other dune classes, these dunes are typically found at higher elevations and further from the shoreline. Woody vegetation cover should generally be greater than or equal to about 30%. See the dune-bare class for a general description of dune features.	Supratidal/ upland	Lucas and Carter (2010)
Meadow	Meadow includes areas with sparse to dense herbaceous vegetation located above extreme high water springs found leading up to primary dunes and on the barrier flat (i.e., backslope of dunes). Vegetation coverage should be generally greater than 30%.	Supratidal/ upland	Lucas and Carter (2010)
Unvegetated barrier flat	Unvegetated barrier flat includes flat or gently sloping unvegetated or sparsely vegetated areas (i.e., less than 30% cover) above extreme high water springs that are located on the backslope of dunes, unvegetated washover fans, unvegetated open developed areas, and estuarine shorelines where salinity is less than 30 parts per thousand (ppt).	Supratidal/ upland	Leatherman (1979)
Scrub/shrub	Scrub/shrub includes areas where woody vegetation height is greater than about 0.5 meters, but less than 6 meters. Woody vegetation coverage should generally be greater than 30%.	Supratidal/ upland	Cowardin et al. (1979)
Forest	Forest includes upland areas where woody vegetation height is greater than 6 meters. Woody vegetation coverage is generally greater than 30%.	Supratidal/ upland	Cowardin et al. (1979)
Forested wetland	Forested wetland includes all nontidal wetlands dominated by woody vegetation with a height greater than or equal to 6 meters. Woody vegetation coverage should generally be greater than 30%.	Supratidal/ upland	Cowardin et al. (1979)
Intertidal beach	Intertidal beach includes bare or sparsely vegetated areas along the ocean-facing side of the island found between extreme low water springs and extreme high water springs that are adjacent to high-energy shorelines which occasionally experience salinity that is greater than or equal to 30 ppt.	Intertidal	Cowardin et al. (1979)

[a]All percent coverage requirements refer to an area of at least 40 m^2 (i.e., the same area as the minimum mapping unit).

(cont'd.)

Habitat	Description[a]	Tidal regime	Source
Beach	Beach includes bare or sparsely vegetated area that is upslope of the intertidal beach zone and marine open water. These habitats occasionally experience inundation by marine water at a concentration of greater than or equal to 30 ppt and include shorelines with high wave energy.	Supratidal/ upland	Cowardin et al. (1979)
Intertidal flat	Intertidal flat includes all tidal wetlands (i.e., wetlands found above extreme low water springs and below extreme high water springs) adjacent to estuarine open water (i.e., water with salinity due to ocean-derived salts that would rarely be above 30 ppt) and along shorelines with low wave energy with vegetation cover of less than 30%.	Intertidal	Cowardin et al. (1979)
Intertidal marsh	Intertidal marsh includes all tidal wetlands (i.e., wetlands that are found above extreme low water springs and below extreme high water springs) with 30% or greater areal cover by erect, rooted, herbaceous hydrophytes.	Intertidal	Cowardin et al. (1979)
Shoreline protection	Shoreline protection includes areas that have any material used to protect shorelines from erosion.	Supratidal/ upland	Fearnley et al. (2009)
Developed	Developed includes areas dominated by constructed materials (i.e., transportation infrastructure, and residential and commercial areas).	Supratidal/ upland	Homer et al. (2015)
Water-fresh	Water-fresh includes all areas of nontidal open water (i.e., isolated low-lying areas that are not influenced from tides associated extreme water springs). These water areas generally have less than 30% cover of vegetation.	Supratidal/ upland	Cowardin et al. (1979)
Water-estuarine	Water-estuarine includes all areas of tidal open water and estuarine water of the back-barrier side of the island (i.e., water bodies that receive regular inundation from tides associated extreme water springs). These areas rarely have salinity greater than 30 ppt. These water areas generally have less than 30% cover of vegetation.	Subtidal	Cowardin et al. (1979)
Water-marine	Water-marine includes all areas of marine open water found offshore of the ocean-facing side of the island. These areas are found along high-energy coastlines and/or occasionally experience salinity levels greater than or equal to 30 ppt.	Subtidal	Cowardin et al. (1979)

[a]All percent coverage requirements refer to an area of at least 40 m^2 (i.e., the same area as the minimum mapping unit).

APPENDIX B: HABITAT MAPPING THRESHOLDS

Table B.1. Examples of general thresholds used for the barrier island habitat mapping effort for Dauphin Island, Alabama, 2015. B: Beach; DB: Dune-bare; DH: Dune-herbaceous; DV: Developed; DW: Dune-wooded; F: Forest; IB: Intertidal beach; IF: Intertidal flat; IM: Intertidal marsh; M: Meadow; NDVI: Normalized difference vegetation index; NIR: Near infrared band; SD: Standard deviation; SS: Scrub/shrub; TPI: Upper ridges and slopes processed from the topographic position index (Weiss, 2001); UBF: Unvegetated barrier flat; VH: Vegetation height in m; WE: Water-estuarine; WF: Water-fresh; and WM: Water-marine.

General class	Threshold(s)	Detailed class	Thresholds/rules
Non-vegetated	Mean NDVI < -0.01 & Mean NIR > 29,000	B	Found near the ocean-facing shoreline in front of dune or transitional area (i.e., start of vegetated area)
		DB	Overlap with TPI = TRUE
		UBF	Areas not classified as B where overlap with TPI = False and Overlap with probability of being intertidal = FALSE
		IB	Overlap with probability of being intertidal = TRUE & along the ocean-facing shoreline
		IF	Overlap with probability of being intertidal = TRUE & along the back-barrier-facing shoreline
		DV	Buildings: Median VH > 1 & Mean NDVI < -0.06 & Mean NIR > 16,000; Non-buildings: Mean VH < 1 & Mean NDVI < -0.06 & Mean NDVI > -0.02 & Mean NIR < 33,000 & Mean NIR > 12,000
Vegetated	Mean NDVI < -0.07 & Mean NIR < 29,000; Mean NDVI > 0	DW	Areas classified as either SS or F where overlap with TPI = TRUE
		DH	Areas not classified as either SS or F where overlap with TPI = TRUE
		M	Overlap with probability of being intertidal = FALSE
		SS	Mean VH >= 0.05 & Mean VH < 6 & SD VH < 3 & Mean NDVI > 0.20
		F	Mean VH >= 6 & Mean NDVI > 0.25; Mean VH >=0.05 & Mean VH < 6 & SD VH < 3 & Mean NDVI > 0.20
		IM	Overlap with probability of being intertidal = TRUE
Water	Mean NDVI < -0.25 & Mean NIR < 1,500	WE	Found near the back-barrier-facing shoreline
		WF	Overlap with probability of being intertidal = FALSE
		WM	Found near the ocean-facing shoreline

APPENDIX C: HABITAT MODELING

Table C.1. Model presets and overall accuracy results using five-fold cross validation by algorithm (i.e., K-nearest neighbor, support vector machine, and random forest models) for the subtidal zone for the contemporary habitat model development for Dauphin Island, Alabama, USA. D: Distance; K = Number of neighbors; KT: Kernel type; KS: Kernel scale; SD: Standard deviation; W: Weight.

			Overall accuracy	
Algorithm	**Name**	**Configuration**	**Mean**	**SD**
K-nearest neighbor (KNN)	Fine KNN	K = 1; D = Euclidean	94.60	0.15
	Medium KNN	K = 10; D = Euclidean	96.16	0.16
	Coarse KNN	K = 100; D = Euclidean	96.54	0.05
	Cosine KNN	K = 10; D = cosine	96.20	0.14
	Cubic KNN	K = 10; D = cubic	96.16	0.16
	Weighted KNN	K = 10; D = Euclidean; W = inverse squared	94.82	0.10
Support vector machine (SVM)	Linear SVM	KT = linear; KS = automatic	96.48	0.04
	Quadratic SVM	KT = quadratic; KS = automatic	96.50	0.00
	Cubic SVM	KT = cubic; KS = automatic	92.62	4.50
	Fine Gaussian SVM	KT = Gaussian; KS = 0.56	96.52	0.04
	Medium Gaussian SVM	KT = Gaussian; KS = 2.2	96.50	0.06
	Coarse Gaussian SVM	KT = Gaussian; KS = 8.9	93.30	0.00
Random forest (RF)	Random forest	30 trees	94.64	0.20

Table C.2. Model presets and overall accuracy results using five-fold cross validation by algorithm (i.e., K-nearest neighbor, support vector machine, and random forest models) for the intertidal zone for the contemporary habitat model development for Dauphin Island, Alabama, USA. D: Distance; K = Number of neighbors; KT: Kernel type; KS: Kernel scale; SD: Standard deviation; W: Weight.

			Overall accuracy	
Algorithm	**Name**	**Configuration**	**Mean**	**SD**
K-nearest neighbor (KNN)	Fine KNN	K = 1; D = Euclidean	82.54	0.82
	Medium KNN	K = 10; D = Euclidean	82.46	1.15
	Coarse KNN	K = 100; D = Euclidean	72.66	0.23
	Cosine KNN	K = 10; D = cosine	81.22	0.84
	Cubic KNN	K = 10; D = cubic	81.22	1.65
	Weighted KNN	K = 10; D = Euclidean; W = inverse squared	84.68	1.63
Support vector machine (SVM)	Linear SVM	KT = linear; KS = automatic	80.74	0.53
	Quadratic SVM	KT = quadratic; KS = automatic	84.22	0.48
	Cubic SVM	KT = cubic; KS = automatic	85.54	1.00
	Fine Gaussian SVM	KT = Gaussian; KS = 0.56	84.34	0.55
	Medium Gaussian SVM	KT = Gaussian; KS = 2.2	81.60	0.60
	Coarse Gaussian SVM	KT = Gaussian; KS = 8.9	71.58	0.48
Random forest (RF)	Random forest	30 trees	88.78	0.63

Table C.3. Model presets and overall accuracy results using five-fold cross validation by algorithm (i.e., K-nearest neighbor, support vector machine, and random forest models) for the supratidal/upland zone for the contemporary habitat model development for Dauphin Island, Alabama, USA. D: Distance; K = Number of neighbors; KT: Kernel type; KS: Kernel scale; SD: Standard deviation; W: Weight.

			Overall accuracy	
Algorithm	**Name**	**Configuration**	**Mean**	**SD**
K-nearest neighbor (KNN)	Fine KNN	K = 1; D = Euclidean	71.26	0.35
	Medium KNN	K = 10; D = Euclidean	74.02	0.51
	Coarse KNN	K = 100; D = Euclidean	66.22	0.19
	Cosine KNN	K = 10; D = cosine	72.64	0.42
	Cubic KNN	K = 10; D = cubic	73.56	0.67
	Weighted KNN	K = 10; D = Euclidean; W = inverse squared	75.74	0.87
Support vector machine (SVM)	Linear SVM	KT = linear; KS = automatic	72.74	0.22
	Quadratic SVM	KT = quadratic; KS = automatic	76.36	0.34
	Cubic SVM	KT = cubic; KS = automatic	75.62	0.65
	Fine Gaussian SVM	KT = Gaussian; KS = 0.56	70.74	0.52
	Medium Gaussian SVM	KT = Gaussian; KS = 2.2	74.08	0.43
	Coarse Gaussian SVM	KT = Gaussian; KS = 8.9	64.62	0.12
Random forest (RF)	Random forest	30 trees	78.02	0.64

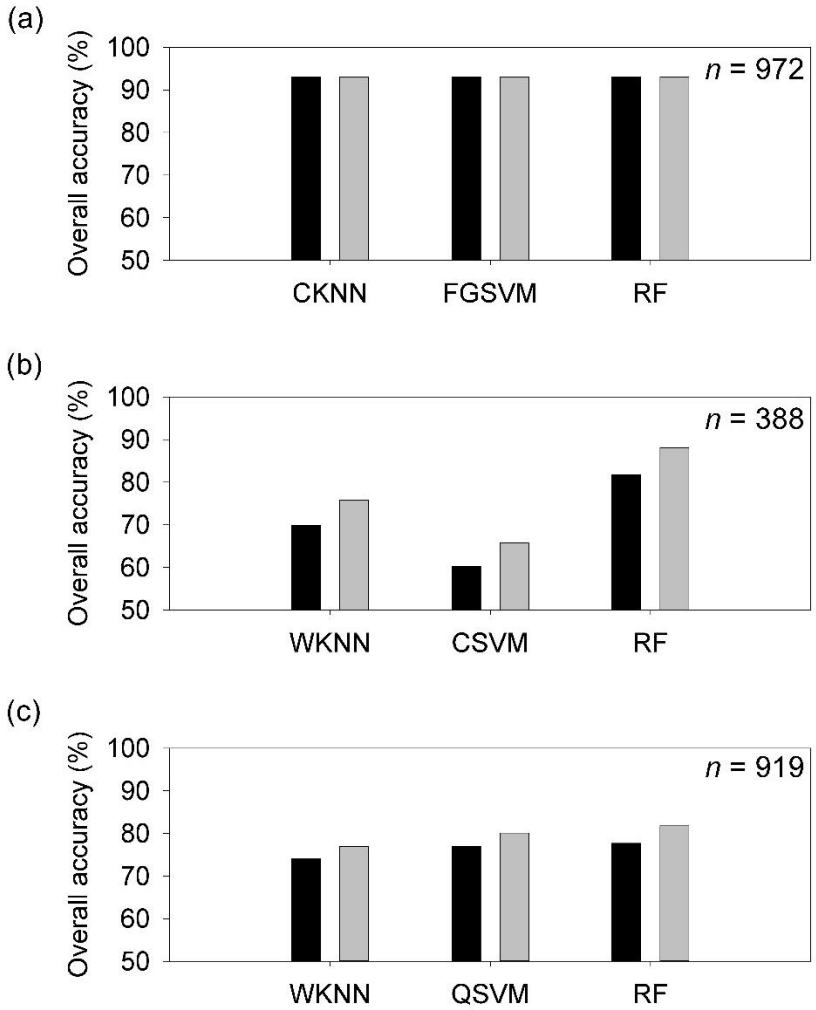

Figure C.1. Deterministic accuracy (black bar) and fuzzy overall accuracy (gray bar) by zone for top three models for the contemporary habitat model development for Dauphin Island, Alabama, USA. (a) Subtidal zone; (b) Intertidal zone; and (c) Supratidal/upland zone. CKNN: Coarse K-nearest neighbor model; CSVM: Cubic support vector machine model; FGSVM: Fine-scaled Gaussian support vector machine model; RF: Random forest model; QSVM: Quadratic support vector machine model; WKNN: Weighted K-nearest neighbor model.

Table C.4. Error matrix with deterministic and fuzzy accuracies for the initial contemporary model results (i.e., without post-processing and a four-pixel minimum mapping unit) for Dauphin Island, Alabama, USA. For the off-diagonal cells, the first value indicates deterministic count and the second value indicates the fuzzy count. BF: Barrier flat; B: Beach; CT: Column total; D: Dune; DPA: Deterministic producer's accuracy; DOA: Deterministic overall accuracy; DUA: Deterministic user's accuracy; FOA: Fuzzy overall accuracy; FPA: Fuzzy producer's accuracy; FUA: Fuzzy user's accuracy; IB: Intertidal beach; IF: Intertidal flat; IM: Intertidal marsh; RT: Row total; WE: Water-estuarine; WF: Water-fresh; WM: Water-marine; WV: Woody vegetation; WW: Woody wetland.

		Reference data													
	Class	BF	B	D	IB	IF	IM	WE	WF	WM	WV	WW	RT	DUA (%)	FUA (%)
Model data	BF	**305**	4;2	36;1	1;0	15;8	47;23	13;0	0;0	0;0	31;15	0;0	501	60.9	70.7
	B	4;7	**62**	0;1	2;14	0;3	3;0	1;0	0;0	7;25	0;1	0;0	130	47.7	86.9
	D	38;1	0;1	**99**	0;0	0;0	0;0	0;0	0;0	3;1	5;1	0;0	149	66.4	69.1
	IB	1;0	13;1	0;0	**17**	0;2	1;0	0;10	0;0	2;88	0;0	0;0	135	12.6	87.4
	IF	17;5	4;0	0;0	3;0	**95**	39;34	73;144	0;0	11;0	2;1	0;0	428	22.2	65.2
	IM	13;6	2;0	2;0	0;0	23;4	**307**	54;3	0;0	1;0	1;1	0;0	417	73.6	77.0
	WE	1;0	0;0	0;0	0;0	0;0	0;0	**607**	0;0	0;0	0;0	0;0	608	99.8	99.8
	WF	9;0	0;0	0;0	0;0	0;0	0;0	9;0	**27**	1;0	4;1	0;0	51	52.9	54.9
	WM	0;0	1;0	0;0	0;0	0;0	0;0	68;0	0;0	**314**	0;0	0;0	383	82.0	82.0
	WV	13;8	0;0	0;0	0;0	0;0	6;0	0;0	0;0	0;0	**205**	2;0	234	87.6	91.0
	WW	2;0	0;0	0;0	0;0	0;0	0;0	0;0	1;0	0;0	20;3	**29**	55	52.7	58.2
	CT	430	90	139	37	150	460	982	28	453	291	31	**3,091**		
	DPA (%)	70.9	68.9	71.2	46.0	63.3	66.7	61.8	96.4	69.3	70.5	93.6			
	FPA (%)	77.2	73.3	72.7	83.8	74.7	79.1	77.8	96.4	94.5	78.4	93.6			
		DOA (%): 66.9; FOA (%): 80.3													

VITA

Nicholas Enwright was born in North Central Massachusetts. Before attending the Louisiana State University, Nicholas graduated in 2007 with a Bachelor of Science in Geography from the University of North Texas in Denton, Texas. He continued his studies in Geography at the University of North Texas and received his Master of Science in Applied Geography in 2010. While working on his Master of Science degree, he was awarded the Department of Geography's Outstanding Graduate Student award in 2009. In 2010, he moved to Lafayette, Louisiana to begin work as a contractor providing geospatial analyses and remote sensing support to the U.S. Geological Survey Wetland and Aquatic Research Center. In 2013, he was hired as a geographer by the U.S. Geological Survey Wetland and Aquatic Research Center.